A study of steric chirality: The chiral nematic phase of a system of chiral two-site HGO molecules

George Jackson, Szabolcs Varga

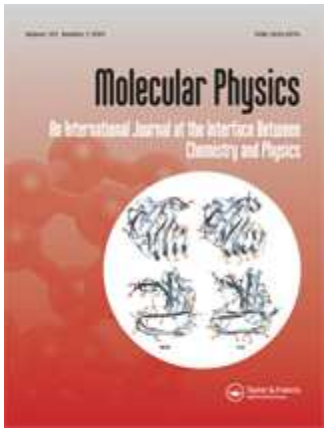

A study of steric chirality: The chiral nematic phase of a system of chiral two-site HGO molecules

Journal:	*Molecular Physics*
Manuscript ID:	TMPH-2010-0450
Manuscript Type:	Special Issue paper - In honour of Bob Evans
Date Submitted by the Author:	18-Nov-2010
Complete List of Authors:	Jackson, George; Imperial College London, Chemical Engineering Varga, Szabolcs; University of Pannonia, Institute of Physics
Keywords:	Liquid Crystals, Density Functional Theory, Chirality, Biaxiality

A study of steric chirality: The chiral nematic phase of a system of chiral two-site HGO molecules

Szabolcs Varga[a] and George Jackson[b]

[a] *Department of Physics and Mechatronics, University of Pannonia, H-8200 Veszprém, PO Box 158, Hungary*

[b] *Department of Chemical Engineering, Imperial College London, South Kensington Campus, London SW7 2AZ, UK.*

PACS Numbers: 64.70.Fx, 05.70.Fh, 75.50.Mm

Number of pages: 49 (including figure captions and figures)

Figures: 12

[a] e-mail: vargasz@almos.vein.hu

[b] e-mail: g.jackson@imperial.ac.uk

Abstract

The liquid crystalline phase behaviour of a chiral two-site hard Gaussian overlap fluid is examined using the well-known Parsons-Lee extension of the theory of Onsager. The hard-core model is constructed such that the vector connecting the centers of two hard Gaussian segments is perpendicular to the long axes of both segments. The microscopic chirality of the particle can be controlled with the dihedral angle between the long axes of the hard Gaussian segments, the distance between the two segments, and the length-to-breath ratios of each segment. In the framework of Parsons-Lee approach three different types of phases are considered, namely, the isotropic liquid, and the nematic and the chiral nematic (cholesteric) liquid crystalline phases. For simplicity, the orientation of the particles is restricted to the plane perpendicular to the twist axis, and the particles do not have internal freedom to rotate around their main symmetry axes. The geometric condition for the formation of a chiral nematic phase, the properties of the helical structure, and the phase boundary of the ordering transition are determined by means of a free energy minimization. It is shown that steric (shape) chirality always gives rise to helical structure in the nematic phase, and that the low density chiral systems can undergo a transition from an isotropic liquid to a twisted nematic phase increasing the density. Analytical expressions are obtained for the twist period (pitch) in the limit of parallel stacking of the rod-like segments in layers normal to the helical axis, which are only valid for systems characterized by weak chiral strengths. A key finding of the numerical calculations is that the pitch is very sensitive to the segment separation, but not to the density or aspect ratio. It is interesting to note that the inverse of the pitch is predicted to depend linearly on the dihedral angle in all of the cases studied.

1. Introduction

The simplest liquid crystalline (meso) phase is a nematic in which the principal axis of the molecules (mesogens) is aligned along a preferential direction (the director) but where the distribution of the molecular centres of mass is otherwise isotropic [1,2]. Molecular (microscopic) chirality is a fascinating property of mesogens because it can give rise to an additional helical structure in the direction normal to the plane of the nematic ordering [1-5]. The helically structured nematic phase is often referred to as a chiral nematic or cholesteric phase. The relation between the bulk (macroscopic) liquid crystal phase behaviour and the inherent chirality of the molecules is still poorly understood. One example is the liquid crystalline behaviour exhibited by aqueous colloidal suspensions of TMV or *pf*1 viruses, where the molecular chirality does not give rise to a helical macroscopic structure, while a stable cholesteric phase is exhibited in aqueous suspensions of *fd* viruses which is structurally very similar to *pf1* [6-8]. It is therefore clear that molecular chirality does not guarantee the existence of the orientational ordered twisted structure.

Liquid crystalline phase behaviour was originally thought to be the consequence of electrostatic (polar) interactions between the molecular species alone [9,10]. The mean-field Maier-Saupe treatment of liquid crystalline order [11-13] is consistent with this energetic standpoint, as is the common application of the phenomenological Landau-de Gennes description [14-16]. It is now well recognised that repulsive (excluded volume) interactions also play a central role in the stabilisation of mesophases as Onsager had first suggested in 1942 [17,18]; extensive molecular simulation studies of hard discs [19,20], ellipsoids of revolution [21,22], hard spherocylinders [23–26], and rigid hard-sphere chains [27] certainly support this view. Though anisotropic repulsive interactions thus appear to a perquisite for the formation of macroscopic liquid crystalline order, the effect of the electrostatic forces cannot be overlooked. The stable orientationally and positionally

ordered structures that are observed are very sensitive to the precise features of the electrostatic interactions (such as their position and orientation) or the presence of flexible tails as has been highlighted in studies of model dipolar hard-core systems [28-32].

The existence of twisted nematic phases can be attributed to microscopic chiral features which are both steric and electrostatic in origin. In most real systems these two types of molecular chirality are present but the separate contribution that each interaction makes to the orientational ordering of the bulk phase is difficult to identify [1-5]. A full armoury of statistical mechanical and continuum theories and molecular simulation techniques has been deployed in studies of model molecules with chiral interactions which are of a steric or electrostatic nature (or both), including the development of suitable indices to characterise the molecular chirality; see [33-97] and references therein as representative examples. Despite this large body of work there is still much debate as to which underlying microscopic feature is responsible for the stabilisation of chiral nematic phase. It is therefore a highly desirable goal to gain a better understanding of the relation between molecular chirality and the helical twist of the bulk phase by studying model systems for which the roles of the steric and electrostatic chirality can be examined independently. The effect of electrostatic chiral interactions on cholesteric order has been examined in detail with Maier-Saupe mean-field [3-5, 33-35, 37, 38, 40, 62, 71, 73, 76, 83-85] and Onsager-like [93, 94, 97] theories. In the opposite vein we focus on a description of the chiral nematic phase of purely repulsive hard body systems characterised by steric chirality in our current work.

Straley [36] was the first to examine the effect of repulsive steric chirality by studying a system of helically threaded hard rods using Onsager's second-virial theory for orientational order in hard anisometric particles [18]. Odijk [44] later extended the approach of Straley to allow for a treatment of the molecular flexibility. A surprising finding of these studies is that the helical twist of the bulk chiral structure does not depend on the degree of molecular chirality, though the wave number (inverse pitch) is found to be proportional to the density, diameter of the molecular core, and the thread depth in very ordered twisted nematic phases. In related work Pelcovits [60] examined a system of rigid and semi-flexible corkscrew particles finding the more physically intuitive

dependence of the cholesteric pitch on the molecular chirality; furthermore, the density dependence found for the pitch is different from that described by Straley or Odijk. The chiral nematic phase formed by twisted biaxial ellipsoids (with and without isotropic attractive interactions) has also been studied by Evans [51] using a Parsons-Lee [98,99] type scaling of the Onsager free energy functional to account for the higher virial coefficients in an approximate manner. In this case Evans did not observe a density dependence of the pitch but the bulk chirality was found to be proportional to the molecular twist of the hard body. Very recently Dhakal and Selinger [96] have examined a lattice model of bent-core molecule with mean-field and Landau-de Gennes theories and by Monte Carlo simulation, describing the temperature dependence of the pitch and the underlying mutual enhancement of biaxial and chiral order. The model we study here is a continuum analogue of this lattice model.

Simulation studies of chiral nematic phases are comparatively rare [54-56, 61, 63, 67-70, 72, 77, 79-81, 86, 88, 92, 93, 96], and tend to focus on particles characterized by the electrostatic dispersive chiral interaction potential devised by Goossens [33] incorporated within a reference system of hard-core or Gay-Berne [100] (GB) mesogens. The first simulations of purely repulsive chiral molecules formed from two hard prolate ellipsoidal cores in a crossed configuration was presented by Allen [54] to study the dependence of the helical twisting power on the addition of these model chiral dopants to the nematic phase of uniaxial molecules; Camp [63] later developed an elegant and simple theoretical framework for such a system. Memmer et al. [61] have considered the steric chirality in a system of particles comprising two fused GB sites, where the dihedral angle between the GB segments governs the chirality of the molecule. With their canonical Monte Carlo simulations they showed that one could stabilize a macroscopic cholesteric structure for the GB dimers. A drawback of the study of Memmer et al. [61] is that the underlying dispersive attractive interactions of the GB cores also affects the structure of the chiral nematic phase, i.e., the contribution due to steric chirality cannot be completely decoupled from the electrostatic chirality. The same issue arises in systems of fused two-site GB models with a bent-core [81] or discotic [88] geometry; interestingly, though the bent-core GB molecules are biaxial but otherwise achiral, they

are found to exhibit twisted grain boundary (TGB) structures with smectic layers rotated relative to each other [81].

To study the effect of steric chirality alone we construct a two-site hard-body model, similar to that of Allen [54], which can be considered as the athermal analogue of the model proposed by Memmer et al. [61]. It also resembles the single-core chiral model of Harris et al. [3]: in this very simple athermal model only the orientational and the packing entropies are active, and the interplay between these two entropic contributions determines the structure of the stable phase.

Two quantities are required to characterize the structure of the twisted nematic phase: one is the local orientational distribution function, and the other is the spatial period of the twist (cholesteric pitch) [4]. It is generally accepted that the twist angle between two nematic layers is proportional to the distance between the layers, while the orientational distribution function has to be biaxial with a higher probability of molecules oriented in the plane than out of the plane. As has been pointed out by Harris et al. [5], the twisted structure cannot propagate without (local) biaxial orientational order otherwise the macroscopic phase would always be of uniaxial nematic symmetry. In our model we assume that the long axes of the molecular segments are always perpendicular to the helix axis of the chiral twist to fulfill the requirement of biaxial orientational order.

The goal of our work is to study the macroscopic manifestation of chirality in the molecular shape for a hard-body system which forms orientationally ordered phases. Using the purely repulsive hard Gaussian overlap (HGO) model as building blocks to form a two-site chiral molecule, the contribution of steric chirality on the formation of a chiral nematic phase can be studied in isolation. No attractive/electrostatic interactions are included, which would otherwise also have an impact on the helical structure of the bulk phase. Our model makes it possible to determine explicitly the role played by the molecular geometry and the aspect ratio in the stabilization of the bulk helical structure. We use the well-known Parsons-Lee [98,99] extension of Onsager's theory for hard cores to determine the stability of the isotropic, nematic, and chiral nematic phases by characterizing the structure of the bulk phases. As we have already mentioned, the principal inertial axes of the particles are always restricted to stay in a plane, and can either rotate freely in the plane or are

orientationally constrained depending on the level of approximation that is employed. The results of both approximations are compared to assess the relationship between the orientational entropy and the helical wave number of the twisted nematic phase.

The paper is organized as follows: In the following section the molecular model is presented and the geometric conditions that have to be satisfied to represent chiral shapes are discussed. In Section 3. we present the Parsons-Lee theory as applied to chiral nematic phases, and derive our working equations using two different approximations for the orientational distribution function. Some applications of the theory are then presented for the system of two-site HGO molecules using a second-order expansion of the free energy of the twisted nematic phase. In Section 4. the effect of the three parameters that govern the molecular chirality, the effect of the aspect ratio, and the effect of the packing fraction on the formation of the cholesteric phase is examined in detail; the role of orientational freedom is also assessed. Our conclusions are summarized in Section 5.

2. Molecular model and the conditions for microscopic chirality

The simplest way to examine steric chirality is to link two uniaxial (achiral) rod-like hard cores in such a way that they form a chiral body. To do this of one of the particle has to be twisted relative to the other with a finite angle. We further suppose that the vector connecting the centres of the two prolate bodies is perpendicular to the long symmetry axis of each hard-core segment. This type of molecular geometry is depicted in Fig. 1, where the dihedral angle (α) between the two main symmetry axes of the segments is chosen to be $\pi/6$, the length-to-breath ratio of the each segment is $\kappa_1 = \kappa_2 = \kappa = 3$, and the distance Δ between the centres of the segments is equal to the segment diameter σ_0 (here σ_0 is the dimension of the short axis of the hard core, i.e., its breadth). There are two ways to control the chirality of the molecule shown in Fig. 1: one involves a change in the dihedral angle between the long axes of the segments, and the other a variation of the distance between the centres of the segments. There are particular cases where the molecule is achiral. The parallel and the perpendicular relative alignment of the cores, and the perfectly fused case (the distance between the two centres is zero) are clearly achiral (see Fig. 2). In the case of two different fused hard bodies ($\kappa_1 \neq \kappa_2$), the chirality is lost by making one of the hard-core segments spherical as shown in Fig. 2 d). The exact form of the hard body interaction will be given later.

3. Parsons-Lee theory of the chiral nematic phase

The approach of Onsager [18] is one of the most popular and successful theories for the description of nematic order in systems of hard-core mesogens [101,102], hard-core mixtures [103], and attractive molecules with anisotropic hard cores [104]. It can be regarded as one of the first applications of density functional theory (DFT), where the free energy of the system is described as a functional of the single particle orientational distribution function. A DFT treatment provides one of the most successful generic platforms for the description of inhomogeneous and anisotropic systems. Evans [105,106] has been a key developer and exponent of the approach in its application to free

interfaces of fluids and fluid mixtures and systems under confinement. The work of Evans and co-workers also provides an excellent example of the use of DFT to represent inhomogeneous liquid crystalline systems, including the effect of confinement on the isotropic-nematic transition [107] and capillary nematization of confined hard rods [108,109].

In its original form the theory of Onsager is cast at the second virial level. This means that it appropriate only at low density. The applicability of the Onsager free energy to higher density isotropic and nematic phases of hard body fluids can be extended by following the methodology of Parsons [98] and of Lee [99] (also see the detailed exposition in references [25,102]). The theory is also appropriate for chiral nematic (cholesteric) phase because the local helical structure is expected to be weak in practice and is not likely to give rise to substantial change in the overall free energy of the system. In the remainder of this section we reformulate the Parsons-Lee theory for the chiral nematic phase in a Cartesian coordinate frame of reference where the helical axis is assumed to be parallel with the z axis.

For the freely rotating case, the total Helmholtz free energy F of the chiral nematic phase can be written as a sum of the ideal and residual contributions $F = F_{ideal} + F_{res}$, where the ideal free energy is given by

$$\frac{\beta F_{ideal}}{V} = \rho \ln(\Lambda^3 \rho) - \rho + \frac{\rho}{V} \int d\underline{r} d\underline{\omega} f(\underline{\omega}, z) \ln[\Omega f(\underline{\omega}, z)], \tag{1}$$

while the residual part is approximated by the Parsons-Lee approximation [98,99] as

$$\frac{\beta F_{res}}{V} = \frac{4\eta - 3\eta^2}{8v_0(1-\eta)^2} \frac{\rho}{V} \int d\underline{r}_1 d\underline{\omega}_1 f(\underline{\omega}_1, z_1) \int d\underline{r}_2 d\underline{\omega}_2 f(\underline{\omega}_2, z_2) f_M(\underline{r}_{12}, \underline{\omega}_1, \underline{\omega}_2). \tag{2}$$

Here, the Mayer function f_M provides a direct link to the pair potential u through the following relation: $f_M(\underline{r}_{12}, \underline{\omega}_{12}) = \exp[-\beta u(\underline{r}_{12}, \underline{\omega}_{12})] - 1$. In these expressions $\beta = 1/k_B T$ (k_B being the Boltzmann constant and T the temperature), N is the total number of particles, $\rho = N/V$ is the number density (V being the volume of the system), $\eta = \rho v_0$ is the packing fraction, v_0 is the volume of the particle, Λ^3 is the de Broglie volume (kinetic contribution to the free energy), and $\Omega = 8\pi^2$ for

biaxial particles. The orientational distribution function $f(\underline{\omega}, z)$ is used to describe the orientation of the particle's principal symmetry axis in the plane at position z along the helical axis. Since the chiral nematic phase is periodic in the direction of the helical axis (chosen as the z axis), the spatial integrations can be performed in the layer normal:

$$\frac{\beta F_{res}}{V} = \frac{4\eta - 3\eta^2}{8v_0(1-\eta)^2}\rho\frac{1}{P}\int_0^P dz_1 \int d\underline{\omega}_1 f(\underline{\omega}_1, z_1) \int_{z_{12}\in V_{exc}} dz_2 \int d\underline{\omega}_2 f(\underline{\omega}_2, z_2) A_{exc}(z_{12}, \gamma_{12}), \quad (3)$$

where P is the helical period (pitch) of the chiral nematic phase, V_{exc} denotes that region which is excluded to a particle around another particle fixed in space, and γ_{12} is the angle between the principal axes of the particles. The excluded area A_{exc} is the result of twofold integration of the Mayer function when the positions of molecular centres are a distance $z_{12} = z_1 - z_2$ apart.

Two simplifying assumptions are applied for the orientation distribution function. In the simplest approximation, the particle's orientational unit vector ($\underline{\omega}$) is constrained to stay in the plane normal to the helical axis, all of the particles are taken to be parallel in a given layer (perfect 2D order), and the local nematic director is assumed to vary linearly from layer to layer along the helical axis:

$$f(\underline{\omega}) = \delta\left(\theta - \frac{\pi}{2}\right)\delta(\psi)\delta(\varphi - qz). \quad (4)$$

In this equation δ represents the Dirac delta function, (θ,ψ,φ) are the conventional Euler's angles, while q is the wave number (which is proportional to the inverse pitch) prescribing the helical structure of the nematic order to vary in a linear fashion along the z axis. The relationship between the wave number and the pitch of the chiral nematic phase is simply $q = 2\pi/P$. In the second, more realistic, case the particles are still orientated perpendicular to the helical axis, but they are allowed to rotate freely within a given plane:

$$f(\underline{\omega}) = \delta\left(\theta - \frac{\pi}{2}\right)\delta(\psi)h(\varphi), \quad (5)$$

where h is the corresponding 2D orientational distribution function. The difference between the two approximations is that we neglect the contribution due to the orientational entropy completely with Eq. (4), while the orientational entropy is partially captured with Eq. (5).

After substitution of the perfect 2D order approximation (Eq. (4)) into the expressions for the ideal and residual free energy (Eqs. (1-3)) we get

$$\frac{\beta F_{ideal}}{V} = \rho \ln(\Lambda^3 \rho) - \rho , \tag{6}$$

and

$$\frac{\beta F_{res}}{V} = \frac{4\eta - 3\eta^2}{8v_0(1-\eta)^2} \rho \int_{z_{12} \in V_{exc}} dz_{12} A_{exc}(z_{12}, qz_{12}) . \tag{7}$$

In this way the total free energy density in the case of the perfect 2D order approximation can be written as

$$\frac{\beta F}{V} = \rho \ln(\Lambda^3 \rho) - \rho + \frac{4\eta - 3\eta^2}{8v_0(1-\eta)^2} \rho \int_{z_{12} \in V_{exc}} dz_{12} A_{exc}(z_{12}, qz_{12}) . \tag{8}$$

For a given molecular model and density, the free energy only depends on the wave number, i.e., the equilibrium free energy of the system can be obtained by means of the minimization of Eq. (8) with respect to the wave number: $\frac{d\beta F / V}{dq} = 0$. As only the excluded area depends on the q parameter, the condition of the free energy minimization reduces to the minimization of the excluded volume,

$$\frac{dV_{exc}(q)}{dq} = 0 . \tag{9}$$

The integral of the excluded area over the excluded volume regime gives the overall excluded volume for a pair of twisted body characterized by the twist q:

$$V_{exc}(q) = \int_{z \in V_{exc}} dz A_{exc}(z, qz) . \tag{10}$$

In this way the problem reduces to looking for the particular helical arrangement which minimizes the excluded volume interactions between the particles, or in other words that which maximizes the free volume available for the particles in space. One trivial result of the perfect 2D order

approximation is that the pitch does not depend on density even at infinitely low densities, and the phase can be either nematic or chiral nematic, but not isotropic. To overcome this deficiency of the theory, the particles must possess some orientational degrees of freedom.

In the case of free planar ordering, after substitution of the orientational distribution function (Eq. (5)) into the ideal and residual free energy terms (Eqs. (1-3)) the following relations be derived:

$$\frac{\beta F_{ideal}}{V} = \rho \ln(\Lambda^3 \rho) - \rho + \frac{\rho}{P} \int_0^P dz \int_0^{2\pi} d\varphi h(\varphi, z) \ln h(\varphi, z), \tag{11}$$

$$\frac{\beta F_{res}}{V} = \frac{4\eta - 3\eta^2}{8v_0 (1-\eta)^2} \frac{\rho}{P} \int_0^P dz_1 \int_0^{2\pi} d\varphi_1 h(\varphi_1, z_1) \int_{z_{12} \in V_{exc}} dz_2 \int_0^{2\pi} d\varphi_2 h(\varphi_2, z_2) A_{exc}(z_{12}, \varphi_{12}). \tag{12}$$

As for the perfect 2D order approximation, the free energy again has to be minimized with respect to q, but in addition the orientational distribution function $h(\varphi, z)$ which minimizes the free energy has to be determined in order to describe the equilibrium free energy of the system. This can be done by solving a nonlinear integral equation for $h(\varphi, z)$, which can be obtained by functional minimization of the free energy. In order to reduce the computational burden of the free energy minimization, we use a simple helical trial function with a variational parameter λ and wave number q to represent the two-dimensional orientational distribution function:

$$h(\varphi, z) = \frac{\exp(\lambda \cos(2(qz - \varphi)))}{\int_0^{2\pi} d\varphi \exp(\lambda \cos(2(qz - \varphi)))}. \tag{13}$$

Depending on the values of λ and q, Eq. (13) leads to isotropic ($\lambda = 0$), nematic ($\lambda \neq 0$ and $q = 0$) or chiral nematic ($\lambda \neq 0$ and $q \neq 0$) solutions for the orientational distributions. After inserting Eq. (13) into the free energy of freely (in the plane) rotating particles (the sum of Eqs. (11 and 12)) the minimization conditions can be written as

$$\frac{d\beta F/V}{dq} = 0 \text{ and } \frac{d\beta F/V}{d\lambda} = 0. \tag{14}$$

In the result section we will present the equilibrium pitch obtained from both approximations.

Before discussing the solution of these coupled equations it is enlightening to first find the lowest density at which the nematic or chiral nematic phase becomes stable. We perform a so-called bifurcation analysis where the corresponding density is referred to as the bifurcation density [101]. After substitution of the trial function into the ideal and residual free energy terms (Eqs. (11) and (12)) we can expand the free energy as a function of variational parameter λ up to second order. The resulting free energy has the form of $\beta F / V = a + b\lambda^2$, where the zeroth order term a corresponds to the free energy of the isotropic phase, and b is the expansion coefficient of the nematic perturbation. Since the free energy of the nematic and the isotorpic phases are identical at the bifurcation point, the expansion coefficient of nematic perturbation has to be zero. After some algebra we obtain the following expression for the packing fraction at the bifurcation point:

$$1+\frac{4\eta-3\eta^2}{(1-\eta)^2 8 v_0 \pi}\int_{z\in V_{exc}} dz \int_0^{2\pi} d\varphi \cos\left(2\left(qz-\varphi\right)\right) A_{exc}(z,\varphi)=0 \ . \tag{15}$$

To determine whether the nematic or the chiral nematic phase is more stable at the bifurcation one has to minimize the free energy with respect to the wave number: in this case this corresponds to $\frac{db}{dq}=0$. The result of this minimization is given by

$$\int_{z\in V_{exc}} dz \int_0^{2\pi} d\varphi \sin\left(2\left(qz-\varphi\right)\right) z\, A_{exc}(z,\varphi)=0 \ . \tag{16}$$

The solution of the coupled equations (15) and (16) gives the bifurcation packing fraction and the bifurcation wave number. The results of the bifurcation analysis are presented in Section 4.

In order to proceed the molecular model has to be specified. In the following we assume that each segment of the dimer molecule is characterised by the so-called hard Gaussian overlap (HGO) potential [110,111]. The main advantage of this model is that the distance of closest approach, the excluded area, and excluded volume can be expressed in closed analytical forms [112]. For example,

the excluded area for a pair of HGO particles (of breadth σ_0, length $\sigma_0\kappa$, and aspect ratio κ) in a 2D planar arrangement is given by

$$A_{exc}(z,\gamma)=\begin{cases}\dfrac{\pi\left(\sigma_0^2-z^2\right)}{1-\chi}\sqrt{1-\chi^2\cos^2(\gamma)}, & -\sigma_0\le z\le\sigma_0\\ 0, & \text{otherwise}\end{cases} \tag{17}$$

where γ is the angle between the two particles, and χ is an anisotropy parameter defined as $\chi=\dfrac{\kappa^2-1}{\kappa^2+1}$. For a spherical shape ($\kappa = 1$) the anisotropy parameter is zero, while it is one for an infinite length-to-breath ratio ($\kappa = \infty$). One should note that a molecular volume can not be associated uniquely to the HGO pair potential, but it is generally accepted that the volume of HGO particles can be taken as that of correspond hard ellipsoid of revolution, i.e., $v_{HGO}=\dfrac{\pi}{6}\kappa\sigma_0^3$.

To construct our chiral dimer HGO particles, two HGO segments are positioned with their centres a distance Δ apart in a planar alignment with the main symmetry axes of the segments twisted relative to each other at a dihedral angle α as shown in Fig. 1; in this particular case the two segments are taken to be in contact corresponding to an intramolecular segment separation of $\Delta=\sigma_0$. The resulting chiral HGO particle interacts through its HGO segments.

It is instructive to start by examining the particular case of a pair of chiral HGO particles with a (rather unrealistic hanging) intersegment separation of $\Delta=2\sigma_0$ and relative orientation γ for which the excluded area can be determined very easily in the planar geometry. The two HGO particles start to exclude each other at a relative distance of $z=-3\sigma_\perp$ through the interaction between the "bottom" segment of the "upper" molecule and "top" segment of the "lower" molecule. Here, "upper" or "top" and "lower" or "bottom" refer to the relative position along the helical axis z. This interaction persists up to a distance $z=-\sigma_0$ for which the excluded area of a single HGO particle can be used (cf. Eq. (17)); one should note, however, that the angle between the long axes of HGO segments making up the particle is not same as the angle between the two chiral molecules, but

is $\gamma + \alpha$ because of the twisted structure of the molecules. In the second regime of $-\sigma_0 \le z \le \sigma_0$ "like" "top-top" and "bottom-bottom" excluded volume segment-segment interactions take place simultaneously, but these interactions are identical and the resulting excluded areas is obtained from Eq. (17), as in this case the angle between the two like "top" or two "bottom" segments is γ. In the third regime of $\sigma_0 \le z \le 3\sigma_0$, only the "bottom" segment of the "upper" molecule is excluded by the "top" segment of the "lower" molecule in the same way as in the first regime but now for a relative angle of $\gamma - \alpha$. The excluded area for a pair of chiral HGO particles with an intramolecular segment separation of $\Delta = 2\sigma_0$ can thus be summarised with the following relation:

$$A_{exc}(z_{12},\gamma) = \begin{cases} \dfrac{\pi\left(\sigma_0^2 - (z-2\sigma_0)^2\right)}{1-\chi}\sqrt{1-\chi^2\cos^2(\gamma-\alpha)}, & \sigma_0 \le z \le 3\sigma_0 \\ \dfrac{\pi\left(\sigma_0^2 - z^2\right)}{1-\chi}\sqrt{1-\chi^2\cos^2(\gamma)}, & -\sigma_0 \le z \le \sigma_0 \\ \dfrac{\pi\left(\sigma_0^2 - (z+2\sigma_0)^2\right)}{1-\chi}\sqrt{1-\chi^2\cos^2(\gamma+\alpha)}, & -3\sigma_0 \le z \le -\sigma_0 \end{cases} . \quad (18)$$

Note that the expression for the excluded area is much more complicated for smaller values of separation between the centres of the two segments making up the HGO molecule ($0 \le \Delta < 2\sigma_0$), because the excluded volume regimes of the segment-segment interactions do not decouple so simply but overlap. In our generalized twisted two-site HGO model, where the HGO segments have the same breadth (σ_0) but different lengths ($\kappa_1\sigma_0 \ne \kappa_2\sigma_0$), analytical relations can also be derived for the excluded area. Without presenting the details, the expression can be written in the following form for the intramolecular segment separation of $\Delta = 2\sigma_0$ (see reference [113] for shape parameters for particles of differnt aspect ratio):

$$A_{exc}(z_{12},\gamma)=\begin{cases}\dfrac{\pi\left(\sigma_0^2-\left(z-2\sigma_0\right)^2\right)}{\sqrt{1-\chi_1}\sqrt{1-\chi_2}}\sqrt{1-\chi_1\chi_2\cos^2(\gamma-\alpha)}, & \sigma_0\le z\le 3\sigma_0\\ \dfrac{\pi\left(\sigma_0^2-z^2\right)}{1-\chi_1}\sqrt{1-\chi_1^2\cos^2(\gamma)}, & -\sigma_0\le z\le\sigma_0\\ \dfrac{\pi\left(\sigma_0^2-\left(z+2\sigma_0\right)^2\right)}{\sqrt{1-\chi_1}\sqrt{1-\chi_2}}\sqrt{1-\chi_1\chi_2\cos^2(\gamma+\alpha)}, & -3\sigma_0\le z\le-\sigma_0\end{cases}, \quad (19)$$

where the anisotropy parameters of the segments are defined in terms of length-to-breath ratios (κ_1 ,κ_2) as $\chi_1=\dfrac{\kappa_1^{\,2}-1}{\kappa_1^{\,2}+1}$ and $\chi_2=\dfrac{\kappa_2^{\,2}-1}{\kappa_2^{\,2}+1}$. We must mention that Eq. (19) represents the excluded area for molecular arrangements where the "top" and "bottom" segments of the two molecules are commensurate (i.e., geometries where both of the shorter segments are on the "top" or "bottom", but not one on the "top" and one on the "bottom"). A more complete treatment of this system would involve a binary mixture with equal numbers of molecules in "up" and "down" arrangements. To maintain the simplicity of the theory the "up-down" excluded areas are not included in the description. In the case of a intramolecular segment separation of $\Delta=2\sigma_0$, Eqs. (18) and (19) can be used, while for $0\le\Delta<2\sigma_0$ tabulated values of excluded areas obtained numerically (not presented here) are used as the input to the theory.

It is widely accepted that one can expand the free energy density of the twisted nematic phase as a function of wave number up to the quadratic term to obtain the twist torque (h) and the twist elastic constant (K_{22}) as

$$\left.\frac{\beta F}{V}\right|_{TN}=\left.\frac{\beta F}{V}\right|_{N}-hq+\frac{1}{2}K_{22}q^2, \quad (20)$$

where the zeroth order term is the free energy density of the nematic phase. This truncated free energy is often referred to as the Frank free energy for a system with a twist deformation [5]. Such an approach can be applied only in those cases where the molecular chirality does not give rise to a substantial change in the free energy. This is the case for weakly chiral systems such as aqueous

suspension of the *fd* viruses [6-8] and DNA [114]. The minimization of Frank free energy (Eq. (20)) with respect to q allows us to determine the equilibrium wave number in terms of the twist torque and twist elastic constant as $q = h / K_{22}$. In our system of two-segment HGO molecules, it is reasonable to assume that the second order expansion will be adequate for small dihedral angles and small segment separation. The result of the method for the wave number in the case of perfect 2D (planar) order, for molecules with equal segment aspect ratios ($\kappa_1 = \kappa_2$ corresponding to $\chi_1 = \chi_2 = \chi$) and an intramolecular segment separation of $\Delta = 2\sigma_0$ can be written as

$$q = \frac{10\sin(2\alpha)}{\left(\frac{\sqrt{1-\chi^2\cos^2(\alpha)}}{\sqrt{1-\chi^2}} + 42\frac{\cos(2\alpha)-\chi^2\cos^4(\alpha)}{1-\chi^2\cos^2(\alpha)}\right)\sigma_\perp} = \frac{20\alpha}{43\sigma_0} + \mathrm{O}(\alpha^3). \tag{21}$$

It is interesting to note that wave number depends on the molecular anisotropy for moderate values the intramolecular dihedral angle α between the segments. This is not the case, however, for a very small dihedral angle where q is found to follow a linear dependence with α. The application of the method for the more general case of HGO molecules with segments of unequal size ($\chi_1 \neq \chi_2$) at a separation of $\Delta = 2\sigma_0$ using Eqs. (9), (16) and (19) results in a more general expression for the wave number of the chiral nematic phase:

$$\begin{aligned} q &= \frac{10\chi_2\sin(2\alpha)}{\left(\chi_1\frac{\sqrt{1-\chi_2}\sqrt{1-\chi_1\chi_2\cos^2(\alpha)}}{\sqrt{1-\chi_1}\sqrt{1-\chi_1^2}} + 42\chi_2\frac{\cos(2\alpha)-\chi_1\chi_2\cos^4(\alpha)}{1-\chi_1\chi_2\cos^2(\alpha)}\right)\sigma_0} \\ &= \frac{20\chi_2}{\sqrt{1-\chi_2}\sqrt{1-\chi_1\chi_2}\left(\frac{\chi_1}{\sqrt{1-\chi_1}\sqrt{1-\chi_1^2}} + 42\frac{\chi_2}{\sqrt{1-\chi_2}\sqrt{1-\chi_1\chi_2}}\right)\sigma_0}\alpha + \mathrm{O}(\alpha^3) \end{aligned}. \tag{22}$$

This equation reduces to Eq. (21) in case of identical HGO segments $\chi_1 = \chi_2 = \chi$. There are now, however, two parameters governing the macroscopic chiral structure of the phase: one is the dihedral angle between the two segments of the molecule, and the other is the anisotropy parameter (χ_2). The

relation leads one to the conclusion that no twist can take place in the nematic phase of a system of achiral particles corresponding to the limits of either $\alpha = 0$ or $\chi_2 = 0$.

4. Results and discussions

Before presenting the results of the free energy minimizations we demonstrate why twisted orientational ordering is favorable in our system of repulsive chiral rod-like particles. As we have shown in the case of the perfect 2D order approximation, the system tends to reduce the excluded volume as much as possible to maximize the packing entropy (translational entropy) or equivalently minimize the free energy (cf. Eq. (9)). In this case the orientational entropy does not counter this effect because of the approximation of perfect 2D orientational order. In the case of an intramolecular segment-segment separation of $\Delta = 2\sigma_0$ it is very easy to determine the most favorable orientations over the entire range of the excluded body (cf. Eq. (18)). In all three regions the smallest excluded area can be achieved for relative intermolecular orientations (γ) corresponding to parallel interacting HGO segments. This happens at different angles for different pair separations: $\gamma = -\alpha$ for $-3\sigma_0 < z < -\sigma_0$; $\gamma = 0$ for $-\sigma_0 < z < \sigma_0$; and $\gamma = \alpha$ for $\sigma_0 < z < 3\sigma_0$. The minimal excluded area and the corresponding relative molecular orientation as a function of intermolecular distance along the helical axis is shown in Fig. 3. The best linear fit to the discontinuous γ-z function, which is given by $\gamma = q\,z$, goes through the middle point of the sectors (continuous line in Fig. 3b). The slope of the line (wave number) can be easily determined and it is given by $q = \alpha / 2\sigma_0$. Interestingly the numerical minimization of the free energy for very low values of the dihedral angle gives very similar result to that of our simple argument because $q = \frac{20\alpha}{43\sigma_0}$ (cf. Eq. (21)). For smaller segment-segment distances the excluded regions overlap and the expression for the excluded area becomes more complicated. The results of the calculations are presented for more realistic values of

the (dimensionless) intramolecular segment separations of $\Delta^* = \Delta / \sigma_0 = 0.5$, 0.75 and 1 in Fig 4. It can be seen that the excluded area is very sensitive to the imposed helical structure. Both weak and strong twists result in very high values of the excluded area at some particular distances, which give rise to high excluded volume (packing entropy cost). As a result there is an optimum value of the wave number where the integrated area (excluded volume) is at a minimum, which is represented by a continuous curve for the three cases depicted in Fig. 4. The shift of the excluded area regions for the different segment-segment separations can be seen very clearly with increasing Δ^*. At $\Delta^* = 0.5$ the presence of the three regions can be seen only at the strongest twist corresponding to a dimensionless wave number of $q^* = q\sigma_0 = 0.3$, while we get still overlapping regions for $\Delta^* = 1$ but the behavior is closer to that of the totally separated case (cf. Fig. 3.). This feature is due to the fact that only two excluded areas can overlap for $1 < \Delta^* < 2$, while three overlap for $0 < \Delta^* < 1$.

In light of these results we minimize the excluded volume numerically (see Eq. 9.) and determined the relation between the molecular chirality and the macroscopic structure. We start with the computationally simplest case of $\Delta^* = 2$ for which the excluded areas have very simple forms (cf. Eqs. (18) and (19)). For molecules comprising identical segments, the dependence of the equilibrium wave number on the length-to-breath and intramolecular dihedral angle are shown in Fig. 5. The numerical results (Eq. (9)) and the results of the analytical solution (Eq. (21)) are compared to determine the range of validity of the Frank analysis. In Fig. 5 a) we show that for small values of the intramolecular dihedral angle both methods gives the same results, but a noticeable deviation can be seen from $\alpha \sim 5°$. The numerical result corresponds to a linear dependence between the wave number and the dihedral angle, while the analytical solution overestimated the wave number at a given α. It is interesting to note that the first-order Taylor expansion of the analytical solution (Eq. (21)) is coincident with the numerical solution at any angle due to the linear dependence of the wave number with α. From Fig. 5 b) one can see that the wave number does not depend on the length-to-breath ratio which unmasks some of the shortcomings of the Frank analysis. While Eq. (21) leads to a strong κ dependence, its linearization does not suggest a length-to-breath ratio dependence (in

coincidental agreement with the numerical results). At this point we must mention that even if the length-to-breath ratio were not to affect the helical structure it has strong influence on the range of stability range of the chiral nematic (and nematic) phase. For molecules with HGO segments of different length, the wave number is still characterized by a linear dependence with the dihedral angle, but the value now depends on the length-to-breath ratio (see Fig. 6). As one segment is made progressively more spherical ($\kappa_2 \to 1$) the system is seen to twist to a lesser extent. It can be seen in Fig. 6b) that the helical structure does not change substantially on decreasing κ_2 to up to 50% of κ_1, but then it suddenly becomes progressively less twisted with a further decrease of κ_2. Finally the system loses its twisted structure at $\kappa_2 = 1$ where a normal nematic phase is formed. The agreement between the numerical and the analytical calculations is good only for small values of the dihedral angles and length-to-breath ratios of one of the segments. The consequence of these findings is that the Frank analysis can be adequately applied only for molecules which are weakly chiral. Finally we turn to the issue of the effect of the intramolecular segment-segment distance on the helical structure using the approximation of perfect orientational planar order. It is easy to explain that a stronger twist is necessary along the helical axis if the segments are brought closer for a given dihedral angle. The reason for this is that though the molecules have to rotate through a similar angle as before to minimize the excluded area, they have to do so over a shorter distance. No bulk helical structure is possible for $\Delta = 0$, because the molecule is not chiral in this limit. As a result of these opposing effects there must be a system with $0 < \Delta^* < 2\sigma_0$, which will have the most twisted nematic structure. The numerical solution of Eq. (9) supports this expectation and the results of the calculations are presented in Fig. 7 for $\kappa = 5$ and $\kappa = 10$. The maximum value of the wave number is located for values of Δ of about a quarter of the particle diameter, but this depends markedly on the dihedral angle. It is interesting to note that the helical structure exhibits a dependence on the length-to-breath ratio for low values of intramolecular segment-segment separation ($\Delta^* < 1$) so that the molecules with shorter segments are seen to be more twisted than those with longer ones.

In order to assess the adequacy of the perfect order approximation (cf. Eq. (4)) we have performed a bifurcation analysis together with free energy calculations to locate the position of the isotropic-chiral nematic transition and determine the packing fraction dependence of the helical structure. By solving Eqs. (15) and (16) we have determined the bifurcation packing fraction (η_{bif}) and the bifurcation wave number (q_{bif}). With these two quantities the lower bound of stability of the ordered phase and the extent of twist at the ordering transition can be determined. The results of the bifurcation analysis are presented in Fig. 8 for the intramolecular segment separation of $\Delta^* = 1$. The most important feature is that the stability of the chiral nematic phase can be enhanced significantly by increasing the length-to-breath ratio which is a well-known characteristic of the rod-like systems. Another observation is that an increase in the intramolecular segment dihedral angle does not affect the lower boundary of stability of the twisted nematic phase to any significant degree, but it induces a phase transition between an isotropic and a chiral nematic phase for $\alpha > 0$, while an isotropic-nematic transition is observed for $\alpha = 0$. The bifurcation wave number is found to depend linearly on the dihedral angle up to very high angles (corresponding to the correlation $q^*_{bif} = 0.7792\alpha$). The results for the perfect order approximation are in very good agreement with those of the bifurcation analysis, which indicates that the incorporation of orientational degrees of freedom will only have a small effect on the wave number of the twist. In the case of non equal molecular segments ($\kappa_1 \neq \kappa_2$), the range of stability of the isotropic-chiral nematic phase transition is very sensitive to the shape anisotropy as can be seen in Fig. 9 (a). As one of the segments of the HGO molecule becomes more and more spherical, the packing fraction of the isotropic-chiral nematic phase boundary increases, i.e., the region of the chiral nematic phase is shifted to higher density. This is in agreement with the fact that a decrease in the shape anisotropy will lead to a destabilization of the liquid crystalline phase. As it can be seen in Fig. 9 (a) the dihedral angle only has a small effect on the phase boundary as the ordering tendency of both segments does not change with the dihedral angle. In Fig. 9 (b) we show that isotropic-nematic transition takes place only in the achiral limit of $\kappa_2 = 1$ as in this case the bifurcation wave number is zero for any dihedral angle. With increasing shape anisotropy of one of

the segments the wave number of the phase transition increases quickly; this dependence becomes very weak as the anisotropy of the segment reaches a certain value. This occurs roughly for a shape anisotropy at which a stable nematic phase would form for a system of HGO particles. Furthermore, it is clear from Fig. 9 (b) that the results obtained with the perfect order approximation (dashed curves) are very close to those for the freely rotating case (continuous curves), i.e,. the bifurcation wave number is not sensitive to the approximation used for the orientational degrees of freedom.

Up to this point we have not performed a thorough stability analysis of the chiral nematic phase with respect to the isotropic and nematic phases. To determine which phase is the most stable at given packing fraction the free energies of all phases are determined by solving Eq. (14). It is found in all cases that the free energy of the chiral nematic phase is the lowest for densities above the bifurcation point as long as the molecules are chiral. This is demonstrated with two examples for systems differing only in the intramolecular segment dihedral angle in Fig. 10. It can be seen that for the molecules characterised by a weaker microscopic chirality, the difference between the free energies of the nematic and chiral nematic phases is very small up to a very high nematic order of $\left(S = \int_0^{2\pi} h(\varphi)\cos(2\varphi)d\varphi \right) = 0.9$, and the bifurcation to the ordered phase take place at almost the same packing fraction. However, the second system with a greater molecular chirality behaves in a different way, as the nematic phase is seen to bifurcate from the isotropic phase at a significantly higher packing fraction than that of chiral nematic phase; differences in the free energies are significant even close to the isotropic-nematic bifurcation point. The reason for this is due to the large dihedral angle since the (artificial) ordering of the molecules with their different segments in one direction gives rise to a large cost in terms of excluded volume as the arrangement with different segments in opposite directions would be preferred. Changing the helical direction of the two molecular segments from a parallel arrangement will reduce the excluded volume and stabilize the ordered phase at lower packing fractions. This is also the reason why the bifurcation packing fraction of the isotropic-chiral nematic phase is not very sensitive to the dihedral angle. In all cases the isotropic-chiral nematic phase transition is found to be second order as the order parameter goes to

zero continuously at the bifurcation point (see the inset of Fig. 10), and apart from at the bifurcation point no common tangent can be constructed between the free energy densities of the isotropic and chiral nematic phases. As far as the helical structure of the bulk chiral nematic phase is concerned, the wave number is plotted as a function of the packing fraction in Fig. 11 for both systems. The strongly chiral system is about three times more twisted than the weakly chiral system. The systems do not appear to exhibit a strong dependence on the packing fraction; a slight dependence can be seen in the inset in which we show the behaviour for a dihedral angle of $\alpha = 30°$ where starting from the bifurcation point the wave number first decreases, exhibits a minimum at around $\eta = 0.18$, and then increases with increasing packing fraction. This tendency can also be observed for weak chiralities ($\alpha = 10°$), but the change in the wave number is even less marked. This kind of density dependence has not been observed in hard-core models of sterically chiral molecules such as twisted ellipsoid [51], threaded hard rod [36,44] or corkscrew [60] models. To assess the adequacy of the perfect order approximation, the wave number obtained from Eq. (9) are also shown in Fig. 11. As can be seen the wave number is found to be constant at any density and is very close to the wave number determined for the freely rotating case. Finally in Fig. 12 we present the effect of varying the segment anisotropy on the order parameter-packing fraction and wave number-packing fraction dependencies obtained from the minimization of the free energy (cf. Eq. (14)). As before the free energy of the chiral nematic phase is always less than that of nematic phase if the molecule is chiral. The order parameter curves suggest that decreasing the shape anisotropy of one of the segments has an effect not only on the location of the bifurcation point but also on the degree of ordering at a given density, as the molecules are less anisotropic are less ordered. The wave number is affected by the value of κ_2 as it decreases with increasing packing fraction. There is a linear decrease in the wave number with density, but the slope increases with decreasing shape anisotropy (see lower panel of the Fig. 12). It can also be seen that the perfect planar order leads to an underestimate in the wave number with decreasing shape anisotropy of one of the segments and it does not take into account the density dependence.

5. Conclusion

We have considered a simple steric molecular model for chiral liquid crystals. The representation is an extension of hard-body models of the nematic phase constructed by fusing two uniaxial hard bodies with a relative twist between the long axes of the segments. The hard Gaussian overlap (HGO) potential is used to represent the interaction between the segments of the chiral molecules to isolate the link between the shape chirality and the bulk properties of the chiral nematic phase. The electrostatic and other dispersive interactions are not included in the model to avoid complicating the analysis due to collective effects of the different types of chiralities. The Parsons-Lee extension of the Onsager theory is used to describe the isotropic, nematic, and chiral nematic (cholesteric) phases of system. To simplify the calculations and at the same time to capture the key physical factors that influence the ordering phenomena we have used several approximations for the orientational distribution function. We have assumed that the long axes of the HGO segments that make up the chiral molecules are constrained to stay in the plane normal to the helical axis. Moreover no internal rotation is allowed around the symmetry axis of the molecule. In this way the molecules are allowed to rotate freely only in the direction normal to the helical axis and the vector connecting the centres the two molecular HGO segments is always parallel to the helical axis. Two types of single particle orientational distribution functions have been introduced to account for the orientational ordering and helical structure inherent in chiral liquid crystals. In the simplest approximation the particles are perfectly aligned in the planes but they twist in a linear fashion in the direction of helical axis. In the second approximation a trial function has been introduced for the representation of the orientational distribution function which is able to describe isotropic, nematic, and chiral nematic phases. Moreover it gives the exact bifurcation densities and wave numbers of the

orientational ordering transitions. Both approximations have proved to be very useful in the determination of the structure and stability of the phases. The first approximation allows one to obtain analytical equations which relate the wave number of the twisted nematic phase and the molecular properties such as the intramolecular segment dihedral angle and length-to-breath ratios. The second approximation gives rise to two coupled equations for the wave number and variational parameter which makes it possible to determine the phase boundaries and the order parameter of the nematic phases.

From our findings it is clear that the intramolecular dihedral angle (between the two HGO segments) is the only chiral parameter which determines the handedness of the molecules and the bulk phases; the two other chiral parameters, the asymmetry in the shape anisotropy of the HGO segments and the intramolecular distance between the two HGO segments, only have an effect on the wave number of the twisted phase. The wave number is found to depend linearly on the intramolecular segment dihedral angle in all cases, i.e., the handedness of the phase is determined by the sign of the dihedral angle and no twist takes place in the achiral limit of $\alpha = 0$. Decreasing the shape anisotropy of one of the molecular segments does not effect the helical structure substantially up to a weakly anisotropic particle shape, and then the wave number rapidly drops to zero (untwisted structure) in the limit of an achiral shape ($\kappa_2 = 0$). The relation between macroscopic twist and the intramolecular segment-segment distance is more complicated between the achiral ($\Delta = 0$) and the larger separation limits, but in all cases the twist reaches a maximum value at a segment-segment separation close to a quarter of the segment diameter. The free energy calculations reveal that the isotropic-nematic transition is always metastable with respect to isotropic-chiral nematic transition for chiral molecules, the latter only being stable in the achiral limits. Interestingly the pitch depends very weakly on density for molecules with identical HGO segments, but it increases linearly with the density as the shape anisotropy of the one of the segments is decreased. It is also shown that the difference between the numerically obtained free energy and the second order Frank free energy

increases with increasing molecular chirality to such an extent that the Frank expression for the wave number cannot be applied for a molecular twist above $\alpha \sim 5°$.

The effect of higher order (cosine) terms in the orientational distribution function and the case of complete 3D rotational degrees of freedom are not considered in our current work. It would be desirable to see unambiguously the packing fraction dependence of the helical wave number. In addition it would of interest to explore the impact of other types of steric chiralities such as single and double helices, on the macroscopic chirality. In this way it would be possible to determine the separate roles of steric and electrostatic chiralities in the helical structure of chiral macromolecules such as DNA, or viral systems, where both types of chiralities are present. We leave this for future work.

Acknowledgements

We are both grateful to the Royal Society for the award of an International Short Visit grant which has facilitated our collaborative work. Additional funding to the Molecular Systems Engineering Group from the Engineering and Physical Sciences Research Council (EPSRC) of the UK (grants GR/T17595, GR/N35991, GR/R09497, and EP/E016340), the Joint Research Equipment Initiative (JREI) (GR/M94427), and the Royal Society-Wolfson Foundation refurbishment grant is also acknowledged.

References

[1] S. Chandrasekhar, *Liquid Crystals*, 2nd ed. (Cambridge University Press, Cambridge, 1992).

[2] P.-G. de Gennes and J. Prost, *The Physics of Liquid Crystals*, 2nd ed. (Oxford University Press, Oxford, 1993).

[3] A. B. Harris, R. D. Kamien, and T. C. Lubensky, Phys. Rev. Lett., 78, 1476 (1997).

[4] T. C. Lubensky, A. B. Harris, R. D. Kamien, and G. Yan, Ferroelectrics, **212**, 1 (1998).

[5] A. B. Harris, R. D. Kamien, and T. C. Lubensky, Rev. Mod. Phys., **71**, 1745 (1999).

[6] Z. Dogic, S. Fraden, Langmuir, 16, 7820 (2000).

[7] E. Grelet, S. Fraden, Phys. Rev. Lett., **90**, 198302 (2003).

[8] Z. Dogic, S. Fraden, Curr. Opinion Coll. Inter. Sci., **11**, 47 (2006).

[9] M. Born, Sits. Phys. Maths., **25**, 614 (1916).

[10] M. Born, Ann. Phys. **55**, 221 (1918).

[11] W. Maier and A. Saupe, Z. Naturforsch., **13a**, 564 (1958).

[12] W. Maier and A. Saupe, Z. Naturforsch., **14a**, 882 (1959).

[13] W. Maier and A. Saupe, Z. Naturforsch., **15a**, 287 (1960).

[14] L. D. Landau, Phys. Z Sowjetunion, **11**, 26 (1937); reprinted in *Collected Papers of L.D. Landau* , ed. D. ter Haar (Pergamon Press, Oxford, 1965), pp. 193–216.

[15] P.-J. de Gennes, Phys. Lett. A, **30**, 454 (1969).

[16] P.-J. de Gennes, Solid State Comm., **10**, 753 (1972).

[17] L. Onsager, Phys. Rev., **62**, 558 (1942).

[18] L. Onsager, Ann. N.Y. Acad. Sci., **51**, 627 (1949).

[19] D. Frenkel and R. Eppenga, Phys. Rev. Lett., **49**, 1089 (1982).

[20] R. Eppenga and D. Frenkel, Mol. Phys. **52**, 1303 (1984).

[21] D. Frenkel and B. M. Mulder, Mol. Phys. **55**, 1171 (1985).

[22] A. Samborski, G. T. Evans, C. P. Mason, and M. P. Allen, Mol. Phys. **81**, 263 (1994).

[23] D. Frenkel, J. Phys. Chem., **91**, 4912 (1987).

[24] D. Frenkel, H. N. W. Lekkerkerker, and A. Stroobants, Nature, **332**, 822 (1988).

[25] S. C. McGrother, D. C. Williamson, and G. Jackson, J. Chem. Phys., **104**, 6755 (1996).

[26] P. G. Bolhuis and D. Frenkel, J. Chem. Phys., **106**, 666 (1997).

[27] D. C. Williamson and G. Jackson, J. Chem. Phys., **108**, 10294 (1998).

[28] S.C. McGrother, A. Gil-Villegas, and G. Jackson, J. Phys.: Condens. Matter, **8**, 9649 (1996).

[29] A. Gil-Villegas, S. C. McGrother, and G. Jackson, Chem. Phys. Lett., **269**, 441 (1997).

[30] A. Gil-Villegas, S. C. McGrother, and G. Jackson, Mol. Phys., **92**, 723 (1997).

[31] S. C. McGrother, A. Gil-Villegas, and G. Jackson, Mol. Phys., **95**, 657 (1998).

[32] J. S. van Duijneveldt, A. Gil-Villegas, G. Jackson, and M. P. Allen, J. Chem. Phys. **112**, 9092

(2000).

[33] W. J. A. Goossens, Mol. Cryst. Liquid Cryst., **12**, 237 (1970).

[34] R. G. Priest and T. C. Lubensky, Phys. Rev. A, **9**, 893 (1974).

[35] A. Wulf, J. Chem. Phys. **60**, 3994 (1974).

[36] J. P. Straley, Phys. Rev. A, **14**, 1835 (1976).

[37] B. W. van der Meer, G. Vertogen, A. J. Dekker, and J. G. J. Ypma, J. Chem. Phys., **65**, 3935 (1976).

[38] Y. R. Lin-Liu, Y. M. Shih, and C. W. Woo, Phys. Rev. A, **15**, 2550 (1977).

[39] H. Kimura, M. Hosino, and H. Nakano, J. Phys. Soc. Jpn., **51**, 1584 (1982).

[40] Y. R. Lin-Liu and M. A. Lee, Phys. Rev. A, **28**, 2580 (1983).

[41] A. N. Zakhlevnykh and M. I. Shliomis, Zh. Eks. Teo. Fiz., **86**, 1309 (1984).

[42] M. Nakagawa, Mol. Cryst. Liq. Cryst., **130**, 349 (1985).

[43] M. A. Osipov, Chem. Phys., **96**, 259 (1985).

[44] T. Odijk, J. Phys. Chem., **91**, 6060 (1987).

[45] W. J. A. Goossens, Phys. Rev. A, **35**, 1843 (1987).

[46] M. A. Osipov, Khi. Fiz., **6**, 1312 (1987).

[47] M. A. Osipov, Nuovo Cimento Soc Ita. Fis D., **10**, 1249 (1988).

[48] M. Nakagawa, Liq. Cryst., **3**, 63 (1988).

[49] W. J. A. Goossens, Phys. Rev. A, **39**, 4888 (1989).

[50] W. J. A. Goossens, Phys. Rev. A, **40**, 4019 (1989).

[51] G.T. Evans, Mol. Phys., **77**, 969 (1992).

[52] L. Varichon and A. Tenbosch, Macromolecules, **25**, 3812 (1992).

[53] L. Varichon and A. Tenbosch, Liq. Cryst., **14**, 1635 (1993).

[54] M. P. Allen, Phys. Rev. E, **47**, 4611 (1993).

[55] M. P. Allen and A. J. Masters, Mol. Phys., **79**, 277 (1993).

[56] R. Memmer, H.-G. Kuball, and A. Schönhofer, Liq. Cryst., **15**, 345 (1993).

[57] T. Sato, Y. Sato, Y. Umemura, A. Teramoto, Y. Nagamura, J. Wagner, D. Weng, Y. Okamoto, K. Hatada, and M. M. Green, Macromolecules, **26**, 4551 (1993).

[58] M.A. Osipov, B.T. Pickup, and D.A. Dunmur, Mol. Phys., **84**, 6 (1995); ibid. **84**, 1193 (1995).

[59] T. Koda and H. Kimura, J. Phys. Soc. Jpn., **65**, 2880 (1996).

[60] R. A. Pelcovits, Liq. Cryst., **21**, 361 (1996).

[61] R. Memmer, H.-G. Kuball, and A. Schönhofer, Mol. Phys., **89**, 1633 (1996).

[62] A. Ferrarini, G. J. Moro, and P. L. Nordio, Phys. Rev. E, **53**, 681 (1996).

[63] P. J. Camp, Mol. Phys., **91**, 381 (1997).

[64] J. Saha and M. Saha, Mol. Sim., **19**, 227 (1997).

[65] A. A. Kornyshev and S. Leikin, J. Chem. Phys., **107**, 3656 (1997).

[66] T. Sato, J. Nakamura, A. Teramoto, and M. M. Green, Macromolecules **31**, 1398 (1998).

[67] R. Berardi, H.-G. Kuball, R. Memmer, and C. Zannoni, J. Chem. Soc. Faraday Trans., **94**, 1229 (1998).

[68] R. Memmer and F. Janssen, J. Chem. Soc. Faraday Trans., **94**, 267 (1998).

[69] R. Memmer and F. Janssen, Liq. Cryst., **24**, 805 (1998).

[70] R. Memmer, Ber. Buns. Ges. - Phys. Chem. Chem. Phys., **102**, 1002 (1998).

[71] L. Hu, Y. Jiang, T. D. Lee, and R. Tao, Phys. Rev. E, **57**, 4289 (1998).

[72] R. Memmer, Liq. Cryst., **27**, 533 (2000).

[73] A. V. Emelyanenko, M. A. Osipov, and D. A. Dunmur, Phys. Rev. E, **62**, 2340 (2000).

[74] A. A. Kornyshev and S. Leikin, Phys. Rev. Lett., **84**, 2537 (2000).

[75] A. A. Kornyshev and S. Leikin, Phys. Rev. E, **62**, 2576 (2000).

[76] M. A. Osipov and H.-G. Kuball, Eur. Phys. J. E, 5, 589 (2001).

[77] R. Memmer, J. Chem. Phys., **114**, 8210 (2001).

[78] J. Xu, R. L. B. Selinger, J. V. Selinger, and R. Shashidhar, J. Chem. Phys., **115**, 4333 (2001).

[79] M. P. Allen and A. J. Masters, Mater. Chem., **11**, 2678 (2001).

[80] G. Germano, M. P. Allen, and A. J. Masters, J. Chem. Phys., **116**, 9422 (2002).

[81] S. J. Johnston, R. J. Low, and M. P. Neal, Phys. Rev. E, **65**, 051706 (2002).

[82] A. A. Kornyshev, S. Leikin, and S. V. Malinin, Eur. Phys. J. E, **7**, 83 (2002).

[83] Z. D. Zhang, Z. G. Li, and J. L. Liu, Mod. Phys. Lett. B, **16**, 721 (2002).

[84] A. Kapanowski, Z. Naturforsch. A, **57**, 105 (2002).

[85] A. V. Emelyanenko, Phys. Rev. E, **67**, 031704 (2003).

[86] S. Varga and G. Jackson, Chem. Phys. Lett., **377**, 6 (2003).

[87] M. P. Neal, M. Solymosi, M. R. Wilson, and D. J. Earl, J. Chem. Phys., **119**, 3567 (2003).

[88] R. Berardi, M. Cecchini, and C. Zannoni, J. Chem. Phys., **119**, 9933 (2003).

[89] Y. Huh, and N. M. Cann, J. Chem. Phys., **121**, 10299 (2004).

[90] F. Tombolato and A. Ferrarini, J. Chem. Phys., **122**, 054908 (2005).

[91] F. Tombolato, A. Ferrarini, and E. Grelet, Phys. Rev. Lett., **96**, 258302 (2006).

[92] H. Kamberaj, R. J. Low, and M. P. Neal, Mol. Phys., **104**, 335 (2006).

[93] S. Varga and G. Jackson, Mol. Phys., **104**, 3681 (2006).

[94] H. H. Wensink and G. Jackson, J. Chem. Phys., **130**, 234911 (2009).

[95] E. O. Yewande, M. P. Neal, R. J. Low, Mol. Phys., **107**, 281 (2009).

[96] S. Dhakal and J. V. Selinger, to be published (2011).

[97] H. H. Wensink and G. Jackson, J. Phys.: Condens. Matter, in press (2011).

[98] J. D. Parsons, Phys. Rev. A, **19**, 1225 (1979).

[99] S. D. Lee, J. Chem. Phys., **97**, 4972 (1987).

[100] J. G. Gay and B. J. Berne, J. Chem. Phys., **74**, 3316 (1981).

[101] G. J. Vroege and H. N. W. Lekkerkerker, Rep. Prog. Phys., **55**, 1241 (1992).

[102] M. Franco-Melgar, A. J. Haslam, and G. Jackson, Mol. Phys., **106**, 649 (2008).

[103] A. Malijevský , G. Jackson, and S. Varga, J. Chem. Phys., **129**, 144504 (2008).

[104] M. Franco-Melgar, A. J. Haslam, and G. Jackson, Mol. Phys., **107**, 2329 (2009).

[105] R. Evans, Adv. Phys., **28**, 143 (1979).

[106] R. Evans, *Density functionals in the theory of nonuniform fluids*, in *Fundamentals of Inhomogeneous Fluids*, Edited by D. Henderson (Dekker, New York, 1992).

[107] M. M. Telo da Gama, P. Tarazona, M. P. Allen, and R. Evans, Mol. Phys., **71**, 801 (1990).

[108] R. van Roij, M. Dijkstra, and R. Evans, Euro. Phys. Lett., **49**, 350 (2000).

[109] M. Dijkstra, R. van Roij, and R. Evans, Phys. Rev. E, **63**, 051703 (2001).

[110] B. J. Berne and P. Pechukas, J. Chem. Phys., **56**, 4213 (1972).

[111] V. R. Bhethanabotla and W. A. Steele, Mol. Phys., **60**, 249 (1987).

[112] P. Padilla and E. Velasco, J. Chem. Phys., **106**, 10299 (1997).

[113] D. J. Cleaver, C. M. Care, M. P. Allen, and M. P. Neal, Phys. Rev. E, **54**, 559 (1996).

[114] C. B. Stanley, H. Hong, and H. H. Strey, Biophys. J., **89**, 2552 (2005).

Figures

Figure 1)

Top view and side views of a chiral two-segment HGO particle. The intramolecular segment dihedral angle is $\alpha = 30°$, the segment length-to-breadth ratio is $\kappa = 3$, and the intramolecular segment-segment separation is $\Delta = \sigma_0$, where σ_0 is the segment breadth.

Figure 2)

Side views of four achiral two-site HGO particles with α the intramolecular segment dihedral angle, κ the segment length-to-breadth ratio, and Δ the intramolecular segment-segment separation: a) $\alpha = 90°$ for $\kappa = 3$ and $\Delta = \sigma_0$; b) $\alpha = 0°$ for $\kappa = 3$ and $\Delta = \sigma_0$; c) $\alpha = 30°$ for $\kappa = 3$ and $\Delta = 0$; and d) $\alpha = 30°$ for $\kappa_2 = 1$, $\kappa_1 = 3$, and $\Delta = \sigma_0$, where σ_0 is the segment breadth.

Figure 3)

Excluded area of the most favorable configuration for the chiral two-segment HGO particle (with α the intramolecular segment dihedral angle, κ the segment length-to-breadth ratio, and Δ the intramolecular segment-segment separation) and the corresponding twist angle as a function of distance along the helical axis chosen as a z axis for $\alpha = 10°$, $\kappa = 10$ and $\Delta^* = 2$. In lower panel the horizontal dashed segments indicate the most favourable twist angles, while the continuous line is a guide to the eye which is given by $\gamma = \frac{\alpha}{2} z^*$. The excluded area and the distances are in dimensionless unit: $A^*_{exc} = A_{exc} / \sigma_0^2$, $\Delta^* = \Delta / \sigma_0$ and $z^* = z / \sigma_0$, where σ_0 is the segment breadth.

Figure 4)

Excluded area of a chiral two-segment HGO particle (with α the intramolecular segment dihedral angle, κ the segment length-to-breadth ratio, and Δ the intramolecular segment-segment separation) as a function of distance along the direction of helical axis chosen as a z axis for different value of wave number (q) for $\alpha = 10°$ and $\kappa = 10$: a) q^* = 0.1 (dashed), 0.2 (continuous) and 0.3 (short dashed) for $\Delta^* = 0.5$ b) q^*=0.05 (dashed), 0.2 (continuous) and 0.3 (short dashed) for Δ^*=0.75, c) q^*=0.05 (dashed), 0.15 (continuous) and 0.25 (short dashed) for Δ^*=1. The excluded area, centre-to-centre segment separation, distance along the helical axis, and wave number are in dimensionless units: $A^*_{exc} = A_{exc}/\sigma_0^2$, $\Delta^* = \Delta/\sigma_0$, $z^* = z/\sigma_0$, and $q^* = q\sigma_0$, where σ_0 is the segment breadth.

Figure 5)

The wave number $q = 2\pi/P$ (inverse pitch) of a system of chiral two-segment HGO particles as a function of: a) the intramolecular segment dihedral angle α; and b) the segment length-to-breath ratio κ are shown in the case of perfect 2D order for an intramolecular segment-segment separation of $\Delta^* = 2$. The continuous curves represent the results of numerical calculations (cf. Eq. (9)), while the dashed curves the results of the Frank analysis (cf. Eq. (21)). The numerically obtained pitches are depicted in the insets. The wave number and the pitch are in dimensionless units: $q^* = q\sigma_0$, $P^* = P/\sigma_0$, where σ_0 is the segment breadth.

Figure 6)

The effect of varying the length-to-breath ratio κ_2 of a segment for a system of chiral two-segment HGO particles (with α the intramolecular segment dihedral angle, and Δ the intramolecular segment-segment separation) on the helical period of the nematic nematic phase. a) The wave number $q = 2\pi/P$ (inverse pitch) is plotted as a function dihedral angle α for κ_1 = 10 and $\Delta^* = 2$. The values of κ_2 are indicated on the figure. b) The dependence of the wave number on the length-to-breath ratio κ_2 for some values of dihedral angle. The continuous curves correspond to numerically

obtained using Eq. (9), while the dashed curves are the results of the Frank analysis (cf. Eq. (22). In the insets we show the dependence of the pitch $P^* = P/\sigma_0$, where σ_0 is the segment breadth, as a function of the dihedral angle and κ_2 obtained with Eq. (9).

Figure 7)

The effect of varying the intramolecular segment-segment distance Δ of a system of chiral two-segment HGO particles (with α the intramolecular segment dihedral angle, and κ the segment length-to-breath ratio) on the helical structure of the chiral nematic phase in the case of dihedral angles of $\alpha = 5°$, 10° and 20° for different values of molecular elongations: a) $\kappa = 5$ and b) $\kappa = 10$. The curves are the results obtained with Eq. (9). In the inset we show the corresponding pitch $P^* = P/\sigma_0$ and a function of

Figure 8)

Dihedral angle α dependence of the bifurcation packing fraction η of the isotropic-chiral nematic phase transition for a chiral two-segment HGO system (with α the intramolecular segment dihedral angle, κ the segment length-to-breath ratio, and Δ the intramolecular segment-segment separation) with $\Delta^* = \Delta/\sigma_0 = 1$, where σ_0 is the segment breadth. The values of the aspect ratios are indicated on the curves. The results are obtained using Eqs. (15) and (16).

Figure 9)

The effect of varying the anisotropy of one of the segments (κ_2) on the bifurcation packing fraction η and wave number q of the isotropic-chiral nematic phase transition for a chiral two-segment HGO system (with α the intramolecular segment dihedral angle, κ the segment length-to-breadth ratio, and Δ the intramolecular segment-segment separation) with $\Delta^* = 2$ and $\kappa_1 = 5$. Values of the dihedral angle of $\alpha =$ 5°, 10°, and 20° are examined (from bottom to top in the figures). In a) the curves for

$\alpha = 5°$ and $\alpha = 10°$ cannot be distinguished at the current resolution. The curves are obtained with Eqs. (15) and (16). The dashed curves in b) represent the solutions of perfect order approximation (cf. Eq. 22). Dimensionless units are employed: $\Delta^* = \Delta / \sigma_0$ and $q^* = q\sigma_0$, where σ_0 is the segment breadth.

Figure 10)

The free energy density ($f^* = \beta F v_0 / V$) as a function of packing fraction η of the three different phases for a chiral two-segment HGO system (with α the intramolecular segment dihedral angle, κ the segment length-to-breadth ratio, and Δ the intramolecular segment-segment separation) with $\kappa = 10$ and $\Delta^* = \Delta / \sigma_0 = 1$, where σ_0 is the segment breadth. The values of the dihedral angle are $\alpha = 10°$ in a) and $\alpha = 30°$ in b). In the inset we represent the order parameter $\left(S = \int_0^{2\pi} h(\varphi)\cos(2\varphi)d\varphi \right)$ as a function of packing fraction for nematic and chiral nematic phases. The curves are the results of the free energy minimization of Eq. (14).

Figure 11)

The packing fraction η dependence of the wave number q of the chiral nematic phase for a chiral two-segment HGO system (with α the intramolecular segment dihedral angle, κ the segment length-to-breadth ratio, and Δ the intramolecular segment-segment separation) with $\kappa = 10$, $\Delta^* = 1$, $\alpha = 10°$ and $\kappa = 10$, $\Delta^* = 1$, $\alpha = 30°$. The continuous curves represent the results of the free energy minimization of Eq. (14), while the dashed curves are the results of Eq. (9). In the inset we highlight the density dependence of the wave number q for the system of $\kappa = 10$, $\Delta^* = 1$, $\alpha = 30°$. Dimensionless units are employed: $\Delta^* = \Delta / \sigma_0$ and $q^* = q\sigma_0$, where σ_0 is the segment breadth.

Figure 12)

The packing fraction η dependence of the order parameter $\left(S = \int_0^{2\pi} h(\varphi)\cos(2\varphi)d\varphi \right)$ and the wave number q of the twisted nematic phase for a chiral two-segment HGO system (with α the intramolecular segment dihedral angle, κ the segment length-to-breadth ratio, and Δ the intramolecular segment-segment separation) with $\kappa_1 = 5$, $\Delta^* = 2$, $\alpha = 30°$ for a varying anisotropy of the second segment κ_2. The curves are the results of the free energy minimization of Eq. (14), while the dashed curves are the results obtained with Eq. (9). The values of the segment anisotropy are κ_2 = 5, 3, 2, and 1.5 from left to right in a), and from top to bottom in b). Dimensionless units are employed: $\Delta^* = \Delta / \sigma_0$ and $q^* = q\sigma_0$, where σ_0 is the segment breadth.

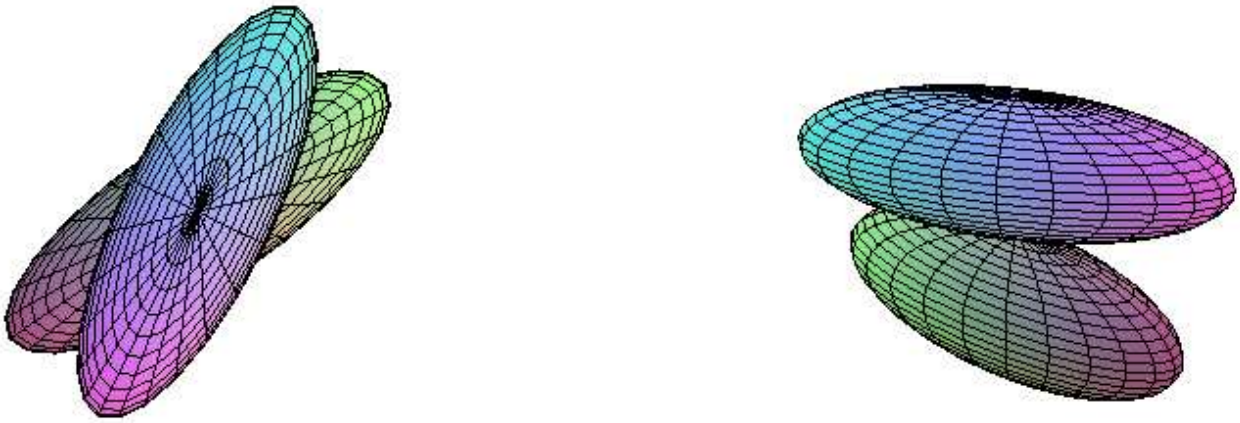

Figure 1.

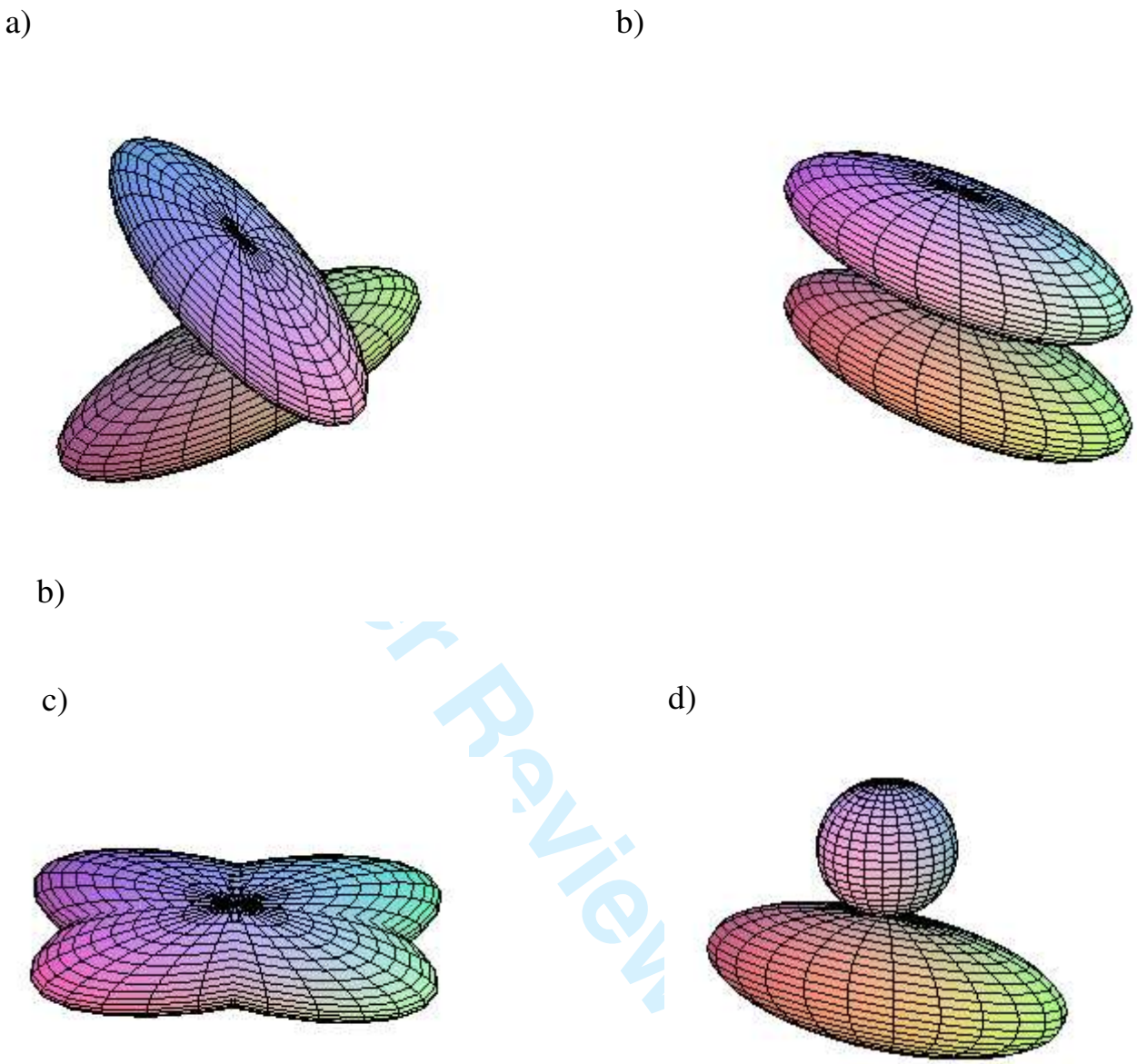

Figure 2.

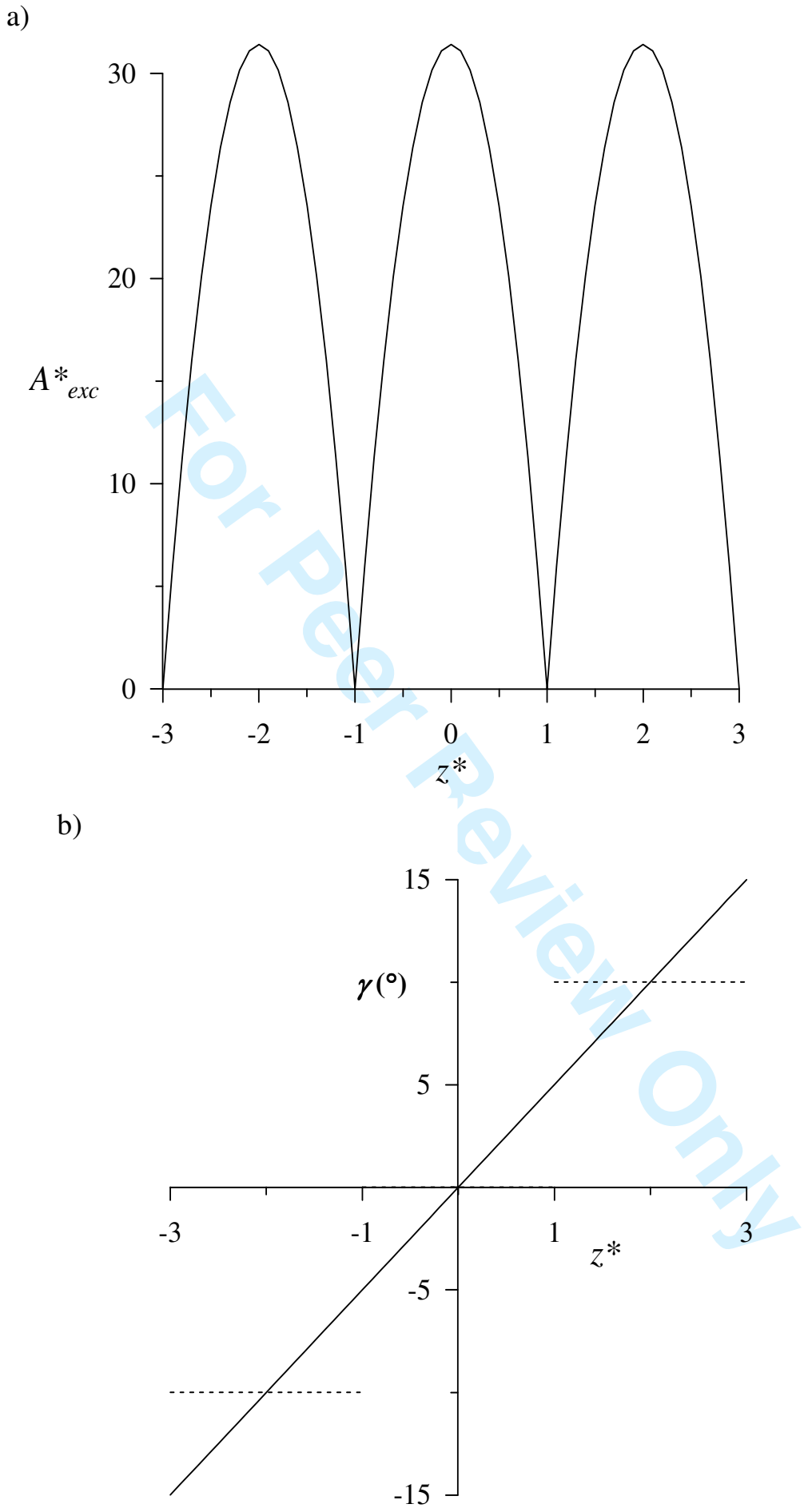

Figure 3

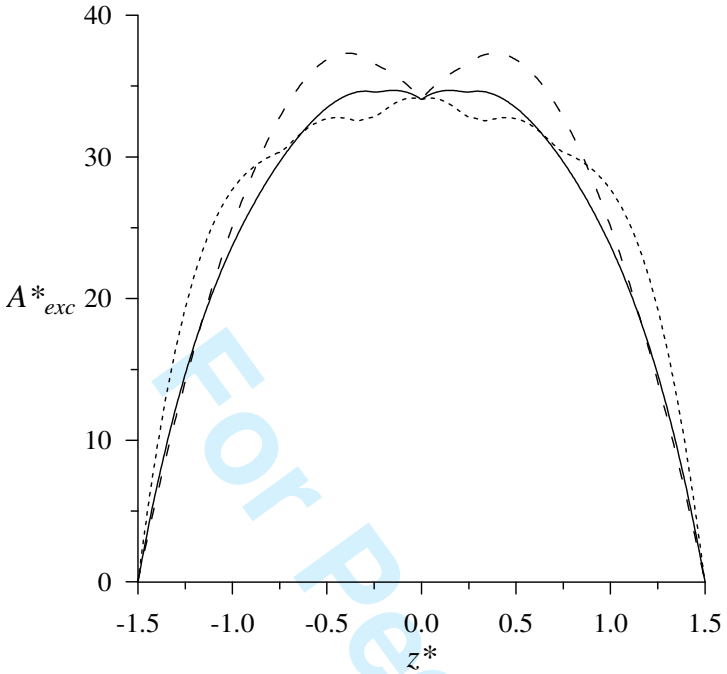

Figure 4 a)

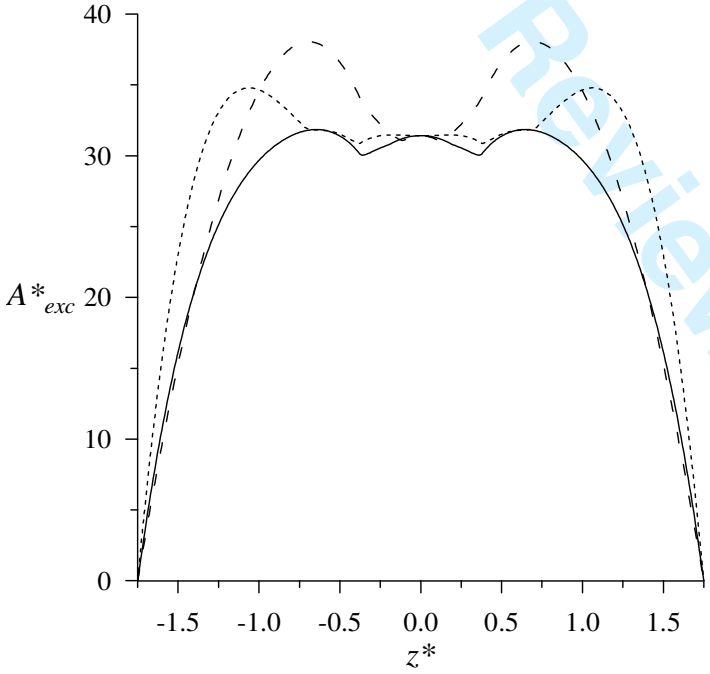

Figure 4 b)

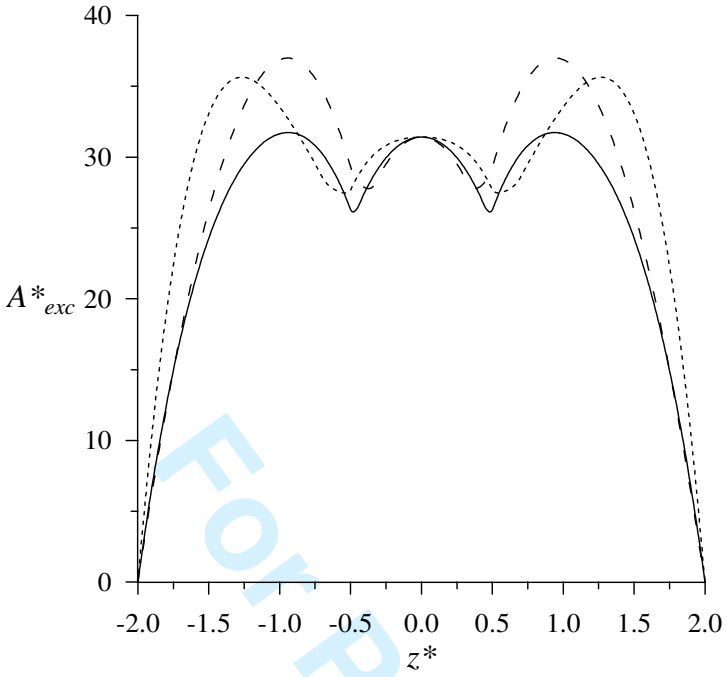

Figure 4 c)

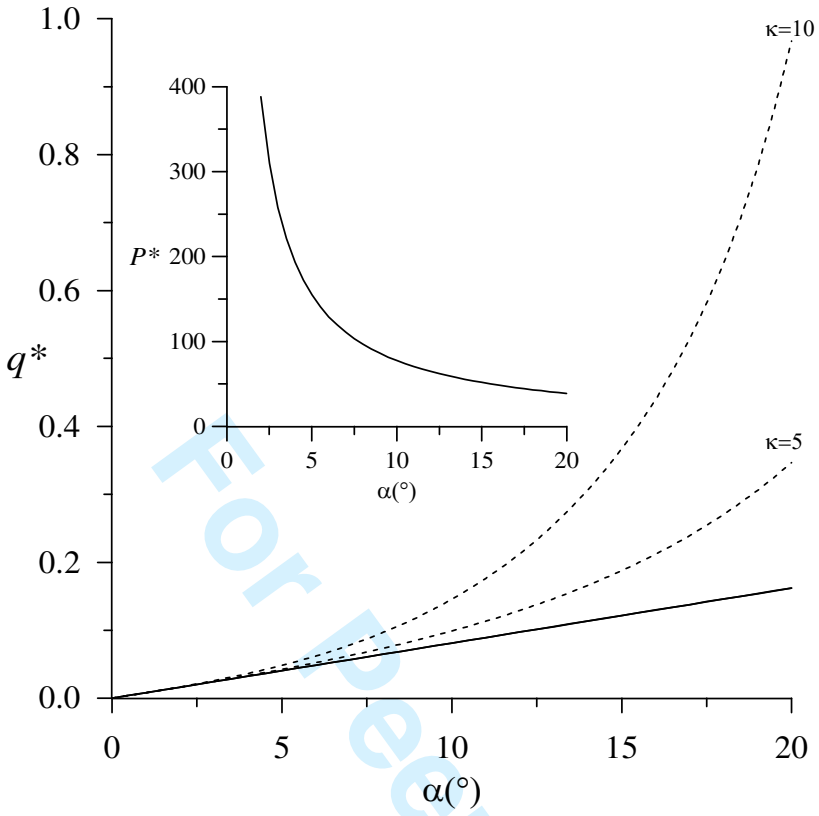

Figure 5 a)

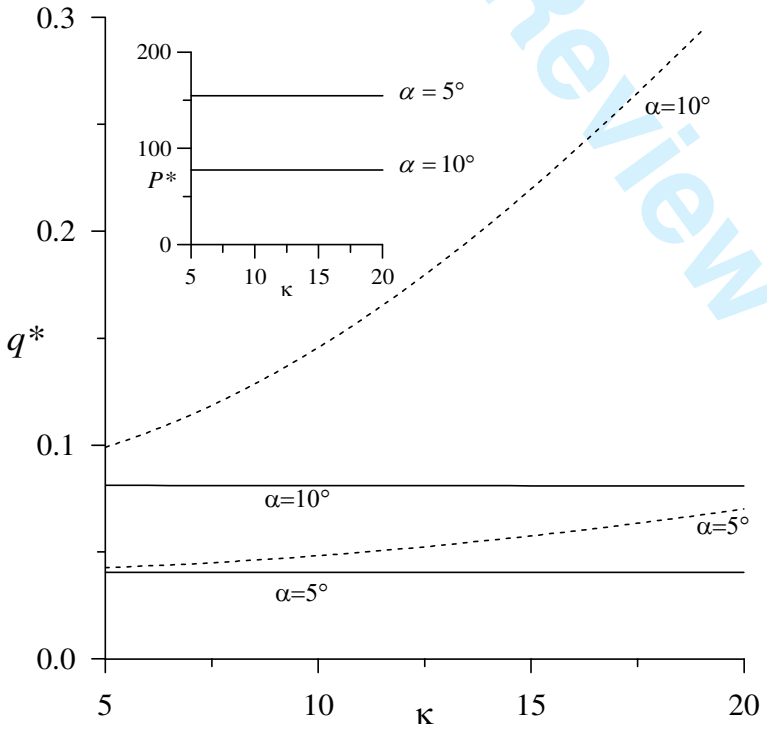

Figure 5 b)

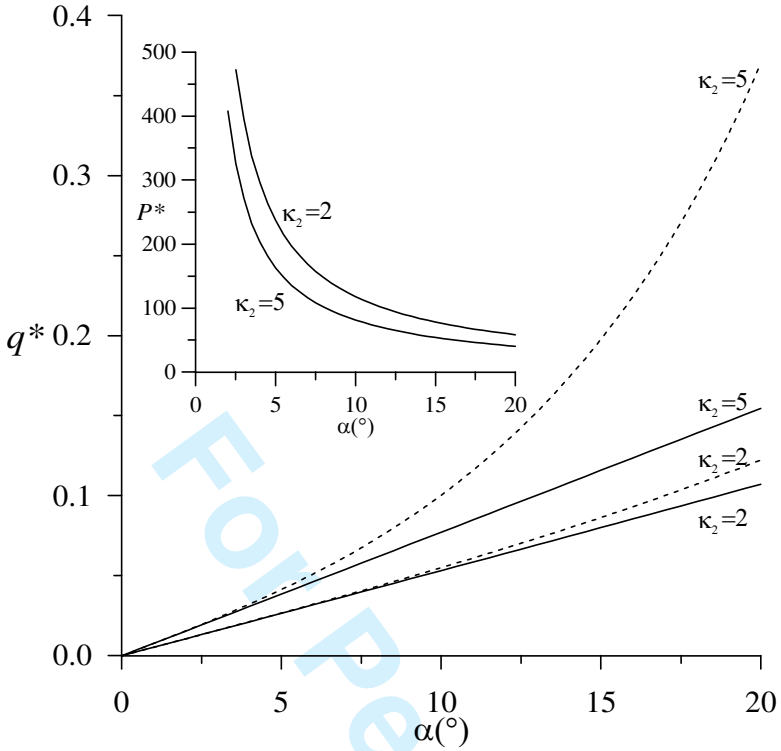

Figure 6 a)

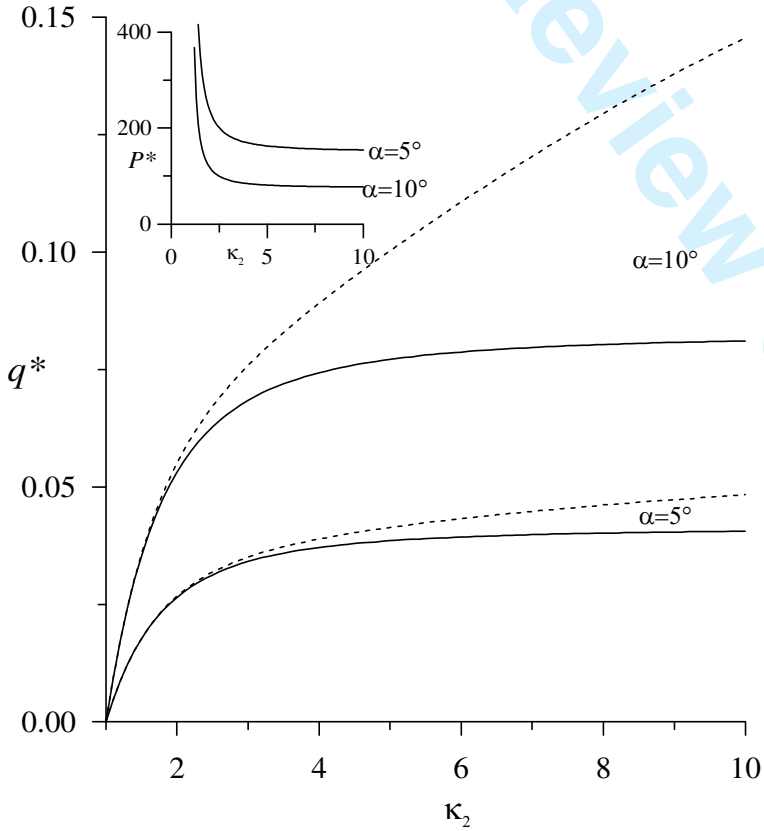

Figure 6 b)

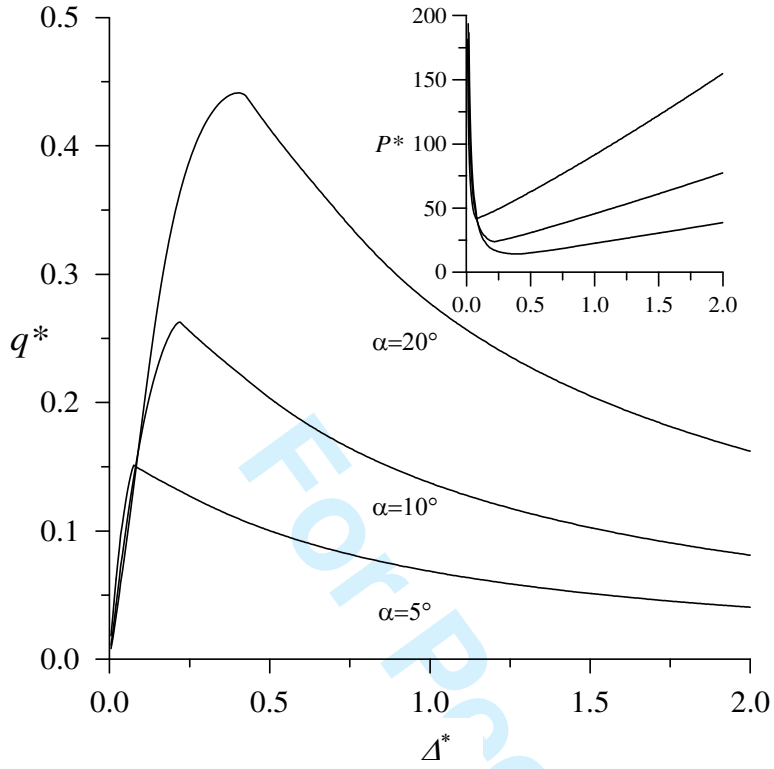

Figure 7 a)

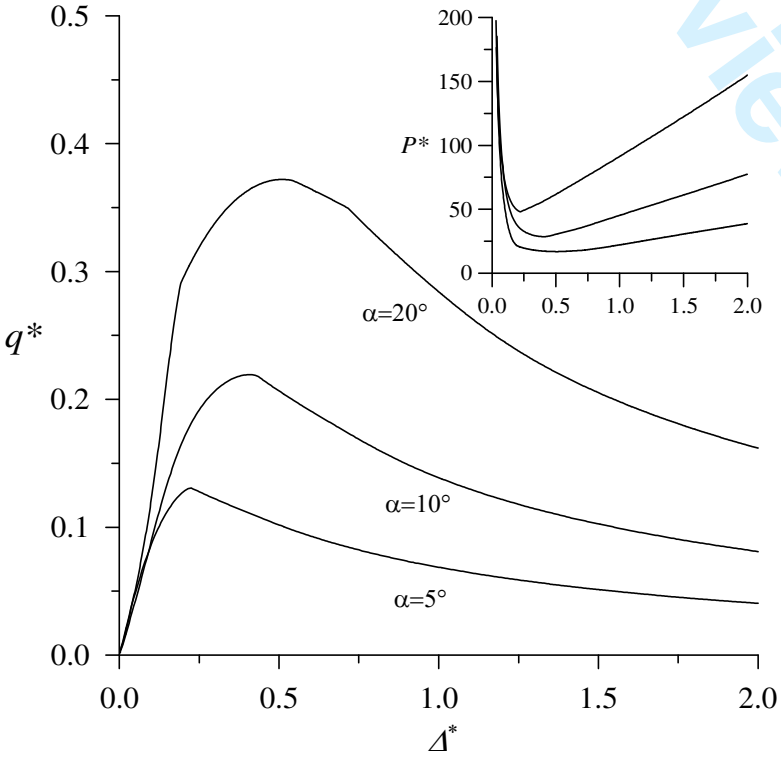

Figure 7 b)

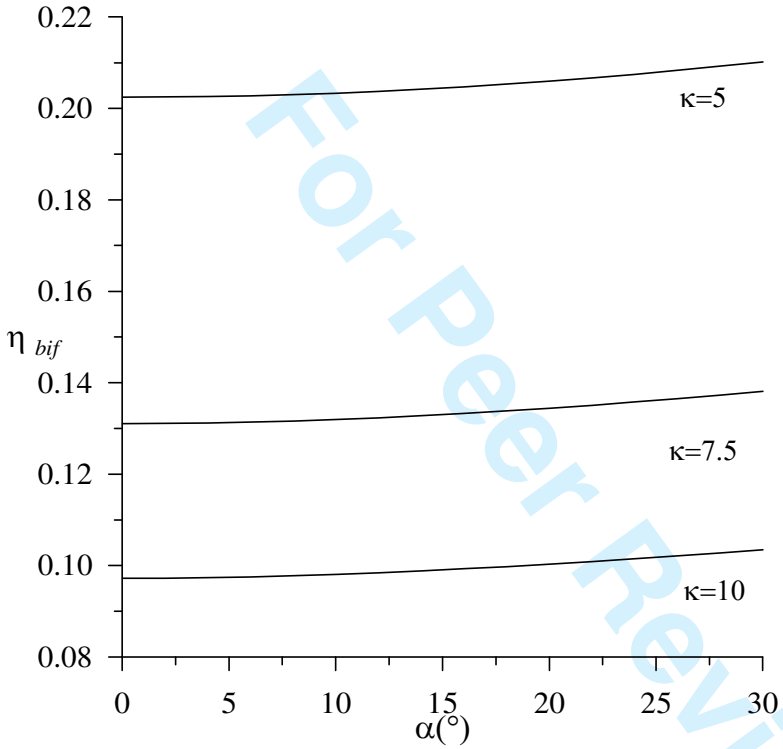

Figure 8)

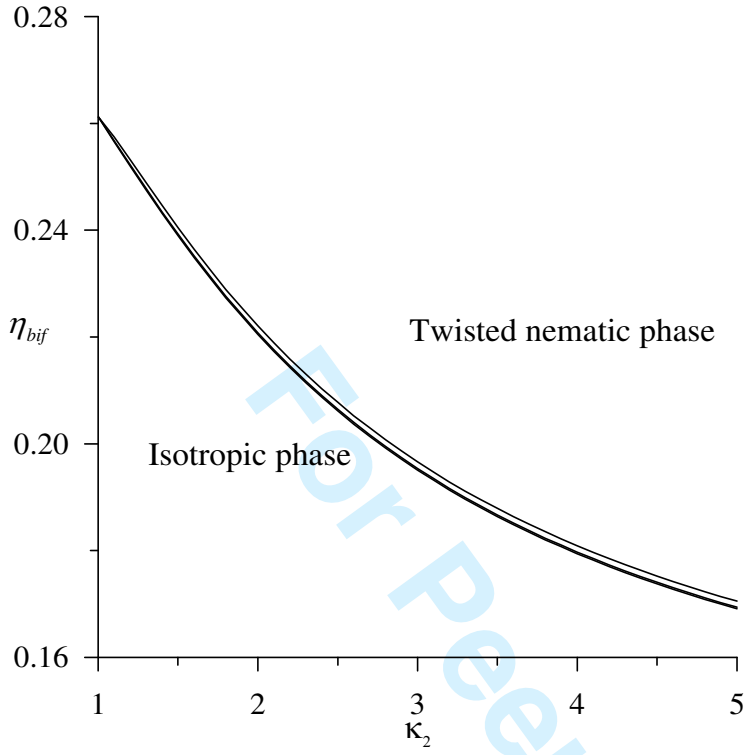

Figure 9 a)

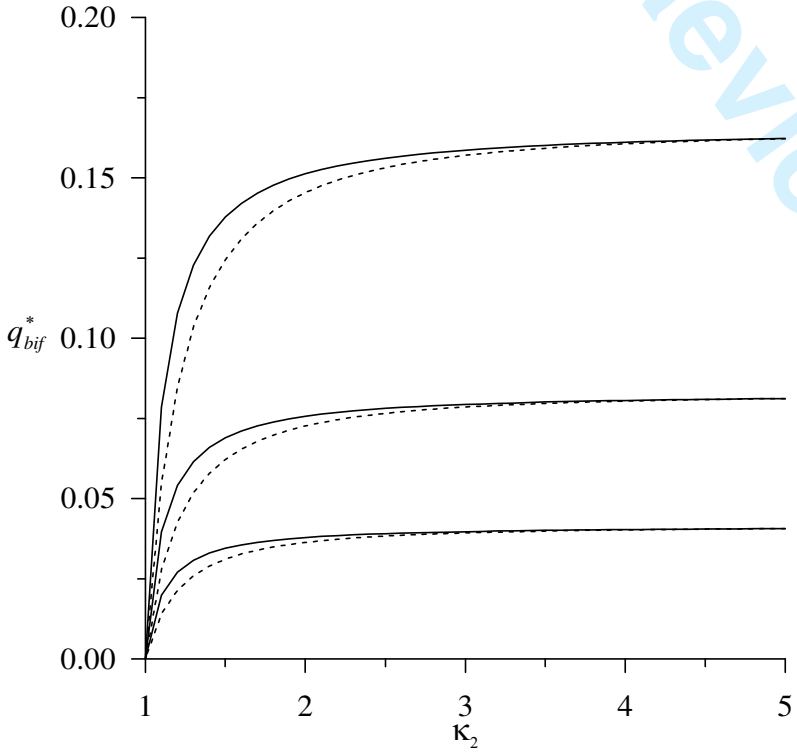

Figure 9 b)

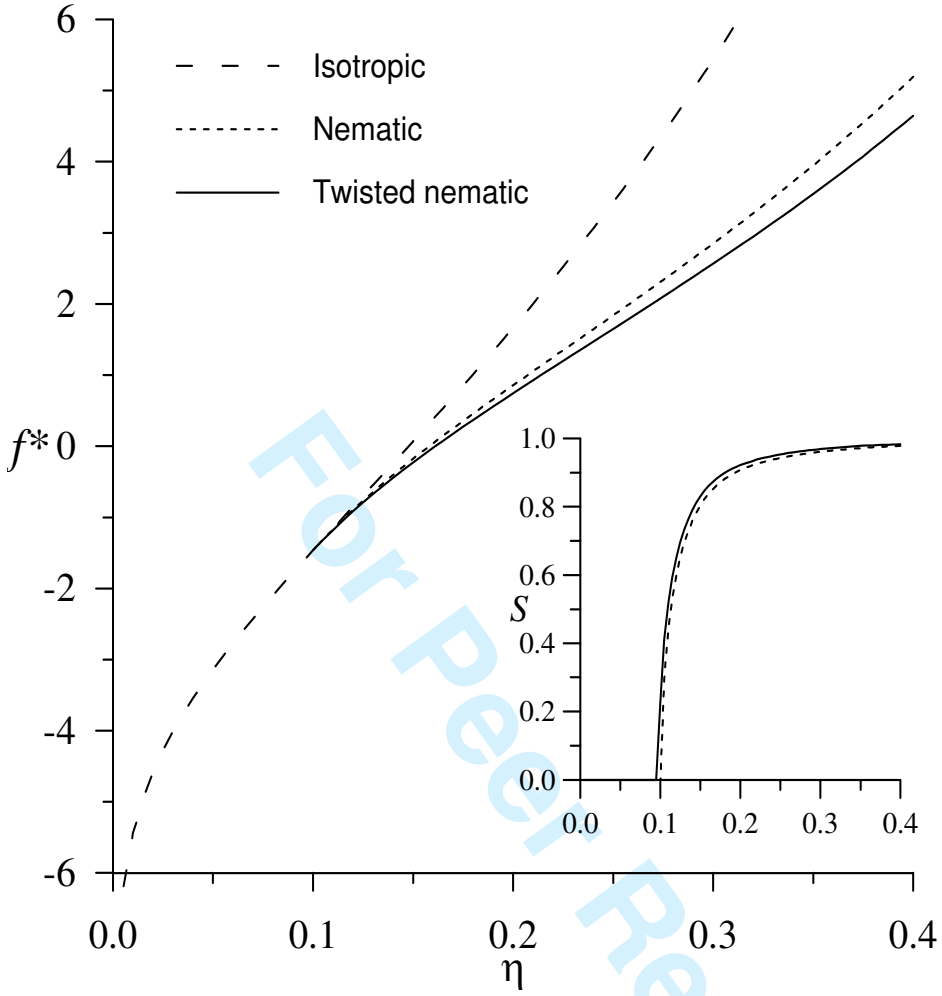

Figure 10 a)

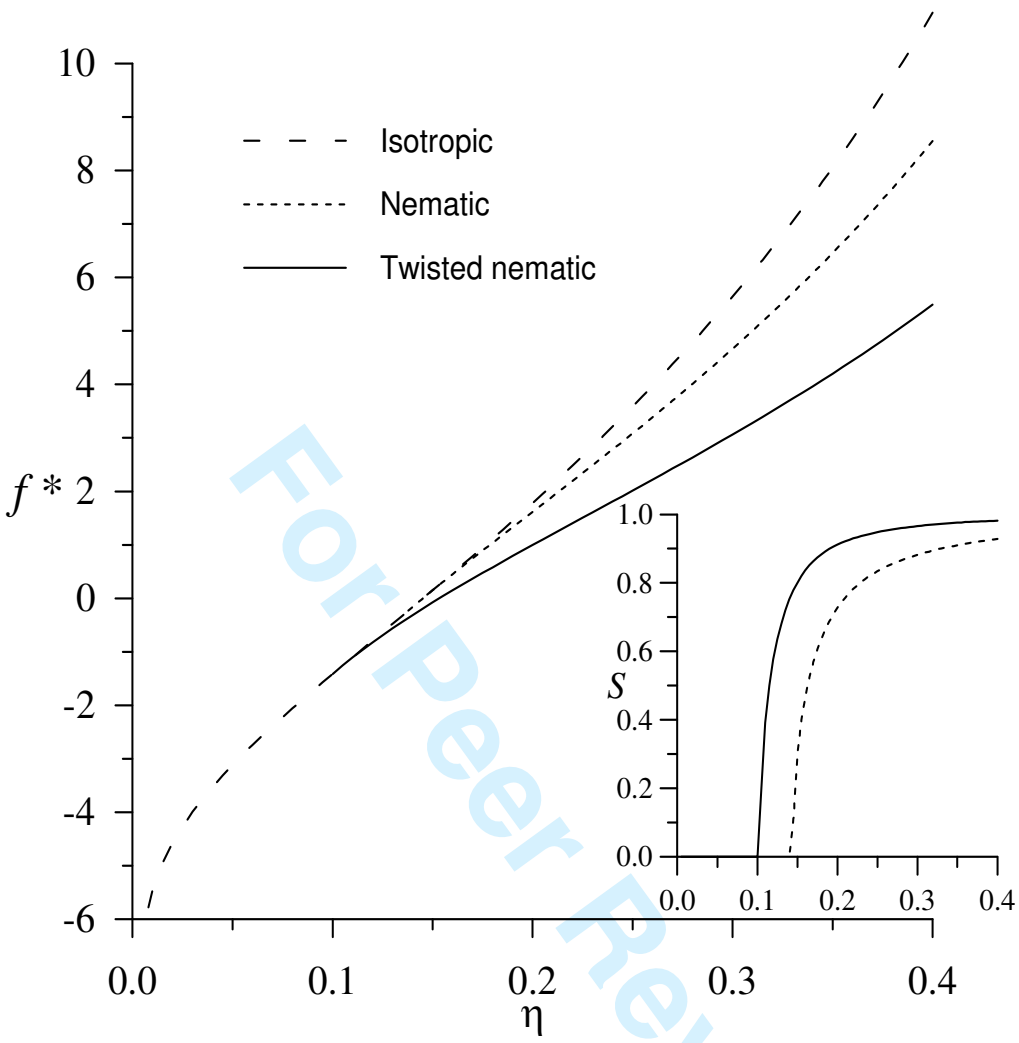

Figure 10 b)

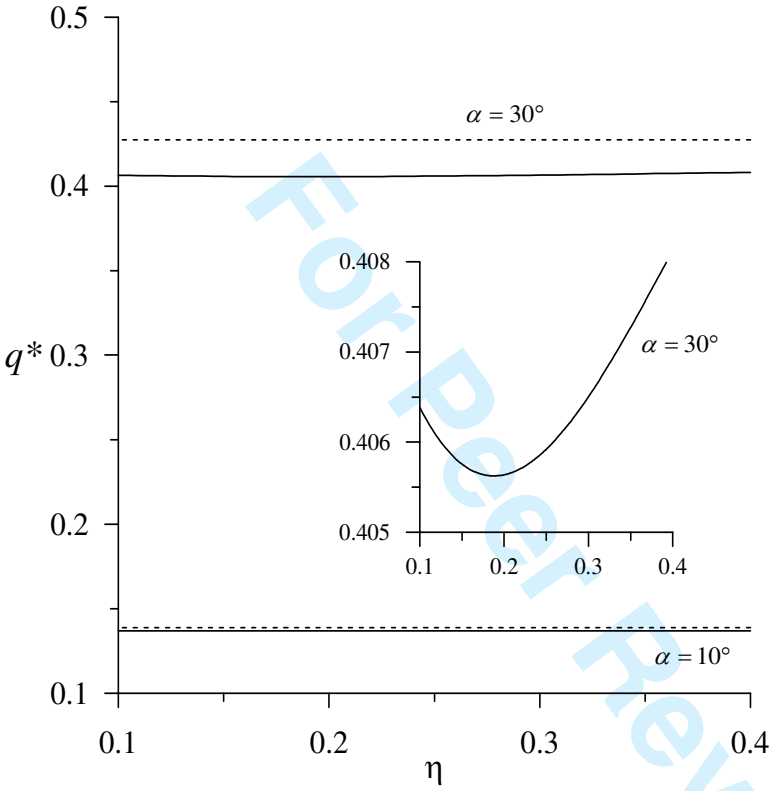

Figure 11

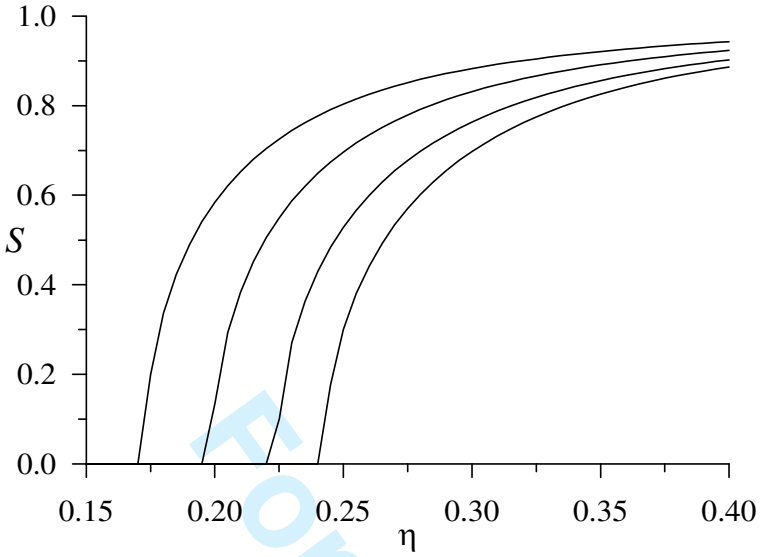

Figure 12 a)

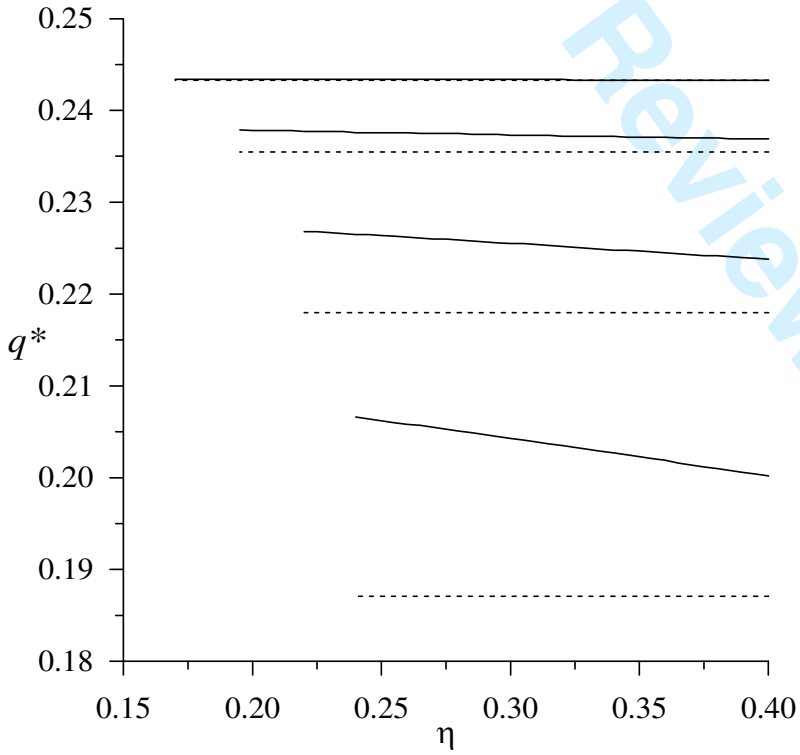

Figure 12 b)

A study of steric chirality: The chiral nematic phase of a system of chiral two-site HGO molecules

Szabolcs Varga[a] and George Jackson[b]

[a] *Department of Physics and Mechatronics, University of Pannonia, H-8200 Veszprém, PO Box 158, Hungary*

[b] *Department of Chemical Engineering, Imperial College London, South Kensington Campus, London SW7 2AZ, UK.*

PACS Numbers: 64.70.Fx, 05.70.Fh, 75.50.Mm

Number of pages: 49 (including figure captions and figures)

Figures: 12

[a] e-mail: vargasz@almos.vein.hu

[b] e-mail: g.jackson@imperial.ac.uk

Abstract

The liquid crystalline phase behaviour of a chiral two-site hard Gaussian overlap fluid is examined using the well-known Parsons-Lee extension of the theory of Onsager. The hard-core model is constructed such that the vector connecting the centers of two hard Gaussian segments is perpendicular to the long axes of both segments. The microscopic chirality of the particle can be controlled with the dihedral angle between the long axes of the hard Gaussian segments, the distance between the two segments, and the length-to-breath ratios of each segment. In the framework of Parsons-Lee approach three different types of phases are considered, namely, the isotropic liquid, and the nematic and the chiral nematic (cholesteric) liquid crystalline phases. For simplicity, the orientation of the particles is restricted to the plane perpendicular to the twist axis, and the particles do not have internal freedom to rotate around their main symmetry axes. The geometric condition for the formation of a chiral nematic phase, the properties of the helical structure, and the phase boundary of the ordering transition are determined by means of a free energy minimization. It is shown that steric (shape) chirality always gives rise to helical structure in the nematic phase, and that the low density chiral systems can undergo a transition from an isotropic liquid to a twisted nematic phase increasing the density. Analytical expressions are obtained for the twist period (pitch) in the limit of parallel stacking of the rod-like segments in layers normal to the helical axis, which are only valid for systems characterized by weak chiral strengths. A key finding of the numerical calculations is that the pitch is very sensitive to the segment separation, but not to the density or aspect ratio. It is interesting to note that the inverse of the pitch is predicted to depend linearly on the dihedral angle in all of the cases studied.

1. Introduction

The simplest liquid crystalline (meso) phase is a nematic in which the principal axis of the molecules (mesogens) is aligned along a preferential direction (the director) but where the distribution of the molecular centres of mass is otherwise isotropic [1,2]. Molecular (microscopic) chirality is a fascinating property of mesogens because it can give rise to an additional helical structure in the direction normal to the plane of the nematic ordering [1-5]. The helically structured nematic phase is often referred to as a chiral nematic or cholesteric phase. The relation between the bulk (macroscopic) liquid crystal phase behaviour and the inherent chirality of the molecules is still poorly understood. One example is the liquid crystalline behaviour exhibited by aqueous colloidal suspensions of TMV or *pf*1 viruses, where the molecular chirality does not give rise to a helical macroscopic structure, while a stable cholesteric phase is exhibited in aqueous suspensions of *fd* viruses which is structurally very similar to *pf1* [6-8]. It is therefore clear that molecular chirality does not guarantee the existence of the orientational ordered twisted structure.

Liquid crystalline phase behaviour was originally thought to be the consequence of electrostatic (polar) interactions between the molecular species alone [9,10]. The mean-field Maier-Saupe treatment of liquid crystalline order [11-13] is consistent with this energetic standpoint, as is the common application of the phenomenological Landau-de Gennes description [14-16]. It is now well recognised that repulsive (excluded volume) interactions also play a central role in the stabilisation of mesophases as Onsager had first suggested in 1942 [17,18]; extensive molecular simulation studies of hard discs [19,20], ellipsoids of revolution [21,22], hard spherocylinders [23–26], and rigid hard-sphere chains [27] certainly support this view. Though anisotropic repulsive interactions thus appear to a perquisite for the formation of macroscopic liquid crystalline order, the effect of the electrostatic forces cannot be overlooked. The stable orientationally and positionally

ordered structures that are observed are very sensitive to the precise features of the electrostatic interactions (such as their position and orientation) or the presence of flexible tails as has been highlighted in studies of model dipolar hard-core systems [28-32].

The existence of twisted nematic phases can be attributed to microscopic chiral features which are both steric and electrostatic in origin. In most real systems these two types of molecular chirality are present but the separate contribution that each interaction makes to the orientational ordering of the bulk phase is difficult to identify [1-5]. A full armoury of statistical mechanical and continuum theories and molecular simulation techniques has been deployed in studies of model molecules with chiral interactions which are of a steric or electrostatic nature (or both), including the development of suitable indices to characterise the molecular chirality; see [33-97] and references therein as representative examples. Despite this large body of work there is still much debate as to which underlying microscopic feature is responsible for the stabilisation of chiral nematic phase. It is therefore a highly desirable goal to gain a better understanding of the relation between molecular chirality and the helical twist of the bulk phase by studying model systems for which the roles of the steric and electrostatic chirality can be examined independently. The effect of electrostatic chiral interactions on cholesteric order has been examined in detail with Maier-Saupe mean-field [3-5, 33-35, 37, 38, 40, 62, 71, 73, 76, 83-85] and Onsager-like [93, 94, 97] theories. In the opposite vein we focus on a description of the chiral nematic phase of purely repulsive hard body systems characterised by steric chirality in our current work.

Straley [36] was the first to examine the effect of repulsive steric chirality by studying a system of helically threaded hard rods using Onsager's second-virial theory for orientational order in hard anisometric particles [18]. Odijk [44] later extended the approach of Straley to allow for a treatment of the molecular flexibility. A surprising finding of these studies is that the helical twist of the bulk chiral structure does not depend on the degree of molecular chirality, though the wave number (inverse pitch) is found to be proportional to the density, diameter of the molecular core, and the thread depth in very ordered twisted nematic phases. In related work Pelcovits [60] examined a system of rigid and semi-flexible corkscrew particles finding the more physically intuitive

dependence of the cholesteric pitch on the molecular chirality; furthermore, the density dependence found for the pitch is different from that described by Straley or Odijk. The chiral nematic phase formed by twisted biaxial ellipsoids (with and without isotropic attractive interactions) has also been studied by Evans [51] using a Parsons-Lee [98,99] type scaling of the Onsager free energy functional to account for the higher virial coefficients in an approximate manner. In this case Evans did not observe a density dependence of the pitch but the bulk chirality was found to be proportional to the molecular twist of the hard body. Very recently Dhakal and Selinger [96] have examined a lattice model of bent-core molecule with mean-field and Landau-de Gennes theories and by Monte Carlo simulation, describing the temperature dependence of the pitch and the underlying mutual enhancement of biaxial and chiral order. The model we study here is a continuum analogue of this lattice model.

Simulation studies of chiral nematic phases are comparatively rare [54-56, 61, 63, 67-70, 72, 77, 79-81, 86, 88, 92, 93, 96], and tend to focus on particles characterized by the electrostatic dispersive chiral interaction potential devised by Goossens [33] incorporated within a reference system of hard-core or Gay-Berne [100] (GB) mesogens. The first simulations of purely repulsive chiral molecules formed from two hard prolate ellipsoidal cores in a crossed configuration was presented by Allen [54] to study the dependence of the helical twisting power on the addition of these model chiral dopants to the nematic phase of uniaxial molecules; Camp [63] later developed an elegant and simple theoretical framework for such a system. Memmer et al. [61] have considered the steric chirality in a system of particles comprising two fused GB sites, where the dihedral angle between the GB segments governs the chirality of the molecule. With their canonical Monte Carlo simulations they showed that one could stabilize a macroscopic cholesteric structure for the GB dimers. A drawback of the study of Memmer et al. [61] is that the underlying dispersive attractive interactions of the GB cores also affects the structure of the chiral nematic phase, i.e., the contribution due to steric chirality cannot be completely decoupled from the electrostatic chirality. The same issue arises in systems of fused two-site GB models with a bent-core [81] or discotic [88] geometry; interestingly, though the bent-core GB molecules are biaxial but otherwise achiral, they

are found to exhibit twisted grain boundary (TGB) structures with smectic layers rotated relative to each other [81].

To study the effect of steric chirality alone we construct a two-site hard-body model, similar to that of Allen [54], which can be considered as the athermal analogue of the model proposed by Memmer et al. [61]. It also resembles the single-core chiral model of Harris et al. [3]: in this very simple athermal model only the orientational and the packing entropies are active, and the interplay between these two entropic contributions determines the structure of the stable phase.

Two quantities are required to characterize the structure of the twisted nematic phase: one is the local orientational distribution function, and the other is the spatial period of the twist (cholesteric pitch) [4]. It is generally accepted that the twist angle between two nematic layers is proportional to the distance between the layers, while the orientational distribution function has to be biaxial with a higher probability of molecules oriented in the plane than out of the plane. As has been pointed out by Harris et al. [5], the twisted structure cannot propagate without (local) biaxial orientational order otherwise the macroscopic phase would always be of uniaxial nematic symmetry. In our model we assume that the long axes of the molecular segments are always perpendicular to the helix axis of the chiral twist to fulfill the requirement of biaxial orientational order.

The goal of our work is to study the macroscopic manifestation of chirality in the molecular shape for a hard-body system which forms orientationally ordered phases. Using the purely repulsive hard Gaussian overlap (HGO) model as building blocks to form a two-site chiral molecule, the contribution of steric chirality on the formation of a chiral nematic phase can be studied in isolation. No attractive/electrostatic interactions are included, which would otherwise also have an impact on the helical structure of the bulk phase. Our model makes it possible to determine explicitly the role played by the molecular geometry and the aspect ratio in the stabilization of the bulk helical structure. We use the well-known Parsons-Lee [98,99] extension of Onsager's theory for hard cores to determine the stability of the isotropic, nematic, and chiral nematic phases by characterizing the structure of the bulk phases. As we have already mentioned, the principal inertial axes of the particles are always restricted to stay in a plane, and can either rotate freely in the plane or are

orientationally constrained depending on the level of approximation that is employed. The results of both approximations are compared to assess the relationship between the orientational entropy and the helical wave number of the twisted nematic phase.

The paper is organized as follows: In the following section the molecular model is presented and the geometric conditions that have to be satisfied to represent chiral shapes are discussed. In Section 3. we present the Parsons-Lee theory as applied to chiral nematic phases, and derive our working equations using two different approximations for the orientational distribution function. Some applications of the theory are then presented for the system of two-site HGO molecules using a second-order expansion of the free energy of the twisted nematic phase. In Section 4. the effect of the three parameters that govern the molecular chirality, the effect of the aspect ratio, and the effect of the packing fraction on the formation of the cholesteric phase is examined in detail; the role of orientational freedom is also assessed. Our conclusions are summarized in Section 5.

2. Molecular model and the conditions for microscopic chirality

The simplest way to examine steric chirality is to link two uniaxial (achiral) rod-like hard cores in such a way that they form a chiral body. To do this of one of the particle has to be twisted relative to the other with a finite angle. We further suppose that the vector connecting the centres of the two prolate bodies is perpendicular to the long symmetry axis of each hard-core segment. This type of molecular geometry is depicted in Fig. 1, where the dihedral angle (α) between the two main symmetry axes of the segments is chosen to be $\pi/6$, the length-to-breath ratio of the each segment is $\kappa_1 = \kappa_2 = \kappa = 3$, and the distance Δ between the centres of the segments is equal to the segment diameter σ_0 (here σ_0 is the dimension of the short axis of the hard core, i.e., its breadth). There are two ways to control the chirality of the molecule shown in Fig. 1: one involves a change in the dihedral angle between the long axes of the segments, and the other a variation of the distance between the centres of the segments. There are particular cases where the molecule is achiral. The parallel and the perpendicular relative alignment of the cores, and the perfectly fused case (the distance between the two centres is zero) are clearly achiral (see Fig. 2). In the case of two different fused hard bodies ($\kappa_1 \neq \kappa_2$), the chirality is lost by making one of the hard-core segments spherical as shown in Fig. 2 d). The exact form of the hard body interaction will be given later.

3. Parsons-Lee theory of the chiral nematic phase

The approach of Onsager [18] is one of the most popular and successful theories for the description of nematic order in systems of hard-core mesogens [101,102], hard-core mixtures [103], and attractive molecules with anisotropic hard cores [104]. It can be regarded as one of the first applications of density functional theory (DFT), where the free energy of the system is described as a functional of the single particle orientational distribution function. A DFT treatment provides one of the most successful generic platforms for the description of inhomogeneous and anisotropic systems. Evans [105,106] has been a key developer and exponent of the approach in its application to free

interfaces of fluids and fluid mixtures and systems under confinement. The work of Evans and co-workers also provides an excellent example of the use of DFT to represent inhomogeneous liquid crystalline systems, including the effect of confinement on the isotropic-nematic transition [107] and capillary nematization of confined hard rods [108,109].

In its original form the theory of Onsager is cast at the second virial level. This means that it appropriate only at low density. The applicability of the Onsager free energy to higher density isotropic and nematic phases of hard body fluids can be extended by following the methodology of Parsons [98] and of Lee [99] (also see the detailed exposition in references [25,102]). The theory is also appropriate for chiral nematic (cholesteric) phase because the local helical structure is expected to be weak in practice and is not likely to give rise to substantial change in the overall free energy of the system. In the remainder of this section we reformulate the Parsons-Lee theory for the chiral nematic phase in a Cartesian coordinate frame of reference where the helical axis is assumed to be parallel with the z axis.

For the freely rotating case, the total Helmholtz free energy F of the chiral nematic phase can be written as a sum of the ideal and residual contributions $F = F_{ideal} + F_{res}$, where the ideal free energy is given by

$$\frac{\beta F_{ideal}}{V} = \rho \ln(\Lambda^3 \rho) - \rho + \frac{\rho}{V} \int d\underline{r} d\underline{\omega} f(\underline{\omega}, z) \ln[\Omega f(\underline{\omega}, z)], \tag{1}$$

while the residual part is approximated by the Parsons-Lee approximation [98,99] as

$$\frac{\beta F_{res}}{V} = \frac{4\eta - 3\eta^2}{8v_0(1-\eta)^2} \frac{\rho}{V} \int d\underline{r}_1 d\underline{\omega}_1 f(\underline{\omega}_1, z_1) \int d\underline{r}_2 d\underline{\omega}_2 f(\underline{\omega}_2, z_2) f_M(\underline{r}_{12}, \underline{\omega}_1, \underline{\omega}_2). \tag{2}$$

Here, the Mayer function f_M provides a direct link to the pair potential u through the following relation: $f_M(\underline{r}_{12}, \underline{\omega}_{12}) = \exp[-\beta u(\underline{r}_{12}, \underline{\omega}_{12})] - 1$. In these expressions $\beta = 1/k_B T$ (k_B being the Boltzmann constant and T the temperature), N is the total number of particles, $\rho = N/V$ is the number density (V being the volume of the system), $\eta = \rho v_0$ is the packing fraction, v_0 is the volume of the particle, Λ^3 is the de Broglie volume (kinetic contribution to the free energy), and $\Omega = 8\pi^2$ for

biaxial particles. The orientational distribution function $f(\underline{\omega},z)$ is used to describe the orientation of the particle's principal symmetry axis in the plane at position z along the helical axis. Since the chiral nematic phase is periodic in the direction of the helical axis (chosen as the z axis), the spatial integrations can be performed in the layer normal:

$$\frac{\beta F_{res}}{V}=\frac{4\eta-3\eta^2}{8v_0(1-\eta)^2}\rho\frac{1}{P}\int_0^P dz_1\int d\underline{\omega}_1 f(\underline{\omega}_1,z_1)\int_{z_{12}\in V_{exc}} dz_2\int d\underline{\omega}_2 f(\underline{\omega}_2,z_2)A_{exc}(z_{12},\gamma_{12}), \tag{3}$$

where P is the helical period (pitch) of the chiral nematic phase, V_{exc} denotes that region which is excluded to a particle around another particle fixed in space, and γ_{12} is the angle between the principal axes of the particles. The excluded area A_{exc} is the result of twofold integration of the Mayer function when the positions of molecular centres are a distance $z_{12} = z_1 - z_2$ apart.

Two simplifying assumptions are applied for the orientation distribution function. In the simplest approximation, the particle's orientational unit vector ($\underline{\omega}$) is constrained to stay in the plane normal to the helical axis, all of the particles are taken to be parallel in a given layer (perfect 2D order), and the local nematic director is assumed to vary linearly from layer to layer along the helical axis:

$$f(\underline{\omega})=\delta\left(\theta-\frac{\pi}{2}\right)\delta(\psi)\delta(\varphi-qz). \tag{4}$$

In this equation δ represents the Dirac delta function, (θ,ψ,φ) are the conventional Euler's angles, while q is the wave number (which is proportional to the inverse pitch) prescribing the helical structure of the nematic order to vary in a linear fashion along the z axis. The relationship between the wave number and the pitch of the chiral nematic phase is simply $q = 2\pi/P$. In the second, more realistic, case the particles are still orientated perpendicular to the helical axis, but they are allowed to rotate freely within a given plane:

$$f(\underline{\omega})=\delta\left(\theta-\frac{\pi}{2}\right)\delta(\psi)h(\varphi), \tag{5}$$

where h is the corresponding 2D orientational distribution function. The difference between the two approximations is that we neglect the contribution due to the orientational entropy completely with Eq. (4), while the orientational entropy is partially captured with Eq. (5).

After substitution of the perfect 2D order approximation (Eq. (4)) into the expressions for the ideal and residual free energy (Eqs. (1-3)) we get

$$\frac{\beta F_{ideal}}{V} = \rho \ln(\Lambda^3 \rho) - \rho , \tag{6}$$

and

$$\frac{\beta F_{res}}{V} = \frac{4\eta - 3\eta^2}{8v_0(1-\eta)^2} \rho \int_{z_{12} \in V_{exc}} dz_{12} A_{exc}(z_{12}, qz_{12}) . \tag{7}$$

In this way the total free energy density in the case of the perfect 2D order approximation can be written as

$$\frac{\beta F}{V} = \rho \ln(\Lambda^3 \rho) - \rho + \frac{4\eta - 3\eta^2}{8v_0(1-\eta)^2} \rho \int_{z_{12} \in V_{exc}} dz_{12} A_{exc}(z_{12}, qz_{12}) . \tag{8}$$

For a given molecular model and density, the free energy only depends on the wave number, i.e., the equilibrium free energy of the system can be obtained by means of the minimization of Eq. (8) with respect to the wave number: $\frac{d\beta F / V}{dq} = 0$. As only the excluded area depends on the q parameter, the condition of the free energy minimization reduces to the minimization of the excluded volume,

$$\frac{dV_{exc}(q)}{dq} = 0 . \tag{9}$$

The integral of the excluded area over the excluded volume regime gives the overall excluded volume for a pair of twisted body characterized by the twist q:

$$V_{exc}(q) = \int_{z \in V_{exc}} dz A_{exc}(z, qz) . \tag{10}$$

In this way the problem reduces to looking for the particular helical arrangement which minimizes the excluded volume interactions between the particles, or in other words that which maximizes the free volume available for the particles in space. One trivial result of the perfect 2D order

approximation is that the pitch does not depend on density even at infinitely low densities, and the phase can be either nematic or chiral nematic, but not isotropic. To overcome this deficiency of the theory, the particles must possess some orientational degrees of freedom.

In the case of free planar ordering, after substitution of the orientational distribution function (Eq. (5)) into the ideal and residual free energy terms (Eqs. (1-3)) the following relations be derived:

$$\frac{\beta F_{ideal}}{V} = \rho \ln(\Lambda^3 \rho) - \rho + \frac{\rho}{P} \int_0^P dz \int_0^{2\pi} d\varphi h(\varphi, z) \ln h(\varphi, z), \tag{11}$$

$$\frac{\beta F_{res}}{V} = \frac{4\eta - 3\eta^2}{8v_0 (1-\eta)^2} \frac{\rho}{P} \int_0^P dz_1 \int_0^{2\pi} d\varphi_1 h(\varphi_1, z_1) \int_{z_{12} \in V_{exc}} dz_2 \int_0^{2\pi} d\varphi_2 h(\varphi_2, z_2) A_{exc}(z_{12}, \varphi_{12}). \tag{12}$$

As for the perfect 2D order approximation, the free energy again has to be minimized with respect to q, but in addition the orientational distribution function $h(\varphi, z)$ which minimizes the free energy has to be determined in order to describe the equilibrium free energy of the system. This can be done by solving a nonlinear integral equation for $h(\varphi, z)$, which can be obtained by functional minimization of the free energy. In order to reduce the computational burden of the free energy minimization, we use a simple helical trial function with a variational parameter λ and wave number q to represent the two-dimensional orientational distribution function:

$$h(\varphi, z) = \frac{\exp(\lambda \cos(2(qz - \varphi)))}{\int_0^{2\pi} d\varphi \exp(\lambda \cos(2(qz - \varphi)))}. \tag{13}$$

Depending on the values of λ and q, Eq. (13) leads to isotropic ($\lambda = 0$), nematic ($\lambda \neq 0$ and $q = 0$) or chiral nematic ($\lambda \neq 0$ and $q \neq 0$) solutions for the orientational distributions. After inserting Eq. (13) into the free energy of freely (in the plane) rotating particles (the sum of Eqs. (11 and 12)) the minimization conditions can be written as

$$\frac{d\beta F / V}{dq} = 0 \text{ and } \frac{d\beta F / V}{d\lambda} = 0. \tag{14}$$

In the result section we will present the equilibrium pitch obtained from both approximations.

Before discussing the solution of these coupled equations it is enlightening to first find the lowest density at which the nematic or chiral nematic phase becomes stable. We perform a so-called bifurcation analysis where the corresponding density is referred to as the bifurcation density [101]. After substitution of the trial function into the ideal and residual free energy terms (Eqs. (11) and (12)) we can expand the free energy as a function of variational parameter λ up to second order. The resulting free energy has the form of $\beta F / V = a + b\lambda^2$, where the zeroth order term a corresponds to the free energy of the isotropic phase, and b is the expansion coefficient of the nematic perturbation. Since the free energy of the nematic and the isotorpic phases are identical at the bifurcation point, the expansion coefficient of nematic perturbation has to be zero. After some algebra we obtain the following expression for the packing fraction at the bifurcation point:

$$1 + \frac{4\eta - 3\eta^2}{(1-\eta)^2 8 v_0 \pi} \int_{z \in V_{exc}} dz \int_0^{2\pi} d\varphi \cos\left(2(qz - \varphi)\right) A_{exc}(z, \varphi) = 0 \ . \tag{15}$$

To determine whether the nematic or the chiral nematic phase is more stable at the bifurcation one has to minimize the free energy with respect to the wave number: in this case this corresponds to $\frac{db}{dq} = 0$. The result of this minimization is given by

$$\int_{z \in V_{exc}} dz \int_0^{2\pi} d\varphi \sin\left(2(qz - \varphi)\right) z \, A_{exc}(z, \varphi) = 0 \ . \tag{16}$$

The solution of the coupled equations (15) and (16) gives the bifurcation packing fraction and the bifurcation wave number. The results of the bifurcation analysis are presented in Section 4.

In order to proceed the molecular model has to be specified. In the following we assume that each segment of the dimer molecule is characterised by the so-called hard Gaussian overlap (HGO) potential [110,111]. The main advantage of this model is that the distance of closest approach, the excluded area, and excluded volume can be expressed in closed analytical forms [112]. For example,

the excluded area for a pair of HGO particles (of breadth σ_0, length $\sigma_0\kappa$, and aspect ratio κ) in a 2D planar arrangement is given by

$$A_{exc}(z,\gamma)=\begin{cases}\dfrac{\pi\left(\sigma_0^2-z^2\right)}{1-\chi}\sqrt{1-\chi^2\cos^2(\gamma)}, & -\sigma_0\le z\le\sigma_0\\ 0, & \text{otherwise}\end{cases} \tag{17}$$

where γ is the angle between the two particles, and χ is an anisotropy parameter defined as $\chi=\dfrac{\kappa^2-1}{\kappa^2+1}$. For a spherical shape ($\kappa = 1$) the anisotropy parameter is zero, while it is one for an infinite length-to-breath ratio ($\kappa = \infty$). One should note that a molecular volume can not be associated uniquely to the HGO pair potential, but it is generally accepted that the volume of HGO particles can be taken as that of correspond hard ellipsoid of revolution, i.e., $v_{HGO}=\dfrac{\pi}{6}\kappa\sigma_0^3$.

To construct our chiral dimer HGO particles, two HGO segments are positioned with their centres a distance Δ apart in a planar alignment with the main symmetry axes of the segments twisted relative to each other at a dihedral angle α as shown in Fig. 1; in this particular case the two segments are taken to be in contact corresponding to an intramolecular segment separation of $\Delta=\sigma_0$. The resulting chiral HGO particle interacts through its HGO segments.

It is instructive to start by examining the particular case of a pair of chiral HGO particles with a (rather unrealistic hanging) intersegment separation of $\Delta=2\sigma_0$ and relative orientation γ for which the excluded area can be determined very easily in the planar geometry. The two HGO particles start to exclude each other at a relative distance of $z=-3\sigma_\perp$ through the interaction between the "bottom" segment of the "upper" molecule and "top" segment of the "lower" molecule. Here, "upper" or "top" and "lower" or "bottom" refer to the relative position along the helical axis *z*. This interaction persists up to a distance $z=-\sigma_0$ for which the excluded area of a single HGO particle can be used (cf. Eq. (17)); one should note, however, that the angle between the long axes of HGO segments making up the particle is not same as the angle between the two chiral molecules, but

is $\gamma + \alpha$ because of the twisted structure of the molecules. In the second regime of $-\sigma_0 \le z \le \sigma_0$ "like" "top-top" and "bottom-bottom" excluded volume segment-segment interactions take place simultaneously, but these interactions are identical and the resulting excluded areas is obtained from Eq. (17), as in this case the angle between the two like "top" or two "bottom" segments is γ. In the third regime of $\sigma_0 \le z \le 3\sigma_0$, only the "bottom" segment of the "upper" molecule is excluded by the "top" segment of the "lower" molecule in the same way as in the first regime but now for a relative angle of $\gamma - \alpha$. The excluded area for a pair of chiral HGO particles with an intramolecular segment separation of $\Delta = 2\sigma_0$ can thus be summarised with the following relation:

$$A_{exc}(z_{12},\gamma) = \begin{cases} \dfrac{\pi\left(\sigma_0^2 - \left(z - 2\sigma_0\right)^2\right)}{1-\chi}\sqrt{1-\chi^2\cos^2(\gamma-\alpha)}, & \sigma_0 \le z \le 3\sigma_0 \\ \dfrac{\pi\left(\sigma_0^2 - z^2\right)}{1-\chi}\sqrt{1-\chi^2\cos^2(\gamma)}, & -\sigma_0 \le z \le \sigma_0 \\ \dfrac{\pi\left(\sigma_0^2 - \left(z + 2\sigma_0\right)^2\right)}{1-\chi}\sqrt{1-\chi^2\cos^2(\gamma+\alpha)}, & -3\sigma_0 \le z \le -\sigma_0 \end{cases} . \quad (18)$$

Note that the expression for the excluded area is much more complicated for smaller values of separation between the centres of the two segments making up the HGO molecule ($0 \le \Delta < 2\sigma_0$), because the excluded volume regimes of the segment-segment interactions do not decouple so simply but overlap. In our generalized twisted two-site HGO model, where the HGO segments have the same breadth (σ_0) but different lengths ($\kappa_1\sigma_0 \ne \kappa_2\sigma_0$), analytical relations can also be derived for the excluded area. Without presenting the details, the expression can be written in the following form for the intramolecular segment separation of $\Delta = 2\sigma_0$ (see reference [113] for shape parameters for particles of differnt aspect ratio):

$$A_{exc}(z_{12},\gamma)=\begin{cases}\dfrac{\pi\left(\sigma_0^2-\left(z-2\sigma_0\right)^2\right)}{\sqrt{1-\chi_1}\sqrt{1-\chi_2}}\sqrt{1-\chi_1\chi_2\cos^2(\gamma-\alpha)}, & \sigma_0\le z\le 3\sigma_0\\ \dfrac{\pi\left(\sigma_0^2-z^2\right)}{1-\chi_1}\sqrt{1-\chi_1^2\cos^2(\gamma)}, & -\sigma_0\le z\le\sigma_0\\ \dfrac{\pi\left(\sigma_0^2-\left(z+2\sigma_0\right)^2\right)}{\sqrt{1-\chi_1}\sqrt{1-\chi_2}}\sqrt{1-\chi_1\chi_2\cos^2(\gamma+\alpha)}, & -3\sigma_0\le z\le-\sigma_0\end{cases}, \quad (19)$$

where the anisotropy parameters of the segments are defined in terms of length-to-breath ratios (κ_1 ,κ_2) as $\chi_1=\dfrac{\kappa_1^{\,2}-1}{\kappa_1^{\,2}+1}$ and $\chi_2=\dfrac{\kappa_2^{\,2}-1}{\kappa_2^{\,2}+1}$. We must mention that Eq. (19) represents the excluded area for molecular arrangements where the "top" and "bottom" segments of the two molecules are commensurate (i.e., geometries where both of the shorter segments are on the "top" or "bottom", but not one on the "top" and one on the "bottom"). A more complete treatment of this system would involve a binary mixture with equal numbers of molecules in "up" and "down" arrangements. To maintain the simplicity of the theory the "up-down" excluded areas are not included in the description. In the case of a intramolecular segment separation of $\Delta=2\sigma_0$, Eqs. (18) and (19) can be used, while for $0\le\Delta<2\sigma_0$ tabulated values of excluded areas obtained numerically (not presented here) are used as the input to the theory.

It is widely accepted that one can expand the free energy density of the twisted nematic phase as a function of wave number up to the quadratic term to obtain the twist torque (h) and the twist elastic constant (K_{22}) as

$$\left.\frac{\beta F}{V}\right|_{TN}=\left.\frac{\beta F}{V}\right|_{N}-hq+\frac{1}{2}K_{22}q^2, \quad (20)$$

where the zeroth order term is the free energy density of the nematic phase. This truncated free energy is often referred to as the Frank free energy for a system with a twist deformation [5]. Such an approach can be applied only in those cases where the molecular chirality does not give rise to a substantial change in the free energy. This is the case for weakly chiral systems such as aqueous

suspension of the *fd* viruses [6-8] and DNA [114]. The minimization of Frank free energy (Eq. (20)) with respect to q allows us to determine the equilibrium wave number in terms of the twist torque and twist elastic constant as $q = h / K_{22}$. In our system of two-segment HGO molecules, it is reasonable to assume that the second order expansion will be adequate for small dihedral angles and small segment separation. The result of the method for the wave number in the case of perfect 2D (planar) order, for molecules with equal segment aspect ratios ($\kappa_1 = \kappa_2$ corresponding to $\chi_1 = \chi_2 = \chi$) and an intramolecular segment separation of $\Delta = 2\sigma_0$ can be written as

$$q = \frac{10\sin(2\alpha)}{\left(\frac{\sqrt{1-\chi^2\cos^2(\alpha)}}{\sqrt{1-\chi^2}} + 42\frac{\cos(2\alpha)-\chi^2\cos^4(\alpha)}{1-\chi^2\cos^2(\alpha)}\right)\sigma_\perp} = \frac{20\alpha}{43\sigma_0} + \mathrm{O}(\alpha^3). \tag{21}$$

It is interesting to note that wave number depends on the molecular anisotropy for moderate values the intramolecular dihedral angle α between the segments. This is not the case, however, for a very small dihedral angle where q is found to follow a linear dependence with α. The application of the method for the more general case of HGO molecules with segments of unequal size ($\chi_1 \neq \chi_2$) at a separation of $\Delta = 2\sigma_0$ using Eqs. (9), (16) and (19) results in a more general expression for the wave number of the chiral nematic phase:

$$\begin{aligned} q &= \frac{10\chi_2\sin(2\alpha)}{\left(\chi_1\frac{\sqrt{1-\chi_2}\sqrt{1-\chi_1\chi_2\cos^2(\alpha)}}{\sqrt{1-\chi_1}\sqrt{1-\chi_1^2}} + 42\chi_2\frac{\cos(2\alpha)-\chi_1\chi_2\cos^4(\alpha)}{1-\chi_1\chi_2\cos^2(\alpha)}\right)\sigma_0} \\ &= \frac{20\chi_2}{\sqrt{1-\chi_2}\sqrt{1-\chi_1\chi_2}\left(\frac{\chi_1}{\sqrt{1-\chi_1}\sqrt{1-\chi_1^2}} + 42\frac{\chi_2}{\sqrt{1-\chi_2}\sqrt{1-\chi_1\chi_2}}\right)\sigma_0}\alpha + \mathrm{O}(\alpha^3) \end{aligned} \tag{22}$$

This equation reduces to Eq. (21) in case of identical HGO segments $\chi_1 = \chi_2 = \chi$. There are now, however, two parameters governing the macroscopic chiral structure of the phase: one is the dihedral angle between the two segments of the molecule, and the other is the anisotropy parameter (χ_2). The

relation leads one to the conclusion that no twist can take place in the nematic phase of a system of achiral particles corresponding to the limits of either $\alpha = 0$ or $\chi_2 = 0$.

4. Results and discussions

Before presenting the results of the free energy minimizations we demonstrate why twisted orientational ordering is favorable in our system of repulsive chiral rod-like particles. As we have shown in the case of the perfect 2D order approximation, the system tends to reduce the excluded volume as much as possible to maximize the packing entropy (translational entropy) or equivalently minimize the free energy (cf. Eq. (9)). In this case the orientational entropy does not counter this effect because of the approximation of perfect 2D orientational order. In the case of an intramolecular segment-segment separation of $\Delta = 2\sigma_0$ it is very easy to determine the most favorable orientations over the entire range of the excluded body (cf. Eq. (18)). In all three regions the smallest excluded area can be achieved for relative intermolecular orientations (γ) corresponding to parallel interacting HGO segments. This happens at different angles for different pair separations: $\gamma = -\alpha$ for $-3\sigma_0 < z < -\sigma_0$; $\gamma = 0$ for $-\sigma_0 < z < \sigma_0$; and $\gamma = \alpha$ for $\sigma_0 < z < 3\sigma_0$. The minimal excluded area and the corresponding relative molecular orientation as a function of intermolecular distance along the helical axis is shown in Fig. 3. The best linear fit to the discontinuous γ-z function, which is given by $\gamma = q\,z$, goes through the middle point of the sectors (continuous line in Fig. 3b). The slope of the line (wave number) can be easily determined and it is given by $q = \alpha / 2\sigma_0$. Interestingly the numerical minimization of the free energy for very low values of the dihedral angle gives very similar result to that of our simple argument because $q = \frac{20\alpha}{43\sigma_0}$ (cf. Eq. (21)). For smaller segment-segment distances the excluded regions overlap and the expression for the excluded area becomes more complicated. The results of the calculations are presented for more realistic values of

the (dimensionless) intramolecular segment separations of $\Delta^* = \Delta/\sigma_0 = 0.5$, 0.75 and 1 in Fig 4. It can be seen that the excluded area is very sensitive to the imposed helical structure. Both weak and strong twists result in very high values of the excluded area at some particular distances, which give rise to high excluded volume (packing entropy cost). As a result there is an optimum value of the wave number where the integrated area (excluded volume) is at a minimum, which is represented by a continuous curve for the three cases depicted in Fig. 4. The shift of the excluded area regions for the different segment-segment separations can be seen very clearly with increasing Δ^*. At $\Delta^* = 0.5$ the presence of the three regions can be seen only at the strongest twist corresponding to a dimensionless wave number of $q^* = q\sigma_0 = 0.3$, while we get still overlapping regions for $\Delta^* = 1$ but the behavior is closer to that of the totally separated case (cf. Fig. 3.). This feature is due to the fact that only two excluded areas can overlap for $1 < \Delta^* < 2$, while three overlap for $0 < \Delta^* < 1$.

In light of these results we minimize the excluded volume numerically (see Eq. 9.) and determined the relation between the molecular chirality and the macroscopic structure. We start with the computationally simplest case of $\Delta^* = 2$ for which the excluded areas have very simple forms (cf. Eqs. (18) and (19)). For molecules comprising identical segments, the dependence of the equilibrium wave number on the length-to-breath and intramolecular dihedral angle are shown in Fig. 5. The numerical results (Eq. (9)) and the results of the analytical solution (Eq. (21)) are compared to determine the range of validity of the Frank analysis. In Fig. 5 a) we show that for small values of the intramolecular dihedral angle both methods gives the same results, but a noticeable deviation can be seen from $\alpha \sim 5°$. The numerical result corresponds to a linear dependence between the wave number and the dihedral angle, while the analytical solution overestimated the wave number at a given α. It is interesting to note that the first-order Taylor expansion of the analytical solution (Eq. (21)) is coincident with the numerical solution at any angle due to the linear dependence of the wave number with α. From Fig. 5 b) one can see that the wave number does not depend on the length-to-breath ratio which unmasks some of the shortcomings of the Frank analysis. While Eq. (21) leads to a strong κ dependence, its linearization does not suggest a length-to-breath ratio dependence (in

coincidental agreement with the numerical results). At this point we must mention that even if the length-to-breath ratio were not to affect the helical structure it has strong influence on the range of stability range of the chiral nematic (and nematic) phase. For molecules with HGO segments of different length, the wave number is still characterized by a linear dependence with the dihedral angle, but the value now depends on the length-to-breath ratio (see Fig. 6). As one segment is made progressively more spherical ($\kappa_2 \to 1$) the system is seen to twist to a lesser extent. It can be seen in Fig. 6b) that the helical structure does not change substantially on decreasing κ_2 to up to 50% of κ_1, but then it suddenly becomes progressively less twisted with a further decrease of κ_2. Finally the system loses its twisted structure at $\kappa_2 = 1$ where a normal nematic phase is formed. The agreement between the numerical and the analytical calculations is good only for small values of the dihedral angles and length-to-breath ratios of one of the segments. The consequence of these findings is that the Frank analysis can be adequately applied only for molecules which are weakly chiral. Finally we turn to the issue of the effect of the intramolecular segment-segment distance on the helical structure using the approximation of perfect orientational planar order. It is easy to explain that a stronger twist is necessary along the helical axis if the segments are brought closer for a given dihedral angle. The reason for this is that though the molecules have to rotate through a similar angle as before to minimize the excluded area, they have to do so over a shorter distance. No bulk helical structure is possible for $\Delta = 0$, because the molecule is not chiral in this limit. As a result of these opposing effects there must be a system with $0 < \Delta^* < 2\sigma_0$, which will have the most twisted nematic structure. The numerical solution of Eq. (9) supports this expectation and the results of the calculations are presented in Fig. 7 for $\kappa = 5$ and $\kappa = 10$. The maximum value of the wave number is located for values of Δ of about a quarter of the particle diameter, but this depends markedly on the dihedral angle. It is interesting to note that the helical structure exhibits a dependence on the length-to-breath ratio for low values of intramolecular segment-segment separation ($\Delta^* < 1$) so that the molecules with shorter segments are seen to be more twisted than those with longer ones.

In order to assess the adequacy of the perfect order approximation (cf. Eq. (4)) we have performed a bifurcation analysis together with free energy calculations to locate the position of the isotropic-chiral nematic transition and determine the packing fraction dependence of the helical structure. By solving Eqs. (15) and (16) we have determined the bifurcation packing fraction (η_{bif}) and the bifurcation wave number (q_{bif}). With these two quantities the lower bound of stability of the ordered phase and the extent of twist at the ordering transition can be determined. The results of the bifurcation analysis are presented in Fig. 8 for the intramolecular segment separation of $\Delta^* = 1$. The most important feature is that the stability of the chiral nematic phase can be enhanced significantly by increasing the length-to-breath ratio which is a well-known characteristic of the rod-like systems. Another observation is that an increase in the intramolecular segment dihedral angle does not affect the lower boundary of stability of the twisted nematic phase to any significant degree, but it induces a phase transition between an isotropic and a chiral nematic phase for $\alpha > 0$, while an isotropic-nematic transition is observed for $\alpha = 0$. The bifurcation wave number is found to depend linearly on the dihedral angle up to very high angles (corresponding to the correlation $q^*_{bif} = 0.7792\alpha$). The results for the perfect order approximation are in very good agreement with those of the bifurcation analysis, which indicates that the incorporation of orientational degrees of freedom will only have a small effect on the wave number of the twist. In the case of non equal molecular segments ($\kappa_1 \neq \kappa_2$), the range of stability of the isotropic-chiral nematic phase transition is very sensitive to the shape anisotropy as can be seen in Fig. 9 (a). As one of the segments of the HGO molecule becomes more and more spherical, the packing fraction of the isotropic-chiral nematic phase boundary increases, i.e., the region of the chiral nematic phase is shifted to higher density. This is in agreement with the fact that a decrease in the shape anisotropy will lead to a destabilization of the liquid crystalline phase. As it can be seen in Fig. 9 (a) the dihedral angle only has a small effect on the phase boundary as the ordering tendency of both segments does not change with the dihedral angle. In Fig. 9 (b) we show that isotropic-nematic transition takes place only in the achiral limit of $\kappa_2 = 1$ as in this case the bifurcation wave number is zero for any dihedral angle. With increasing shape anisotropy of one of

the segments the wave number of the phase transition increases quickly; this dependence becomes very weak as the anisotropy of the segment reaches a certain value. This occurs roughly for a shape anisotropy at which a stable nematic phase would form for a system of HGO particles. Furthermore, it is clear from Fig. 9 (b) that the results obtained with the perfect order approximation (dashed curves) are very close to those for the freely rotating case (continuous curves), i.e,. the bifurcation wave number is not sensitive to the approximation used for the orientational degrees of freedom.

Up to this point we have not performed a thorough stability analysis of the chiral nematic phase with respect to the isotropic and nematic phases. To determine which phase is the most stable at given packing fraction the free energies of all phases are determined by solving Eq. (14). It is found in all cases that the free energy of the chiral nematic phase is the lowest for densities above the bifurcation point as long as the molecules are chiral. This is demonstrated with two examples for systems differing only in the intramolecular segment dihedral angle in Fig. 10. It can be seen that for the molecules characterised by a weaker microscopic chirality, the difference between the free energies of the nematic and chiral nematic phases is very small up to a very high nematic order of $\left(S = \int_0^{2\pi} h(\varphi)\cos(2\varphi)d\varphi \right) = 0.9$, and the bifurcation to the ordered phase take place at almost the same packing fraction. However, the second system with a greater molecular chirality behaves in a different way, as the nematic phase is seen to bifurcate from the isotropic phase at a significantly higher packing fraction than that of chiral nematic phase; differences in the free energies are significant even close to the isotropic-nematic bifurcation point. The reason for this is due to the large dihedral angle since the (artificial) ordering of the molecules with their different segments in one direction gives rise to a large cost in terms of excluded volume as the arrangement with different segments in opposite directions would be preferred. Changing the helical direction of the two molecular segments from a parallel arrangement will reduce the excluded volume and stabilize the ordered phase at lower packing fractions. This is also the reason why the bifurcation packing fraction of the isotropic-chiral nematic phase is not very sensitive to the dihedral angle. In all cases the isotropic-chiral nematic phase transition is found to be second order as the order parameter goes to

zero continuously at the bifurcation point (see the inset of Fig. 10), and apart from at the bifurcation point no common tangent can be constructed between the free energy densities of the isotropic and chiral nematic phases. As far as the helical structure of the bulk chiral nematic phase is concerned, the wave number is plotted as a function of the packing fraction in Fig. 11 for both systems. The strongly chiral system is about three times more twisted than the weakly chiral system. The systems do not appear to exhibit a strong dependence on the packing fraction; a slight dependence can be seen in the inset in which we show the behaviour for a dihedral angle of $\alpha = 30°$ where starting from the bifurcation point the wave number first decreases, exhibits a minimum at around $\eta = 0.18$, and then increases with increasing packing fraction. This tendency can also be observed for weak chiralities ($\alpha = 10°$), but the change in the wave number is even less marked. This kind of density dependence has not been observed in hard-core models of sterically chiral molecules such as twisted ellipsoid [51], threaded hard rod [36,44] or corkscrew [60] models. To assess the adequacy of the perfect order approximation, the wave number obtained from Eq. (9) are also shown in Fig. 11. As can be seen the wave number is found to be constant at any density and is very close to the wave number determined for the freely rotating case. Finally in Fig. 12 we present the effect of varying the segment anisotropy on the order parameter-packing fraction and wave number-packing fraction dependencies obtained from the minimization of the free energy (cf. Eq. (14)). As before the free energy of the chiral nematic phase is always less than that of nematic phase if the molecule is chiral. The order parameter curves suggest that decreasing the shape anisotropy of one of the segments has an effect not only on the location of the bifurcation point but also on the degree of ordering at a given density, as the molecules are less anisotropic are less ordered. The wave number is affected by the value of κ_2 as it decreases with increasing packing fraction. There is a linear decrease in the wave number with density, but the slope increases with decreasing shape anisotropy (see lower panel of the Fig. 12). It can also be seen that the perfect planar order leads to an underestimate in the wave number with decreasing shape anisotropy of one of the segments and it does not take into account the density dependence.

5. Conclusion

We have considered a simple steric molecular model for chiral liquid crystals. The representation is an extension of hard-body models of the nematic phase constructed by fusing two uniaxial hard bodies with a relative twist between the long axes of the segments. The hard Gaussian overlap (HGO) potential is used to represent the interaction between the segments of the chiral molecules to isolate the link between the shape chirality and the bulk properties of the chiral nematic phase. The electrostatic and other dispersive interactions are not included in the model to avoid complicating the analysis due to collective effects of the different types of chiralities. The Parsons-Lee extension of the Onsager theory is used to describe the isotropic, nematic, and chiral nematic (cholesteric) phases of system. To simplify the calculations and at the same time to capture the key physical factors that influence the ordering phenomena we have used several approximations for the orientational distribution function. We have assumed that the long axes of the HGO segments that make up the chiral molecules are constrained to stay in the plane normal to the helical axis. Moreover no internal rotation is allowed around the symmetry axis of the molecule. In this way the molecules are allowed to rotate freely only in the direction normal to the helical axis and the vector connecting the centres the two molecular HGO segments is always parallel to the helical axis. Two types of single particle orientational distribution functions have been introduced to account for the orientational ordering and helical structure inherent in chiral liquid crystals. In the simplest approximation the particles are perfectly aligned in the planes but they twist in a linear fashion in the direction of helical axis. In the second approximation a trial function has been introduced for the representation of the orientational distribution function which is able to describe isotropic, nematic, and chiral nematic phases. Moreover it gives the exact bifurcation densities and wave numbers of the

orientational ordering transitions. Both approximations have proved to be very useful in the determination of the structure and stability of the phases. The first approximation allows one to obtain analytical equations which relate the wave number of the twisted nematic phase and the molecular properties such as the intramolecular segment dihedral angle and length-to-breath ratios. The second approximation gives rise to two coupled equations for the wave number and variational parameter which makes it possible to determine the phase boundaries and the order parameter of the nematic phases.

From our findings it is clear that the intramolecular dihedral angle (between the two HGO segments) is the only chiral parameter which determines the handedness of the molecules and the bulk phases; the two other chiral parameters, the asymmetry in the shape anisotropy of the HGO segments and the intramolecular distance between the two HGO segments, only have an effect on the wave number of the twisted phase. The wave number is found to depend linearly on the intramolecular segment dihedral angle in all cases, i.e., the handedness of the phase is determined by the sign of the dihedral angle and no twist takes place in the achiral limit of $\alpha = 0$. Decreasing the shape anisotropy of one of the molecular segments does not effect the helical structure substantially up to a weakly anisotropic particle shape, and then the wave number rapidly drops to zero (untwisted structure) in the limit of an achiral shape ($\kappa_2 = 0$). The relation between macroscopic twist and the intramolecular segment-segment distance is more complicated between the achiral ($\Delta = 0$) and the larger separation limits, but in all cases the twist reaches a maximum value at a segment-segment separation close to a quarter of the segment diameter. The free energy calculations reveal that the isotropic-nematic transition is always metastable with respect to isotropic-chiral nematic transition for chiral molecules, the latter only being stable in the achiral limits. Interestingly the pitch depends very weakly on density for molecules with identical HGO segments, but it increases linearly with the density as the shape anisotropy of the one of the segments is decreased. It is also shown that the difference between the numerically obtained free energy and the second order Frank free energy

increases with increasing molecular chirality to such an extent that the Frank expression for the wave number cannot be applied for a molecular twist above $\alpha \sim 5°$.

The effect of higher order (cosine) terms in the orientational distribution function and the case of complete 3D rotational degrees of freedom are not considered in our current work. It would be desirable to see unambiguously the packing fraction dependence of the helical wave number. In addition it would of interest to explore the impact of other types of steric chiralities such as single and double helices, on the macroscopic chirality. In this way it would be possible to determine the separate roles of steric and electrostatic chiralities in the helical structure of chiral macromolecules such as DNA, or viral systems, where both types of chiralities are present. We leave this for future work.

Acknowledgements

We are both grateful to the Royal Society for the award of an International Short Visit grant which has facilitated our collaborative work. Additional funding to the Molecular Systems Engineering Group from the Engineering and Physical Sciences Research Council (EPSRC) of the UK (grants GR/T17595, GR/N35991, GR/R09497, and EP/E016340), the Joint Research Equipment Initiative (JREI) (GR/M94427), and the Royal Society-Wolfson Foundation refurbishment grant is also acknowledged.

References

[1] S. Chandrasekhar, *Liquid Crystals*, 2nd ed. (Cambridge University Press, Cambridge, 1992).

[2] P.-G. de Gennes and J. Prost, *The Physics of Liquid Crystals*, 2nd ed. (Oxford University Press, Oxford, 1993).

[3] A. B. Harris, R. D. Kamien, and T. C. Lubensky, Phys. Rev. Lett., 78, 1476 (1997).

[4] T. C. Lubensky, A. B. Harris, R. D. Kamien, and G. Yan, Ferroelectrics, **212**, 1 (1998).

[5] A. B. Harris, R. D. Kamien, and T. C. Lubensky, Rev. Mod. Phys., **71**, 1745 (1999).

[6] Z. Dogic, S. Fraden, Langmuir, 16, 7820 (2000).

[7] E. Grelet, S. Fraden, Phys. Rev. Lett., **90**, 198302 (2003).

[8] Z. Dogic, S. Fraden, Curr. Opinion Coll. Inter. Sci., **11**, 47 (2006).

[9] M. Born, Sits. Phys. Maths., **25**, 614 (1916).

[10] M. Born, Ann. Phys. **55**, 221 (1918).

[11] W. Maier and A. Saupe, Z. Naturforsch., **13a**, 564 (1958).

[12] W. Maier and A. Saupe, Z. Naturforsch., **14a**, 882 (1959).

[13] W. Maier and A. Saupe, Z. Naturforsch., **15a**, 287 (1960).

[14] L. D. Landau, Phys. Z Sowjetunion, **11**, 26 (1937); reprinted in *Collected Papers of L.D. Landau* , ed. D. ter Haar (Pergamon Press, Oxford, 1965), pp. 193–216.

[15] P.-J. de Gennes, Phys. Lett. A, **30**, 454 (1969).

[16] P.-J. de Gennes, Solid State Comm., **10**, 753 (1972).

[17] L. Onsager, Phys. Rev., **62**, 558 (1942).

[18] L. Onsager, Ann. N.Y. Acad. Sci., **51**, 627 (1949).

[19] D. Frenkel and R. Eppenga, Phys. Rev. Lett., **49**, 1089 (1982).

[20] R. Eppenga and D. Frenkel, Mol. Phys. **52**, 1303 (1984).

[21] D. Frenkel and B. M. Mulder, Mol. Phys. **55**, 1171 (1985).

[22] A. Samborski, G. T. Evans, C. P. Mason, and M. P. Allen, Mol. Phys. **81**, 263 (1994).

[23] D. Frenkel, J. Phys. Chem., **91**, 4912 (1987).

[24] D. Frenkel, H. N. W. Lekkerkerker, and A. Stroobants, Nature, **332**, 822 (1988).

[25] S. C. McGrother, D. C. Williamson, and G. Jackson, J. Chem. Phys., **104**, 6755 (1996).

[26] P. G. Bolhuis and D. Frenkel, J. Chem. Phys., **106**, 666 (1997).

[27] D. C. Williamson and G. Jackson, J. Chem. Phys., **108**, 10294 (1998).

[28] S.C. McGrother, A. Gil-Villegas, and G. Jackson, J. Phys.: Condens. Matter, **8**, 9649 (1996).

[29] A. Gil-Villegas, S. C. McGrother, and G. Jackson, Chem. Phys. Lett., **269**, 441 (1997).

[30] A. Gil-Villegas, S. C. McGrother, and G. Jackson, Mol. Phys., **92**, 723 (1997).

[31] S. C. McGrother, A. Gil-Villegas, and G. Jackson, Mol. Phys., **95**, 657 (1998).

[32] J. S. van Duijneveldt, A. Gil-Villegas, G. Jackson, and M. P. Allen, J. Chem. Phys. **112**, 9092

(2000).

[33] W. J. A. Goossens, Mol. Cryst. Liquid Cryst., **12**, 237 (1970).

[34] R. G. Priest and T. C. Lubensky, Phys. Rev. A, **9**, 893 (1974).

[35] A. Wulf, J. Chem. Phys. **60**, 3994 (1974).

[36] J. P. Straley, Phys. Rev. A, **14**, 1835 (1976).

[37] B. W. van der Meer, G. Vertogen, A. J. Dekker, and J. G. J. Ypma, J. Chem. Phys., **65**, 3935 (1976).

[38] Y. R. Lin-Liu, Y. M. Shih, and C. W. Woo, Phys. Rev. A, **15**, 2550 (1977).

[39] H. Kimura, M. Hosino, and H. Nakano, J. Phys. Soc. Jpn., **51**, 1584 (1982).

[40] Y. R. Lin-Liu and M. A. Lee, Phys. Rev. A, **28**, 2580 (1983).

[41] A. N. Zakhlevnykh and M. I. Shliomis, Zh. Eks. Teo. Fiz., **86**, 1309 (1984).

[42] M. Nakagawa, Mol. Cryst. Liq. Cryst., **130**, 349 (1985).

[43] M. A. Osipov, Chem. Phys., **96**, 259 (1985).

[44] T. Odijk, J. Phys. Chem., **91**, 6060 (1987).

[45] W. J. A. Goossens, Phys. Rev. A, **35**, 1843 (1987).

[46] M. A. Osipov, Khi. Fiz., **6**, 1312 (1987).

[47] M. A. Osipov, Nuovo Cimento Soc Ita. Fis D., **10**, 1249 (1988).

[48] M. Nakagawa, Liq. Cryst., **3**, 63 (1988).

[49] W. J. A. Goossens, Phys. Rev. A, **39**, 4888 (1989).

[50] W. J. A. Goossens, Phys. Rev. A, **40**, 4019 (1989).

[51] G.T. Evans, Mol. Phys., **77**, 969 (1992).

[52] L. Varichon and A. Tenbosch, Macromolecules, **25**, 3812 (1992).

[53] L. Varichon and A. Tenbosch, Liq. Cryst., **14**, 1635 (1993).

[54] M. P. Allen, Phys. Rev. E, **47**, 4611 (1993).

[55] M. P. Allen and A. J. Masters, Mol. Phys., **79**, 277 (1993).

[56] R. Memmer, H.-G. Kuball, and A. Schönhofer, Liq. Cryst., **15**, 345 (1993).

[57] T. Sato, Y. Sato, Y. Umemura, A. Teramoto, Y. Nagamura, J. Wagner, D. Weng, Y. Okamoto, K. Hatada, and M. M. Green, Macromolecules, **26**, 4551 (1993).

[58] M.A. Osipov, B.T. Pickup, and D.A. Dunmur, Mol. Phys., **84**, 6 (1995); ibid. **84**, 1193 (1995).

[59] T. Koda and H. Kimura, J. Phys. Soc. Jpn., **65**, 2880 (1996).

[60] R. A. Pelcovits, Liq. Cryst., **21**, 361 (1996).

[61] R. Memmer, H.-G. Kuball, and A. Schönhofer, Mol. Phys., **89**, 1633 (1996).

[62] A. Ferrarini, G. J. Moro, and P. L. Nordio, Phys. Rev. E, **53**, 681 (1996).

[63] P. J. Camp, Mol. Phys., **91**, 381 (1997).

[64] J. Saha and M. Saha, Mol. Sim., **19**, 227 (1997).

[65] A. A. Kornyshev and S. Leikin, J. Chem. Phys., **107**, 3656 (1997).

[66] T. Sato, J. Nakamura, A. Teramoto, and M. M. Green, Macromolecules **31**, 1398 (1998).

[67] R. Berardi, H.-G. Kuball, R. Memmer, and C. Zannoni, J. Chem. Soc. Faraday Trans., **94**, 1229 (1998).

[68] R. Memmer and F. Janssen, J. Chem. Soc. Faraday Trans., **94**, 267 (1998).

[69] R. Memmer and F. Janssen, Liq. Cryst., **24**, 805 (1998).

[70] R. Memmer, Ber. Buns. Ges. - Phys. Chem. Chem. Phys., **102**, 1002 (1998).

[71] L. Hu, Y. Jiang, T. D. Lee, and R. Tao, Phys. Rev. E, **57**, 4289 (1998).

[72] R. Memmer, Liq. Cryst., **27**, 533 (2000).

[73] A. V. Emelyanenko, M. A. Osipov, and D. A. Dunmur, Phys. Rev. E, **62**, 2340 (2000).

[74] A. A. Kornyshev and S. Leikin, Phys. Rev. Lett., **84**, 2537 (2000).

[75] A. A. Kornyshev and S. Leikin, Phys. Rev. E, **62**, 2576 (2000).

[76] M. A. Osipov and H.-G. Kuball, Eur. Phys. J. E, 5, 589 (2001).

[77] R. Memmer, J. Chem. Phys., **114**, 8210 (2001).

[78] J. Xu, R. L. B. Selinger, J. V. Selinger, and R. Shashidhar, J. Chem. Phys., **115**, 4333 (2001).

[79] M. P. Allen and A. J. Masters, Mater. Chem., **11**, 2678 (2001).

[80] G. Germano, M. P. Allen, and A. J. Masters, J. Chem. Phys., **116**, 9422 (2002).

[81] S. J. Johnston, R. J. Low, and M. P. Neal, Phys. Rev. E, **65**, 051706 (2002).

[82] A. A. Kornyshev, S. Leikin, and S. V. Malinin, Eur. Phys. J. E, **7**, 83 (2002).

[83] Z. D. Zhang, Z. G. Li, and J. L. Liu, Mod. Phys. Lett. B, **16**, 721 (2002).

[84] A. Kapanowski, Z. Naturforsch. A, **57**, 105 (2002).

[85] A. V. Emelyanenko, Phys. Rev. E, **67**, 031704 (2003).

[86] S. Varga and G. Jackson, Chem. Phys. Lett., **377**, 6 (2003).

[87] M. P. Neal, M. Solymosi, M. R. Wilson, and D. J. Earl, J. Chem. Phys., **119**, 3567 (2003).

[88] R. Berardi, M. Cecchini, and C. Zannoni, J. Chem. Phys., **119**, 9933 (2003).

[89] Y. Huh, and N. M. Cann, J. Chem. Phys., **121**, 10299 (2004).

[90] F. Tombolato and A. Ferrarini, J. Chem. Phys., **122**, 054908 (2005).

[91] F. Tombolato, A. Ferrarini, and E. Grelet, Phys. Rev. Lett., **96**, 258302 (2006).

[92] H. Kamberaj, R. J. Low, and M. P. Neal, Mol. Phys., **104**, 335 (2006).

[93] S. Varga and G. Jackson, Mol. Phys., **104**, 3681 (2006).

[94] H. H. Wensink and G. Jackson, J. Chem. Phys., **130**, 234911 (2009).

[95] E. O. Yewande, M. P. Neal, R. J. Low, Mol. Phys., **107**, 281 (2009).

[96] S. Dhakal and J. V. Selinger, to be published (2011).

[97] H. H. Wensink and G. Jackson, J. Phys.: Condens. Matter, in press (2011).

[98] J. D. Parsons, Phys. Rev. A, **19**, 1225 (1979).

[99] S. D. Lee, J. Chem. Phys., **97**, 4972 (1987).

[100] J. G. Gay and B. J. Berne, J. Chem. Phys., **74**, 3316 (1981).

[101] G. J. Vroege and H. N. W. Lekkerkerker, Rep. Prog. Phys., **55**, 1241 (1992).

[102] M. Franco-Melgar, A. J. Haslam, and G. Jackson, Mol. Phys., **106**, 649 (2008).

[103] A. Malijevský , G. Jackson, and S. Varga, J. Chem. Phys., **129**, 144504 (2008).

[104] M. Franco-Melgar, A. J. Haslam, and G. Jackson, Mol. Phys., **107**, 2329 (2009).

[105] R. Evans, Adv. Phys., **28**, 143 (1979).

[106] R. Evans, *Density functionals in the theory of nonuniform fluids*, in *Fundamentals of Inhomogeneous Fluids*, Edited by D. Henderson (Dekker, New York, 1992).

[107] M. M. Telo da Gama, P. Tarazona, M. P. Allen, and R. Evans, Mol. Phys., **71**, 801 (1990).

[108] R. van Roij, M. Dijkstra, and R. Evans, Euro. Phys. Lett., **49**, 350 (2000).

[109] M. Dijkstra, R. van Roij, and R. Evans, Phys. Rev. E, **63**, 051703 (2001).

[110] B. J. Berne and P. Pechukas, J. Chem. Phys., **56**, 4213 (1972).

[111] V. R. Bhethanabotla and W. A. Steele, Mol. Phys., **60**, 249 (1987).

[112] P. Padilla and E. Velasco, J. Chem. Phys., **106**, 10299 (1997).

[113] D. J. Cleaver, C. M. Care, M. P. Allen, and M. P. Neal, Phys. Rev. E, **54**, 559 (1996).

[114] C. B. Stanley, H. Hong, and H. H. Strey, Biophys. J., **89**, 2552 (2005).

Figures

Figure 1)

Top view and side views of a chiral two-segment HGO particle. The intramolecular segment dihedral angle is $\alpha = 30°$, the segment length-to-breadth ratio is $\kappa = 3$, and the intramolecular segment-segment separation is $\Delta = \sigma_0$, where σ_0 is the segment breadth.

Figure 2)

Side views of four achiral two-site HGO particles with α the intramolecular segment dihedral angle, κ the segment length-to-breadth ratio, and Δ the intramolecular segment-segment separation: a) $\alpha = 90°$ for $\kappa = 3$ and $\Delta = \sigma_0$; b) $\alpha = 0°$ for $\kappa = 3$ and $\Delta = \sigma_0$; c) $\alpha = 30°$ for $\kappa = 3$ and $\Delta = 0$; and d) $\alpha = 30°$ for $\kappa_2 = 1$, $\kappa_1 = 3$, and $\Delta = \sigma_0$, where σ_0 is the segment breadth.

Figure 3)

Excluded area of the most favorable configuration for the chiral two-segment HGO particle (with α the intramolecular segment dihedral angle, κ the segment length-to-breadth ratio, and Δ the intramolecular segment-segment separation) and the corresponding twist angle as a function of distance along the helical axis chosen as a z axis for α = 10°, κ = 10 and $\Delta^* = 2$. In lower panel the horizontal dashed segments indicate the most favourable twist angles, while the continuous line is a guide to the eye which is given by $\gamma = \frac{\alpha}{2} z^*$. The excluded area and the distances are in dimensionless unit: $A^*_{exc} = A_{exc} / \sigma_0^2$, $\Delta^* = \Delta / \sigma_0$ and $z^* = z / \sigma_0$, where σ_0 is the segment breadth.

Figure 4)

Excluded area of a chiral two-segment HGO particle (with α the intramolecular segment dihedral angle, κ the segment length-to-breadth ratio, and Δ the intramolecular segment-segment separation) as a function of distance along the direction of helical axis chosen as a z axis for different value of wave number (q) for $\alpha = 10°$ and $\kappa = 10$: a) q^* = 0.1 (dashed), 0.2 (continuous) and 0.3 (short dashed) for $\Delta^* = 0.5$ b) q^*=0.05 (dashed), 0.2 (continuous) and 0.3 (short dashed) for Δ^*=0.75, c) q^*=0.05 (dashed), 0.15 (continuous) and 0.25 (short dashed) for Δ^*=1. The excluded area, centre-to-centre segment separation, distance along the helical axis, and wave number are in dimensionless units: $A^*_{exc} = A_{exc}/\sigma_0^2$, $\Delta^* = \Delta/\sigma_0$, $z^* = z/\sigma_0$, and $q^* = q\sigma_0$, where σ_0 is the segment breadth.

Figure 5)

The wave number $q = 2\pi/P$ (inverse pitch) of a system of chiral two-segment HGO particles as a function of: a) the intramolecular segment dihedral angle α; and b) the segment length-to-breath ratio κ are shown in the case of perfect 2D order for an intramolecular segment-segment separation of $\Delta^* = 2$. The continuous curves represent the results of numerical calculations (cf. Eq. (9)), while the dashed curves the results of the Frank analysis (cf. Eq. (21)). The numerically obtained pitches are depicted in the insets. The wave number and the pitch are in dimensionless units: $q^* = q\sigma_0$, $P^* = P/\sigma_0$, where σ_0 is the segment breadth.

Figure 6)

The effect of varying the length-to-breath ratio κ_2 of a segment for a system of chiral two-segment HGO particles (with α the intramolecular segment dihedral angle, and Δ the intramolecular segment-segment separation) on the helical period of the nematic nematic phase. a) The wave number $q = 2\pi/P$ (inverse pitch) is plotted as a function dihedral angle α for $\kappa_1 = 10$ and $\Delta^* = 2$. The values of κ_2 are indicated on the figure. b) The dependence of the wave number on the length-to-breath ratio κ_2 for some values of dihedral angle. The continuous curves correspond to numerically

obtained using Eq. (9), while the dashed curves are the results of the Frank analysis (cf. Eq. (22). In the insets we show the dependence of the pitch $P^* = P/\sigma_0$, where σ_0 is the segment breadth, as a function of the dihedral angle and κ_2 obtained with Eq. (9).

Figure 7)

The effect of varying the intramolecular segment-segment distance Δ of a system of chiral two-segment HGO particles (with α the intramolecular segment dihedral angle, and κ the segment length-to-breath ratio) on the helical structure of the chiral nematic phase in the case of dihedral angles of $\alpha = 5°$, 10° and 20° for different values of molecular elongations: a) $\kappa = 5$ and b) $\kappa = 10$. The curves are the results obtained with Eq. (9). In the inset we show the corresponding pitch $P^* = P/\sigma_0$ and a function of

Figure 8)

Dihedral angle α dependence of the bifurcation packing fraction η of the isotropic-chiral nematic phase transition for a chiral two-segment HGO system (with α the intramolecular segment dihedral angle, κ the segment length-to-breath ratio, and Δ the intramolecular segment-segment separation) with $\Delta^* = \Delta/\sigma_0 = 1$, where σ_0 is the segment breadth. The values of the aspect ratios are indicated on the curves. The results are obtained using Eqs. (15) and (16).

Figure 9)

The effect of varying the anisotropy of one of the segments (κ_2) on the bifurcation packing fraction η and wave number q of the isotropic-chiral nematic phase transition for a chiral two-segment HGO system (with α the intramolecular segment dihedral angle, κ the segment length-to-breadth ratio, and Δ the intramolecular segment-segment separation) with $\Delta^* = 2$ and $\kappa_1 = 5$. Values of the dihedral angle of $\alpha =$ 5°, 10°, and 20° are examined (from bottom to top in the figures). In a) the curves for

$\alpha = 5°$ and $\alpha = 10°$ cannot be distinguished at the current resolution. The curves are obtained with Eqs. (15) and (16). The dashed curves in b) represent the solutions of perfect order approximation (cf. Eq. 22). Dimensionless units are employed: $\Delta^* = \Delta/\sigma_0$ and $q^* = q\sigma_0$, where σ_0 is the segment breadth.

Figure 10)

The free energy density ($f^* = \beta F v_0 / V$) as a function of packing fraction η of the three different phases for a chiral two-segment HGO system (with α the intramolecular segment dihedral angle, κ the segment length-to-breadth ratio, and Δ the intramolecular segment-segment separation) with $\kappa = 10$ and $\Delta^* = \Delta/\sigma_0 = 1$, where σ_0 is the segment breadth. The values of the dihedral angle are $\alpha = 10°$ in a) and $\alpha = 30°$ in b). In the inset we represent the order parameter $\left(S = \int_0^{2\pi} h(\varphi)\cos(2\varphi)d\varphi \right)$ as a function of packing fraction for nematic and chiral nematic phases. The curves are the results of the free energy minimization of Eq. (14).

Figure 11)

The packing fraction η dependence of the wave number q of the chiral nematic phase for a chiral two-segment HGO system (with α the intramolecular segment dihedral angle, κ the segment length-to-breadth ratio, and Δ the intramolecular segment-segment separation) with $\kappa = 10$, $\Delta^* = 1$, $\alpha = 10°$ and $\kappa = 10$, $\Delta^* = 1$, $\alpha = 30°$. The continuous curves represent the results of the free energy minimization of Eq. (14), while the dashed curves are the results of Eq. (9). In the inset we highlight the density dependence of the wave number q for the system of $\kappa = 10$, $\Delta^* = 1$, $\alpha = 30°$. Dimensionless units are employed: $\Delta^* = \Delta/\sigma_0$ and $q^* = q\sigma_0$, where σ_0 is the segment breadth.

Figure 12)

The packing fraction η dependence of the order parameter $\left(S = \int_0^{2\pi} h(\varphi)\cos(2\varphi)d\varphi \right)$ and the wave number q of the twisted nematic phase for a chiral two-segment HGO system (with α the intramolecular segment dihedral angle, κ the segment length-to-breadth ratio, and Δ the intramolecular segment-segment separation) with $\kappa_1 = 5$, $\Delta^* = 2$, $\alpha = 30°$ for a varying anisotropy of the second segment κ_2. The curves are the results of the free energy minimization of Eq. (14), while the dashed curves are the results obtained with Eq. (9). The values of the segment anisotropy are κ_2 = 5, 3, 2, and 1.5 from left to right in a), and from top to bottom in b). Dimensionless units are employed: $\Delta^* = \Delta/\sigma_0$ and $q^* = q\sigma_0$, where σ_0 is the segment breadth.

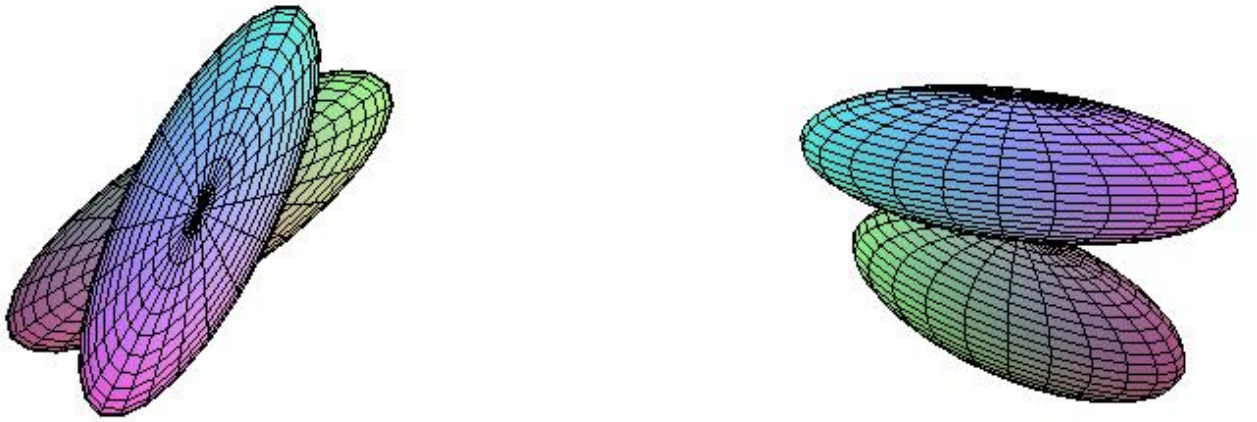

Figure 1.

a) b)

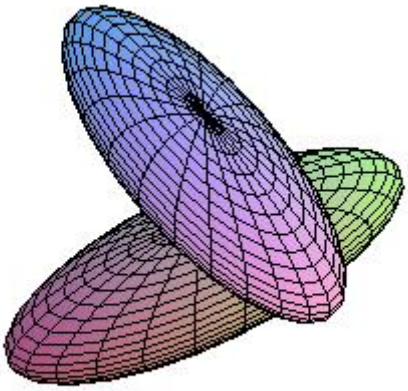

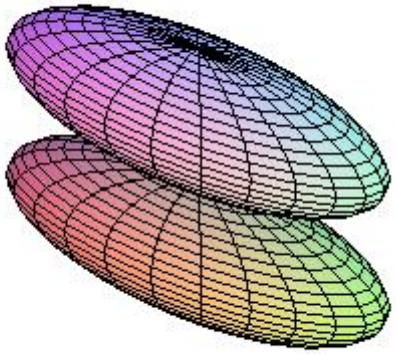

b)

c) d)

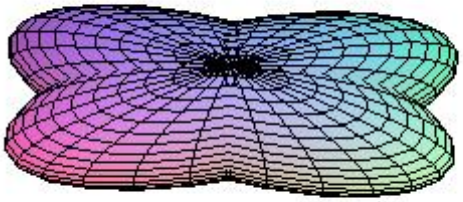

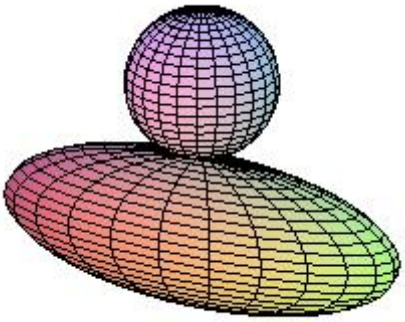

Figure 2.

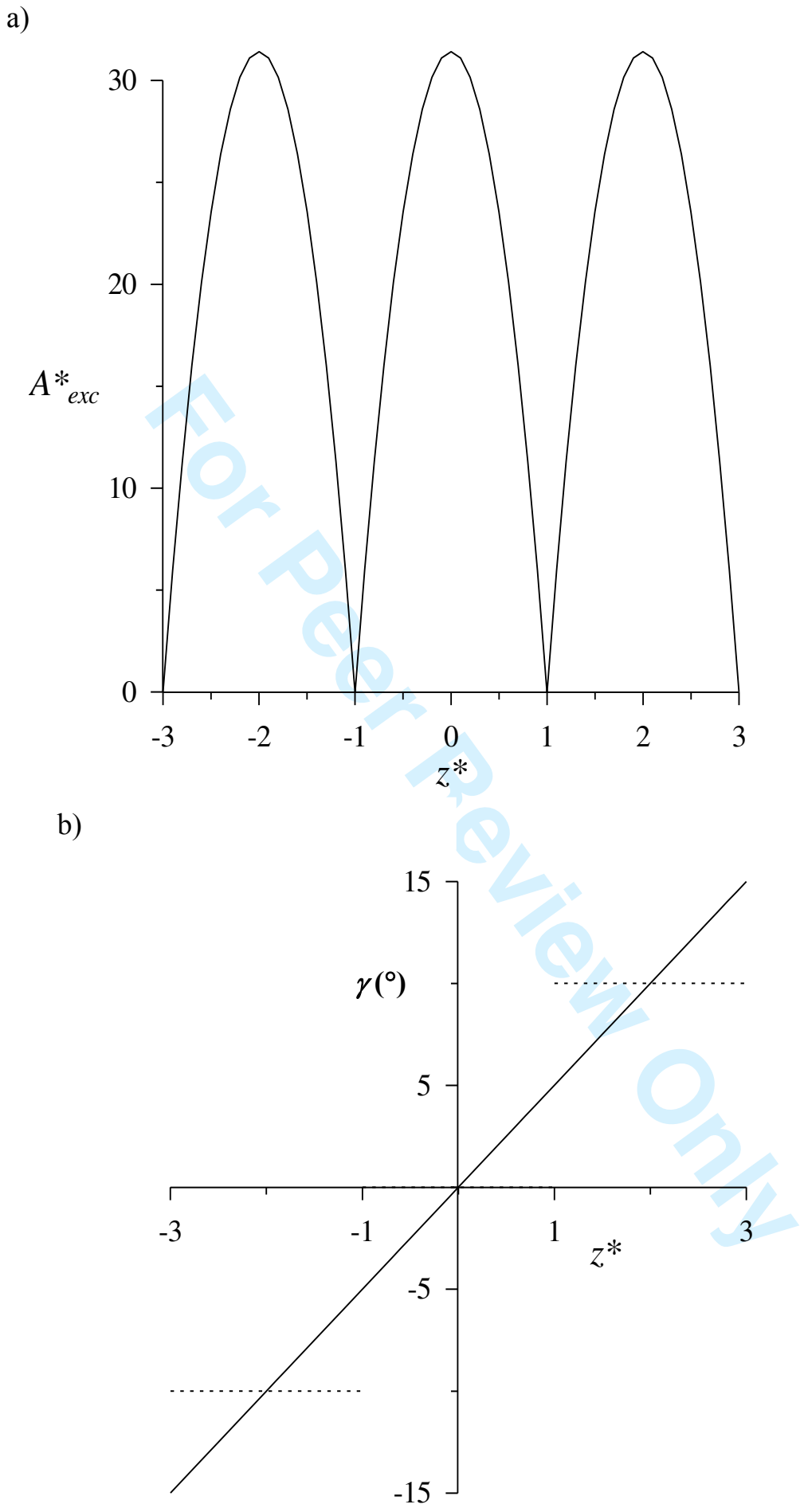

Figure 3

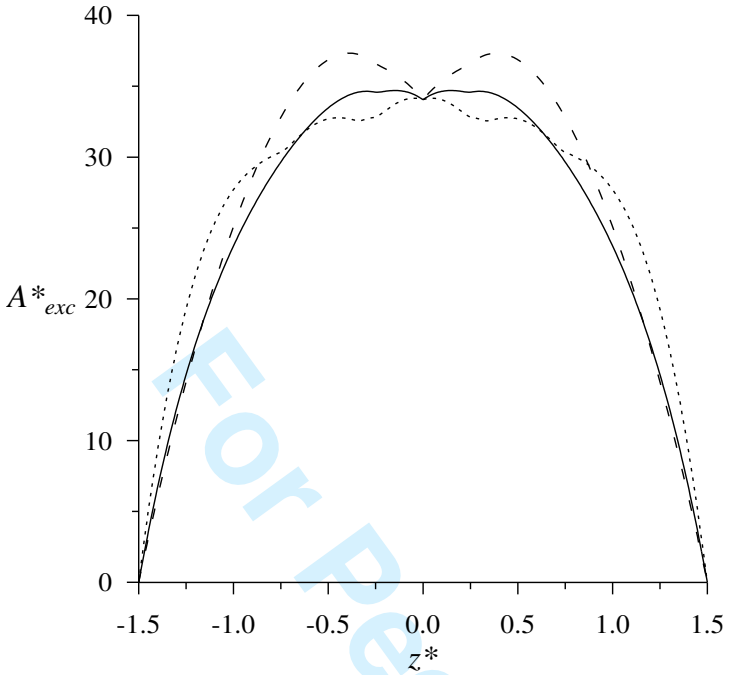

Figure 4 a)

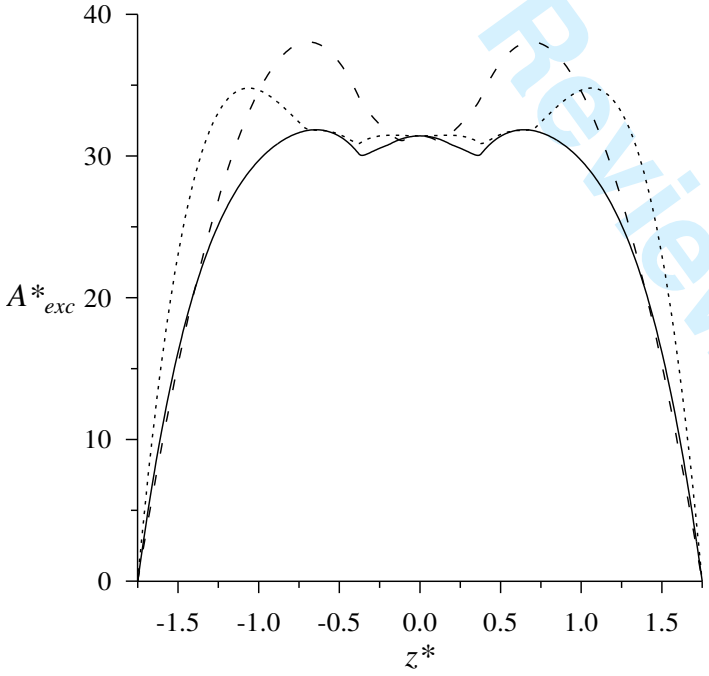

Figure 4 b)

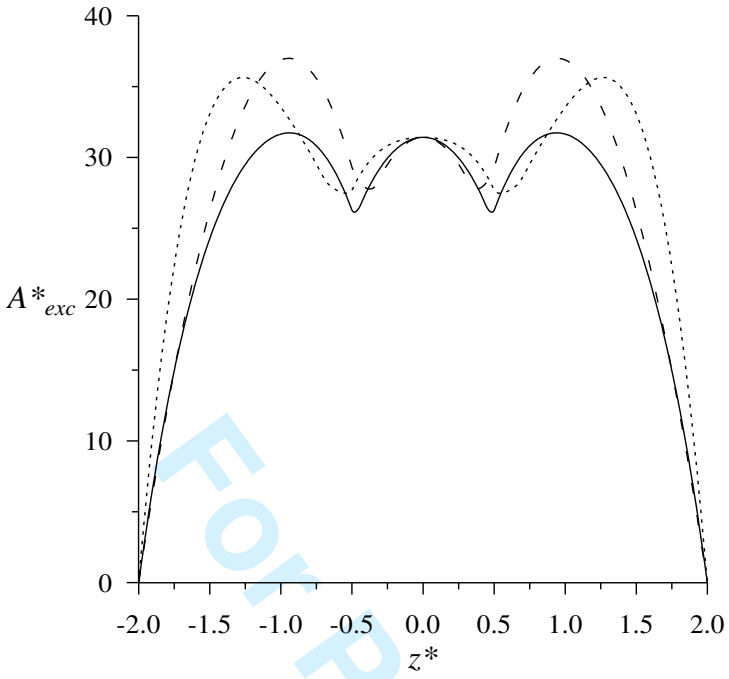

Figure 4 c)

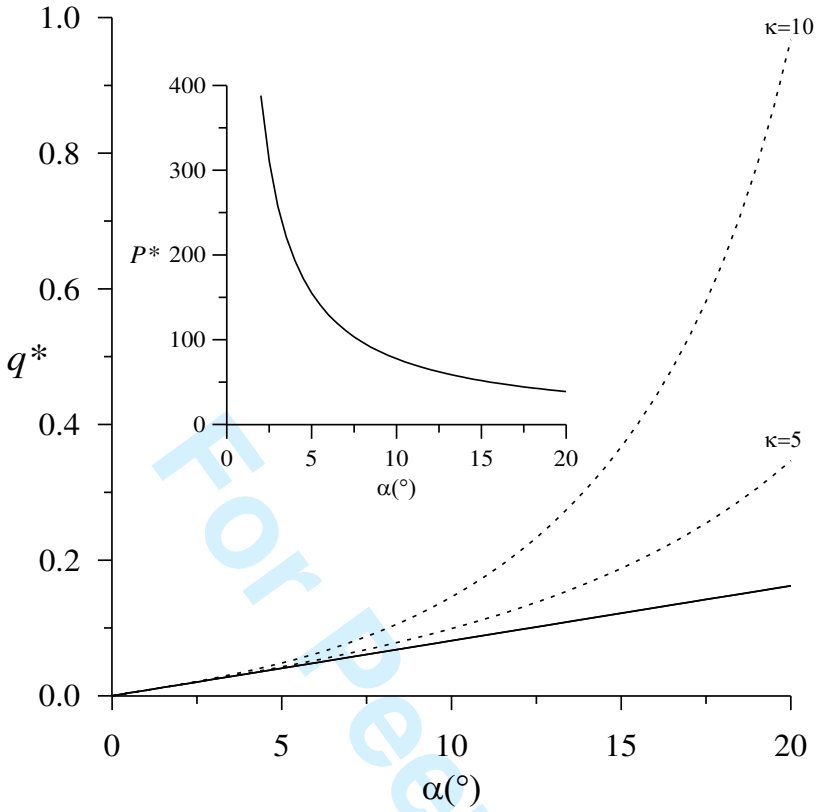

Figure 5 a)

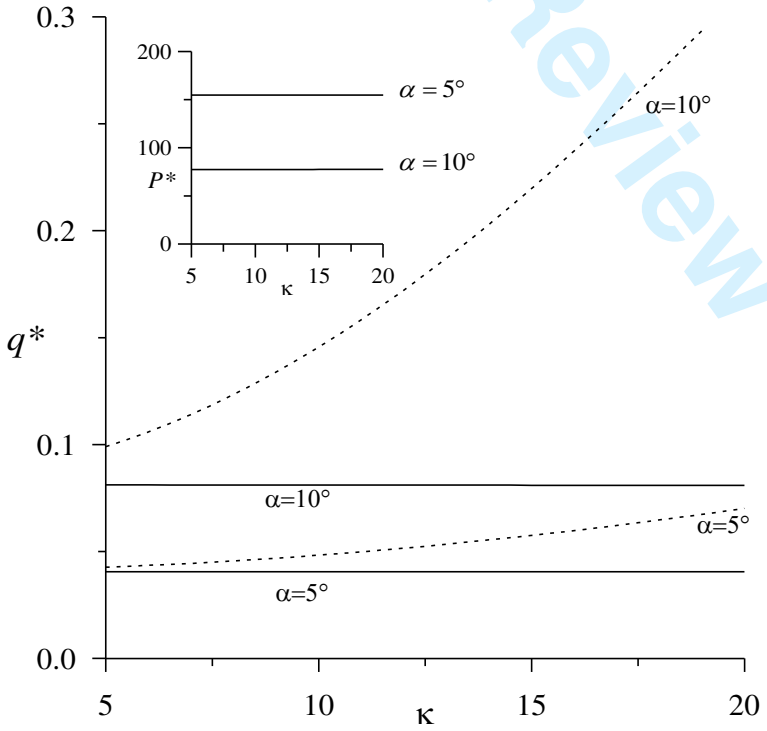

Figure 5 b)

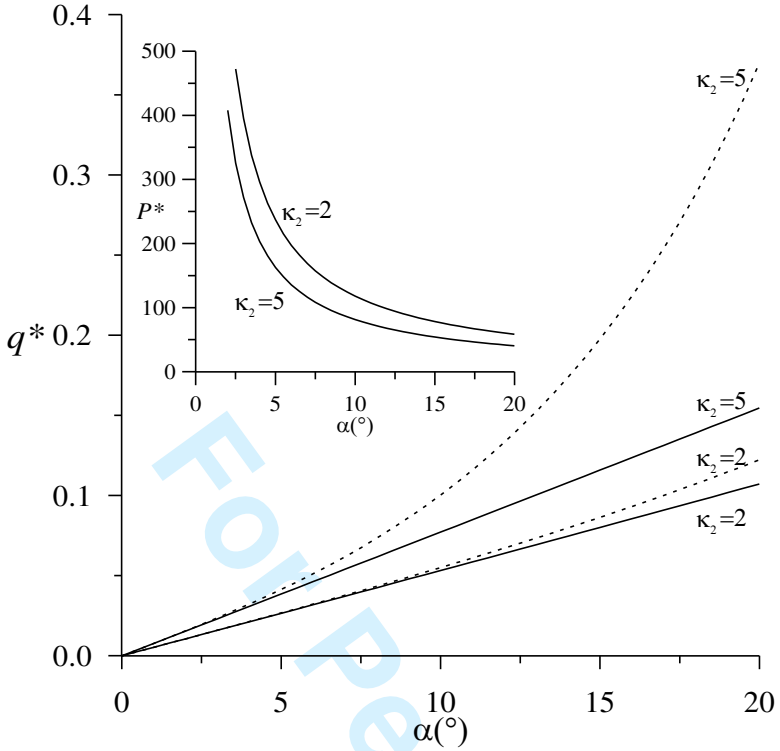

Figure 6 a)

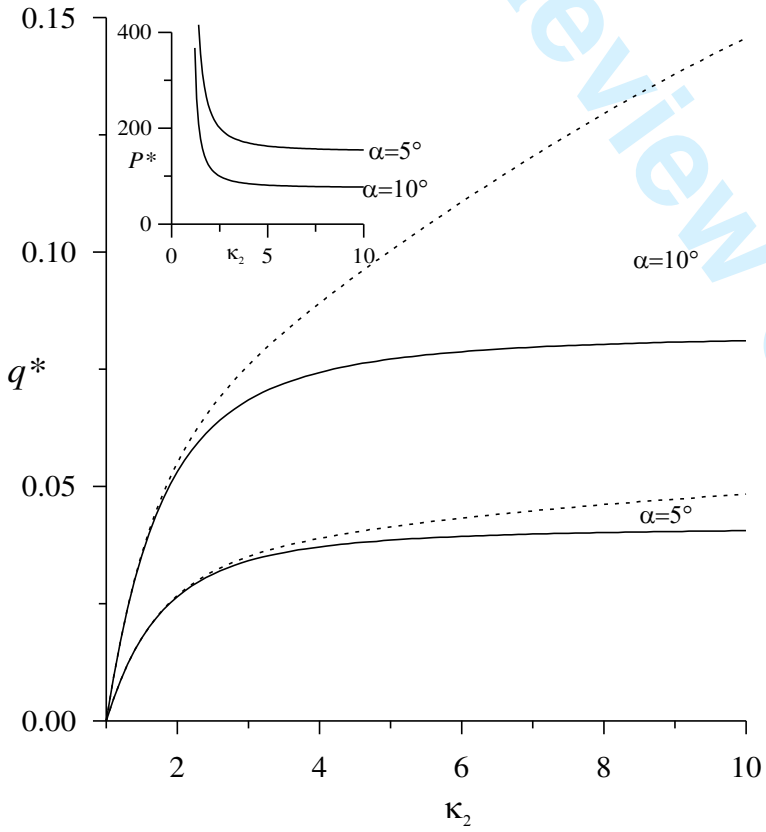

Figure 6 b)

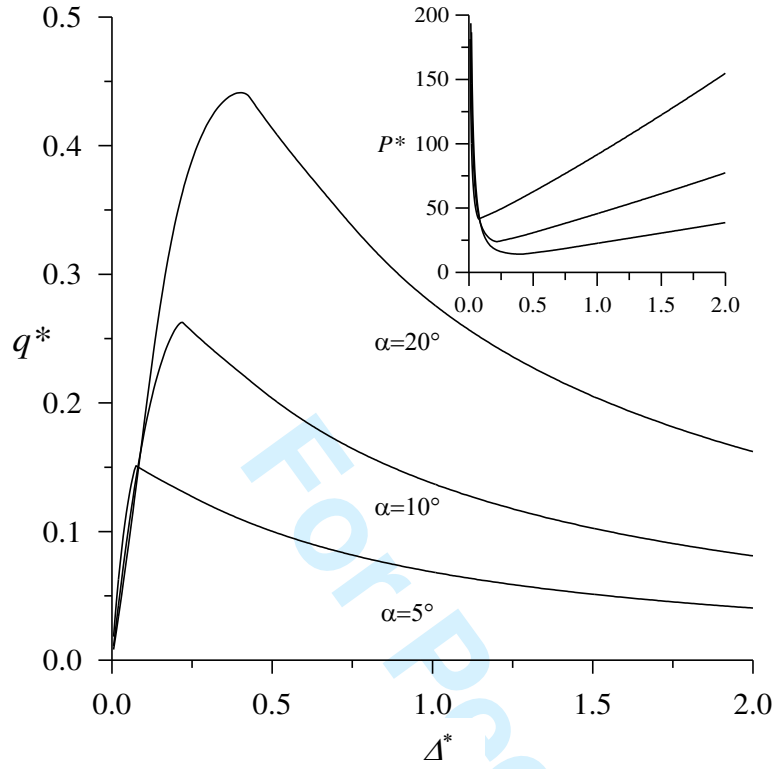

Figure 7 a)

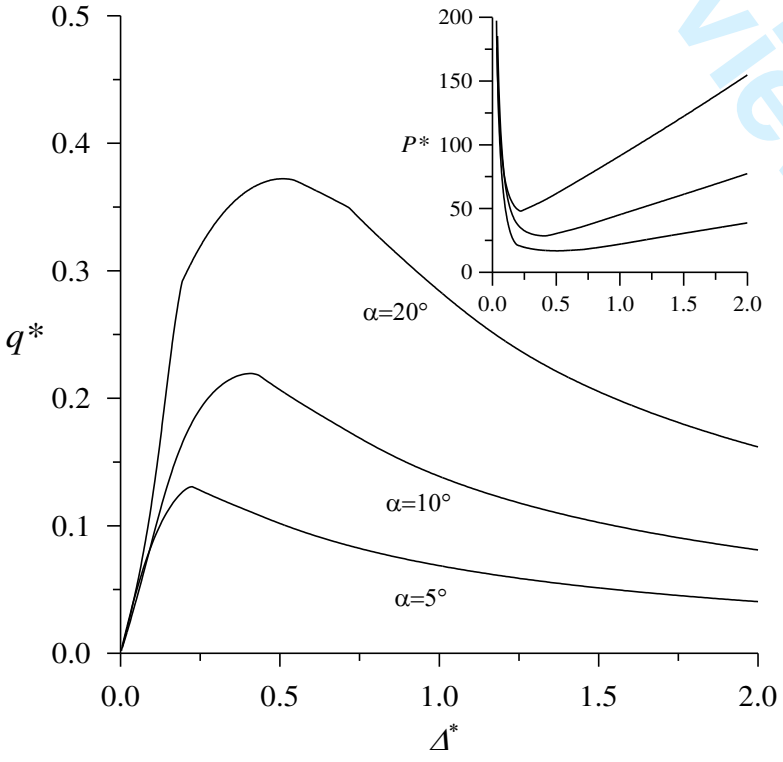

Figure 7 b)

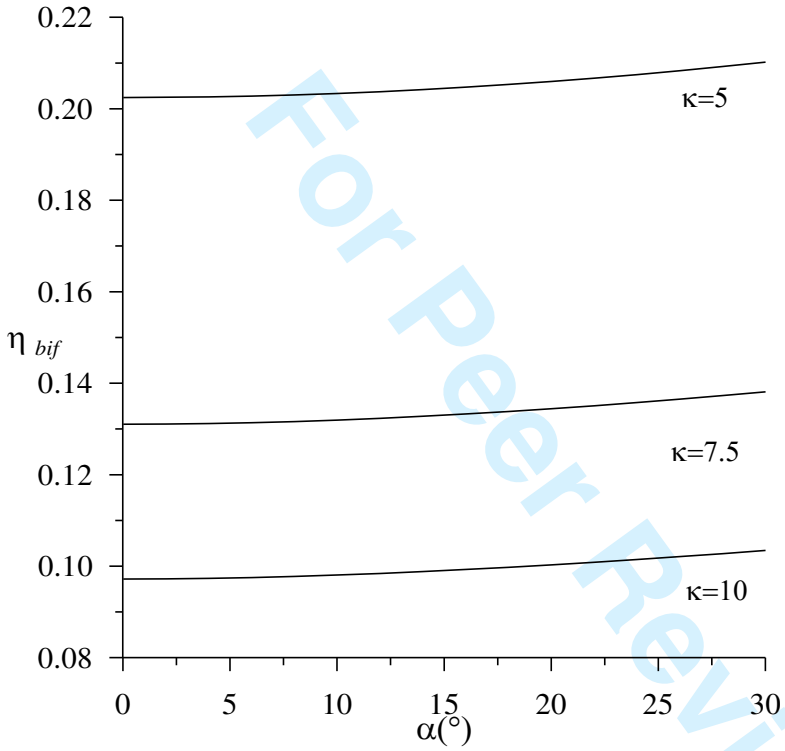

Figure 8)

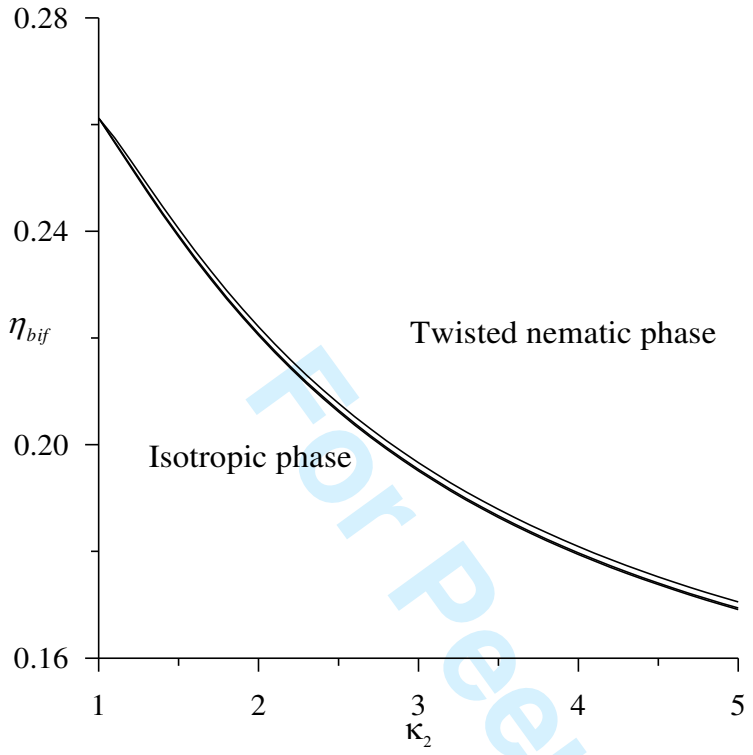

Figure 9 a)

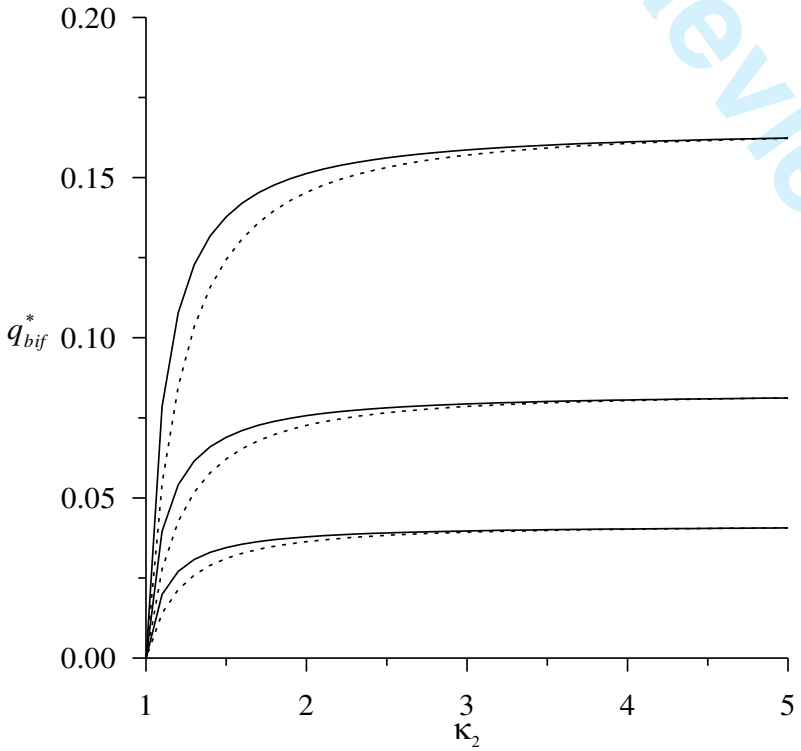

Figure 9 b)

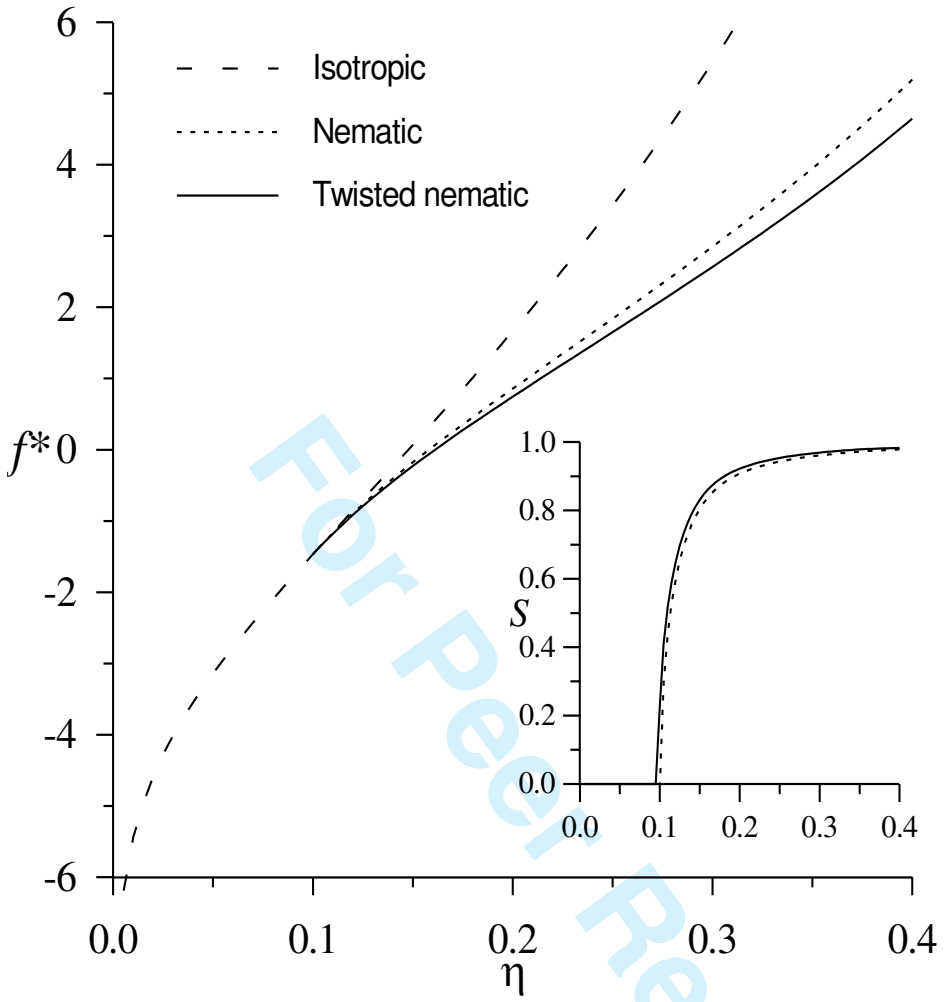

Figure 10 a)

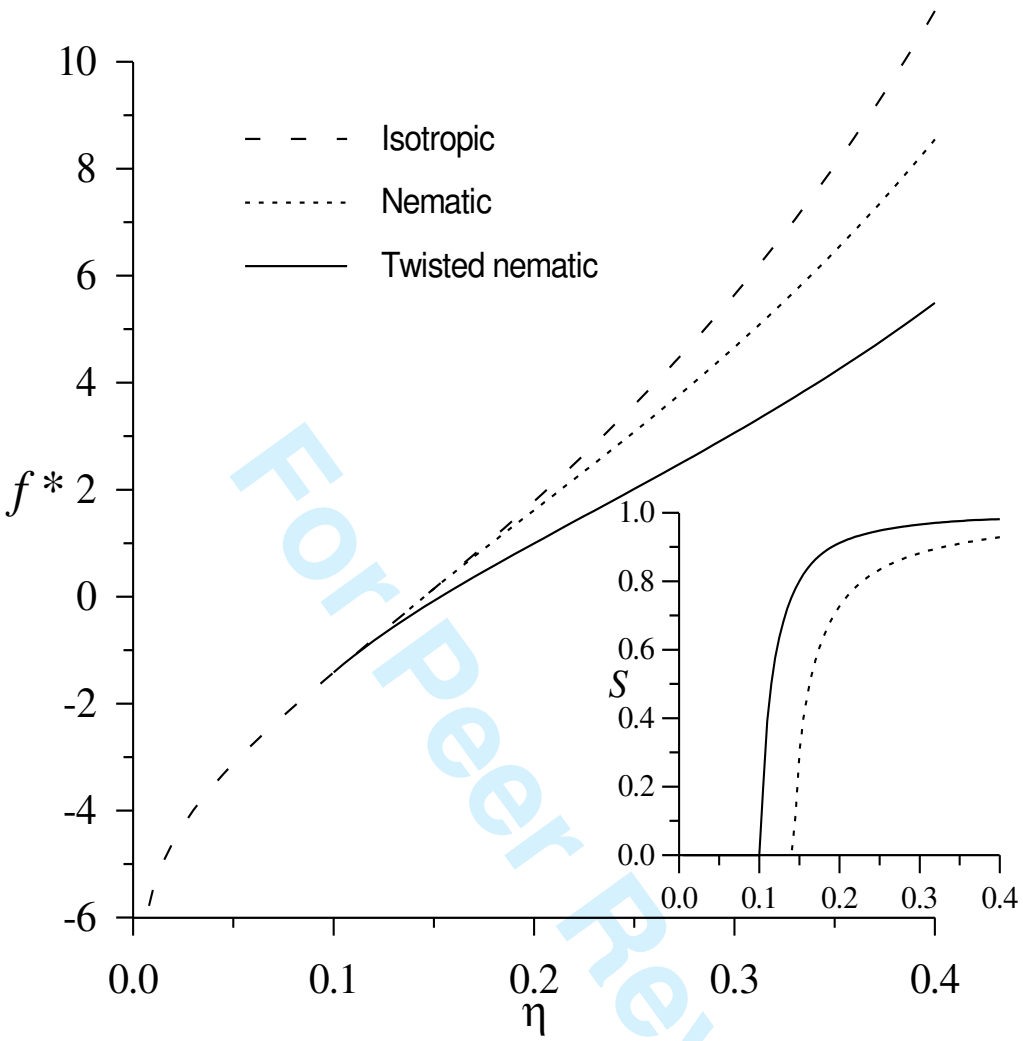

Figure 10 b)

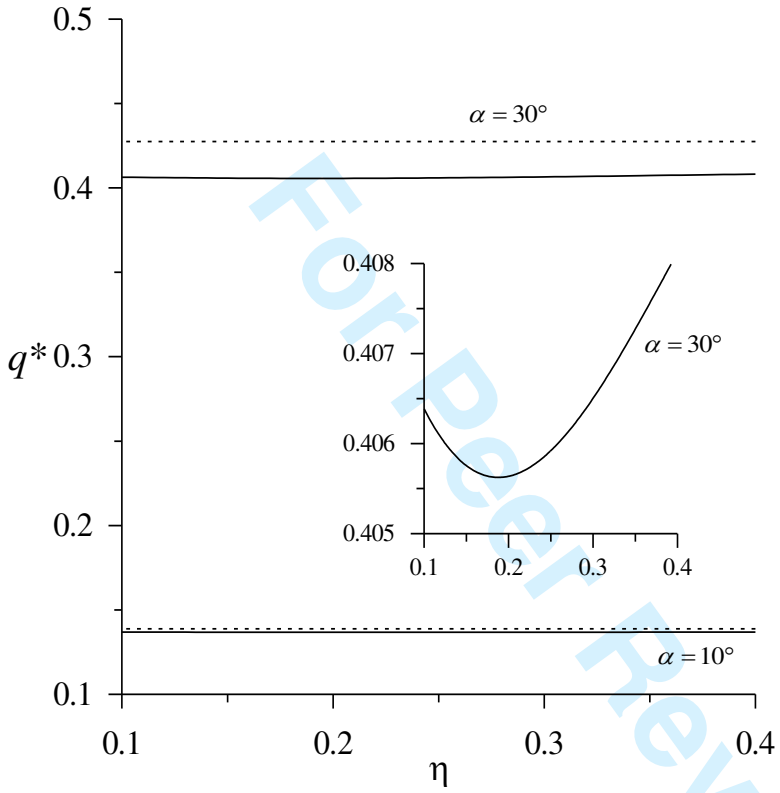

Figure 11

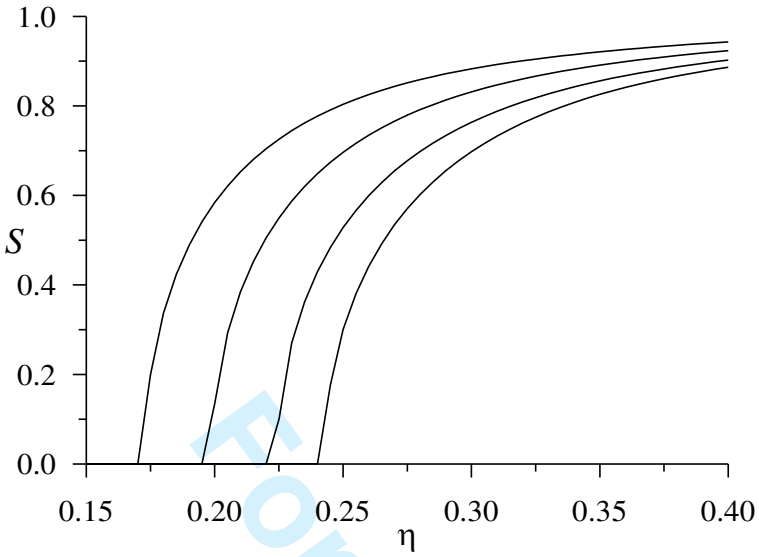

Figure 12 a)

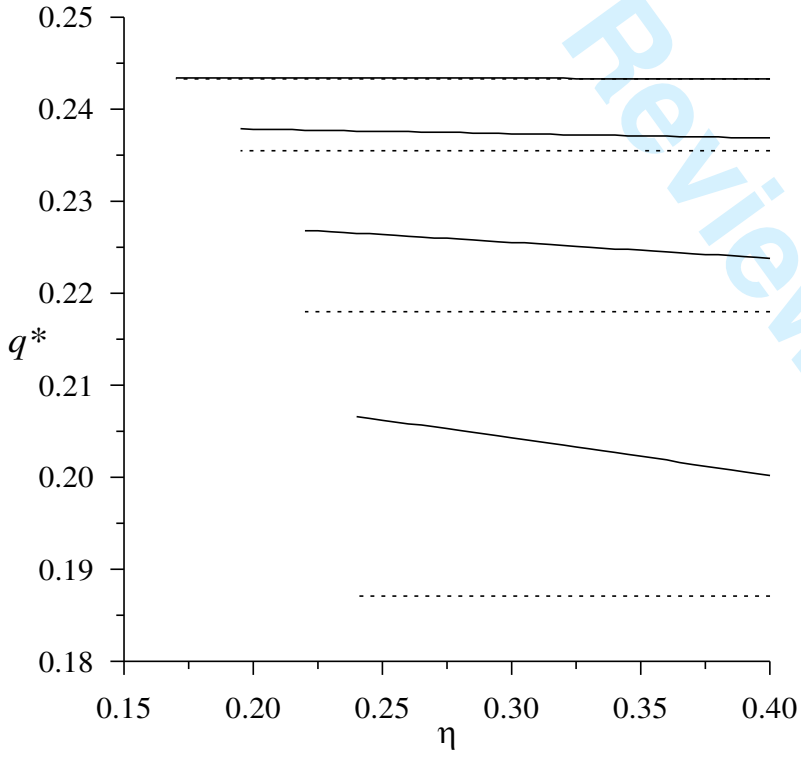

Figure 12 b)